Chapter 1

General introduction: restoration of vertical connectivity in rivers

1.1 Introduction

Hydrological connectivity defines the structure and function of river systems from the geomorphic evolution of watersheds through to temporary biogeochemical microenvironments that promote fundamental ecosystem processes such as the breakdown and remineralization of organic matter (Tockner *et al.* 1999). Many of the impacts of human land use on riverine ecosystems are the direct effects of altering hydrological connectivity via impoundments, extraction and changing patterns of interception, infiltration and runoff; or arise indirectly as altered hydrological connectivity changes patterns of sediment and nutrient delivery, or the quality, quantity or location of food and habitat. Restoration programs in rivers frequently try to treat these impacts, but often fail to address the underlying role of altered hydrological connectivity, limiting their ability to improve self-sustaining ecological functioning and resilience (Buijse *et al.* 2002, Lake *et al.* 2007). Thus, understanding the role of hydrological connectivity in riverine structure and function is necessary to improve the science and practice of riverine restoration ecology.

Hydrological connectivity is defined as "the water-mediated transfer of matter, energy and organisms within or between elements of the hydrological cycle" (Amoros and Roux 1988, Pringle 2001: 981). It has four vectors: longitudinal, lateral, vertical and temporal, and variances in these vectors underpin most ecosystem patterns and processes (Kondolf *et al.* 2006). In rivers, longitudinal hydrological connections predominantly involve the downstream movement of water, sediment, nutrients, organic matter, aquatic vertebrates and macroinvertebrates and seeds of aquatic and riparian plants. However, hydrological connectivity between river reaches also enables the upstream movement of some vertebrate (e.g. platypus, fish) and invertebrate

species. Although less widespread than downstream transport (e.g. invertebrate drift), these upstream movements can have fundamental repercussions for upstream reaches, such as the nutrient input of migrating salmonids in headwater streams (Ben-David *et al.* 1998, Gresh *et al.* 2000).

Lateral connectivity between river channels and floodplains controls successional processes of floodplain vegetation, dynamics of organic matter and nutrients, and maintains the biophysical heterogeneity of floodplains (Ward *et al.* 1999b). Flow variability and channel migration promote diverse arrays of lotic and lentic water bodies and their biota, connected at varying spatial and temporal scales to the active river channel and groundwater (where groundwater is defined as water naturally occurring below ground in an aquifer or otherwise, Tomlinson 2011). Lateral connections may also be biological, such as the energy transfer of aquatic insects to terrestrial predators (e.g. spiders, Dreyer *et al.* 2012) and terrestrial insects to aquatic predators (e.g. fish, Fisher *et al.* 1998a).

The ecology of vertical connectivity has received less attention than longitudinal or lateral linkages (Stanford and Ward 1993), despite early recognition of vertical links between streams and their groundwater aquifers (Freeze and Cherry 1979), the size of stream-groundwater ecotones in some alluvial rivers (Stanford and Gaufin 1974), and their importance to nutrient transformations (Stream Solute Workshop 1990). In general, vertical connectivity promotes resilience and resistance in river systems through the storage, filtration, biogeochemical cycling and biological production that occur in the surface water-groundwater ecotone (Fisher *et al.* 1998a, Boulton 2007). Water and nutrient fluxes between surface and groundwater are moderated as saturated sediments underlying the streambed, bank and floodplain release their stores of water, organic matter and nutrients over varying temporal scales. For example, groundwater input maintains baseflow in many streams, organic matter deposited with sediments during floods is released as bedforms migrate downstream or as the sediments are reworked during successive floods, and nutrients are released as particulates associated with organic matter or as solutes in outwelling water (Mutz and Rohde 2003, Boulton and Hancock 2006, Cornut *et al.* 2010).

The temporal dimension of hydrological connectivity comprises several aspects: when the connection is made (timing), how long the connection lasts (duration), how often the connection is made (frequency), the length of time between connections (recurrence interval), the rate of change in hydrological condition (Walker *et al.* 1995, Thorp *et al.* 2006), and the conditions preceding the connection (context). In rivers, the genetic connectivity of populations is driven by seasonal and lifecycle stages interacting with hydrological connectivity. For example, seed dispersal, macroinvertebrate drift and fish movement all rely on the hydrological connectivity of river reaches and thus, are negatively affected by disruptions to hydrological connectivity such as dams, weirs, excessive extraction and flow regulation (Bunn and Arthington 2002, Pringle 2003b).

It is the combination of spatial and temporal variation in connectivity that is vital to healthy river function (Kondolf *et al.* 2006); biota may need time in certain habitats and to be in these habitats at certain times. For example, habitats may be spatially connected (e.g. feeding, spawning and refuge habitats may be juxtaposed in space), but be unavailable to biota when needed through temporal disconnection (e.g. artificially low discharge from regulation or extraction of flows prevents fish from migrating upstream to spawning habitats). Spatio-temporally variable connectivity also maintains diverse ecological processes. Often, connectivity may be low at one spatiotemporal scale while simultaneously high at another. To illustrate, channelization, incision and widening of river channels may disconnect surface water from groundwater at a catchment scale. However, geomorphic diversity may have increased at the bar-unit scale due to the reworking of sediments deposited within the incised, widened channel (Frothingham *et al.* 2002), leading to increased hydrological connectivity between surface water and shallow groundwater at these much finer temporal and spatial scales. Because the spatiotemporal configuration of vertical connectivity controls many of the biophysical processes that take place in surface and groundwater habitats and across their boundaries, changes to this configuration have widespread repercussions for the ecological integrity of alluvial river systems.

Human land use has dramatically altered the spatial and temporal configuration of vertical connectivity by affecting the biophysical processes that drive surface-subsurface exchange. These disturbances vary across temporal and spatial scales and frequently act in synergy (Hancock 2002). Commonly, this has reduced vertical connectivity within catchments, impairing river function (Kondolf *et al.* 2006). Some disturbances, such as flow regulation, reduce vertical connectivity across multiple scales, while others (e.g. channel straightening removing intrameander flowpaths, or the loss of pool-riffle sequences) remove specific spatiotemporal scales from the mosaic. Where these scales are essential for specific physical and biogeochemical processes or biota, the impacts may be disproportionate to the overall reduction in vertical connectivity (e.g. where intrameander zones are seasonally key nutrient sinks or sources, or where riffles are critical spawning habitats). Additionally, impacts that target processes and habitats at one spatiotemporal scale can influence hydrologic exchange at other scales, often in unexpected ways (Poole *et al.* 2006). From a river management perspective, this means that a disturbance at a given scale may impair surface water-groundwater dynamics at other scales (e.g. fine sediments preferentially clogging the heads of downwelling riffles ('colmation') and reducing reach-scale flux, or channel realignment removing streamflow to a groundwater recharge zone). It also provides a strong argument for targeting restoration works at the appropriate spatial scales so that impacts are not just transferred downstream (e.g. localized flushing of fine sediments may shift the effects of colmation and smothering to the next riffle downstream).

Despite the intensive and extensive effort and resources that have been invested thus far in restoring rivers and catchments worldwide, ecologically successful restoration remains elusive (Wohl *et al.* 2005). According to the fundamental principles of restoration ecology (see Section 1.4), river restoration must be based on a mechanistic understanding of the river system that specifies how the ecosystem works, how it has been impaired and how on-ground strategies will move it along a restoration trajectory (Jansson *et al.* 2005, Palmer *et al.* 2005). Stated simply, until we know how something works and which parts are broken, we can seldom fix it. Thus, framing restoration within the context of disturbances to hydrological connectivity may improve the

science and practice of riverine restoration, not least through targeting restoration works at the appropriate spatial and temporal scales. The first step is to understand the role of vertical connectivity in structuring and maintaining ecological function and resilience in alluvial rivers.

1.2 Ecological functions of vertical connectivity

In many rivers, groundwater and surface water are a single resource, hydrologically connected through multiple interactive pathways that change in space and time (Findlay 1995). These pathways or flowpaths diverge, develop distinct physical and biogeochemical signatures and reconverge at irregular locations and intervals (Brunke and Gonser 1997, Poole *et al.* 2006). The result is a dynamic mosaic of biogeochemically-distinct patches within the alluvial aquifer, the surface stream and the saturated sediments lying below and beside the river channel that form the mediating ecotone between stream, deep groundwater (phreatic water) and floodplain or riparian habitats (Vervier *et al.* 1992, Valett *et al.* 1993, Poole *et al.* 2008). This dynamic mosaic controls lotic and lentic habitat diversity and ecological processes (Battin 2000, Dent *et al.* 2001).

However, the boundaries of this ecotone are hard to define as they fluctuate with variations in the depth and volume of water exchanged with the surface stream (White 1993). These in turn are affected by stream discharge and channel shape (Boulton 1993, Kasahara and Wondzell 2003). Because the boundaries change with fluctuations in surface flow, the ecotone is operationally defined as the interstitial mixing zone comprising 10-98 % advected surface water (Gibert *et al.* 1990). Strictly speaking, the 'hyporheic zone' (*sensu* Orghidan 1959, 'HZ') is defined as the saturated sediments extending vertically under the actual stream (wetted area), and the 'parafluvial zone' (*sensu* Boulton *et al.* 1992, 'PFZ') refers to the saturated sediments extending laterally from the actual stream (Figure 1.1).

Five broad characteristics of hyporheic exchange determine the functional significance of each exchange patch: the direction of exchange, the residence time of water within specific flowpaths, the quantity or volume of surface water–groundwater exchange, the physical and ecological structure of the hyporheic zone (e.g. sediment permeability and microbial communities, respectively), and the physicochemical quality of the water being exchanged. Generally, the direction of hydrologic exchange into or out of biogeochemically-distinct patches governs many of the processes occurring within these patches and across their boundaries (as set out in the Dynamic Ecotone Model, Gibert *et al.* 1990). Surface water entering the streambed ('downwelling' or 'inwelling', Figure 1.1) introduces dissolved oxygen, nutrients such as dissolved organic carbon (DOC), organic matter and small surface invertebrates into the hyporheic zone (Boulton *et al.* 2004). As water percolates through the sediments, it is filtered physically as particulates are caught in the sediment matrix, and biogeochemically as solutes interact with the immense surface areas of the microbial biofilms coating the sediment grains (Boulton *et al.* 1998).

Depending on its residence time in the hyporheic zone, water exiting this ecotone ('upwelling' or 'outwelling', Figure 1.1) may have a very different chemistry and temperature to the receiving surface or groundwater habitat, and provide dissolved oxygen or nutrients that are in limited supply, such as bioavailable nitrogen (Coleman and Dahm 1990, Burkholder *et al.* 2008). Where surface or groundwaters are polluted, the biogeochemical filtration in these saturated sediments may remove or mitigate contaminants, or at least form a barrier to cross-contamination (Hancock 2002). Interstitial biota increase the permeability of the hyporheic zone through burrowing, movement within and across the ecotone (e.g. migration, emergence), and pelletisation (Boulton 2000, 2007, Mermillod-Blondin 2011). Microbial activity and invertebrate detritivory, grazing and excretion influence nutrient dynamics within the ecotone as well as contributing to secondary production in surface waters via the export of nutrients and prey for riverine biota (Fischer *et al.* 2005, Mermillod-Blondin and Rosenberg 2006).

While the physicochemical attributes of water entering the hyporheic zone are determined by its immediate source (i.e. stream, riparian zone or groundwater), the composition of water exiting the hyporheic zone is strongly influenced by its residence time within the ecotone: hyporheic contributions to riverine ecosystems are greatest when a high proportion of total stream discharge travels at intermediate velocities through the hyporheic zone (Boulton *et al.* 1998). For streams, this scenario ensures sufficient supplies of oxygen, solutes and fine particulate organic matter (FPOM) from surface waters to the hyporheic zone, a residence time that enables sufficient contact with interstitial microbes, biofilms and chemical microenvironments, and adequate export of these remineralized nutrients back to surface habitats. If the residence time is too short, there is not enough contact with microbes or biofilms for nutrient remineralization and regeneration. If the residence time is too long, the products of nutrient remineralization processes in the sediments are consumed within these sediments rather than exported to surface or groundwater habitats (Marzadri *et al.* 2011).

Residence time is a function of the velocity of interstitial flow and the length of the flowpath (Findlay 1995). Interstitial velocity is controlled by hydraulic head and the permeability of sediment. Permeability relates to the porosity of the sediment (defined as the ratio of pore volume to sediment volume and determined by grain size distribution, grain shape, surface roughness and particle packing), and the interconnectivity of voids ('hydraulic conductivity'; Brunke and Gonser 1997). Hydraulic head is influenced by precipitation patterns and events (Brunke and Gonser 1997), stream gradients, breaks in stream gradient (e.g. pool-riffle transitions), channel constrictions and meander bends (Boano *et al.* 2007, Revelli *et al.* 2008).

The ecological significance of hyporheic exchange relates to both the quantity and quality of solutes exchanged (Mulholland and DeAngelis 2000, Bencala 2005). Hyporheic exchange typically occurs as multiple, hierarchical flowpaths of various lengths and residence times (Boulton *et al.* 1998, Poole *et al.* 2008). The size and volume of active exchange zones (e.g. downwelling and upwelling, or inwelling and outwelling zones) and the residence times of hyporheic flowpaths are determined by

the hydraulic conductivity of the alluvium, the hydraulic gradient between upstream and downstream ends of the stream reach, and the lateral and vertical flux of groundwater entering the alluvium (Storey *et al.* 2003). Combinations of these mechanisms can produce large hyporheic zones with significant volumes of solutes actively exchanging between surface water and groundwater. For example, the hyporheic zone extends laterally for several kilometres in the Flathead River in Montana, United States (Stanford *et al.* 1994), and vertically for many metres in the Rhône River in France (Marmonier *et al.* 1992). In a Sonoran Desert stream, the hyporheic zone can have a volume several times greater than that of the surface stream (Valett *et al.* 1990).

However, the *quality* – or bioavailability – of solutes exchanged is also fundamental to the ecological services provided by the hyporheic zone. Although the source of water entering the hyporheic zone sets its initial physicochemical composition (e.g. oxygen-rich, nutrient-poor stream water or oxygen-poor, nutrient-rich groundwater), the solute composition changes as the water moves slowly through the sediment matrix with its immense surface area of biofilms (Mulholland and DeAngelis 2000). The heterogeneous and anisotropic (i.e. where properties differ in magnitude depending on the direction of measurement) nature of river bed sediments create areas of different interstitial velocities (Jones and Mulholland 2000, Cardenas and Zlotnik 2003), organic content and therefore chemical environments, in close spatial proximity.

The close spatial juxtaposition of advective (flowing) and non-advective patches with their very different chemical environments is central to the remineralization of organic matter and nutrient regeneration processes (Thomas *et al.* 2003). Organic matter enters streambed sediments either as coarse or fine particulate organic matter (CPOM or FPOM) during sediment reworking by floods, in dissolved (DOM) or particulate form with water entering an interstitial flowpath (Hinkle *et al.* 2001, Crenshaw *et al.* 2002), through bioturbation by hyporheic invertebrates (Mermillod-Blondin 2011), or derived from interstitial biofilms (Findlay 1995, Argerich *et al.* 2011). The rich microbial

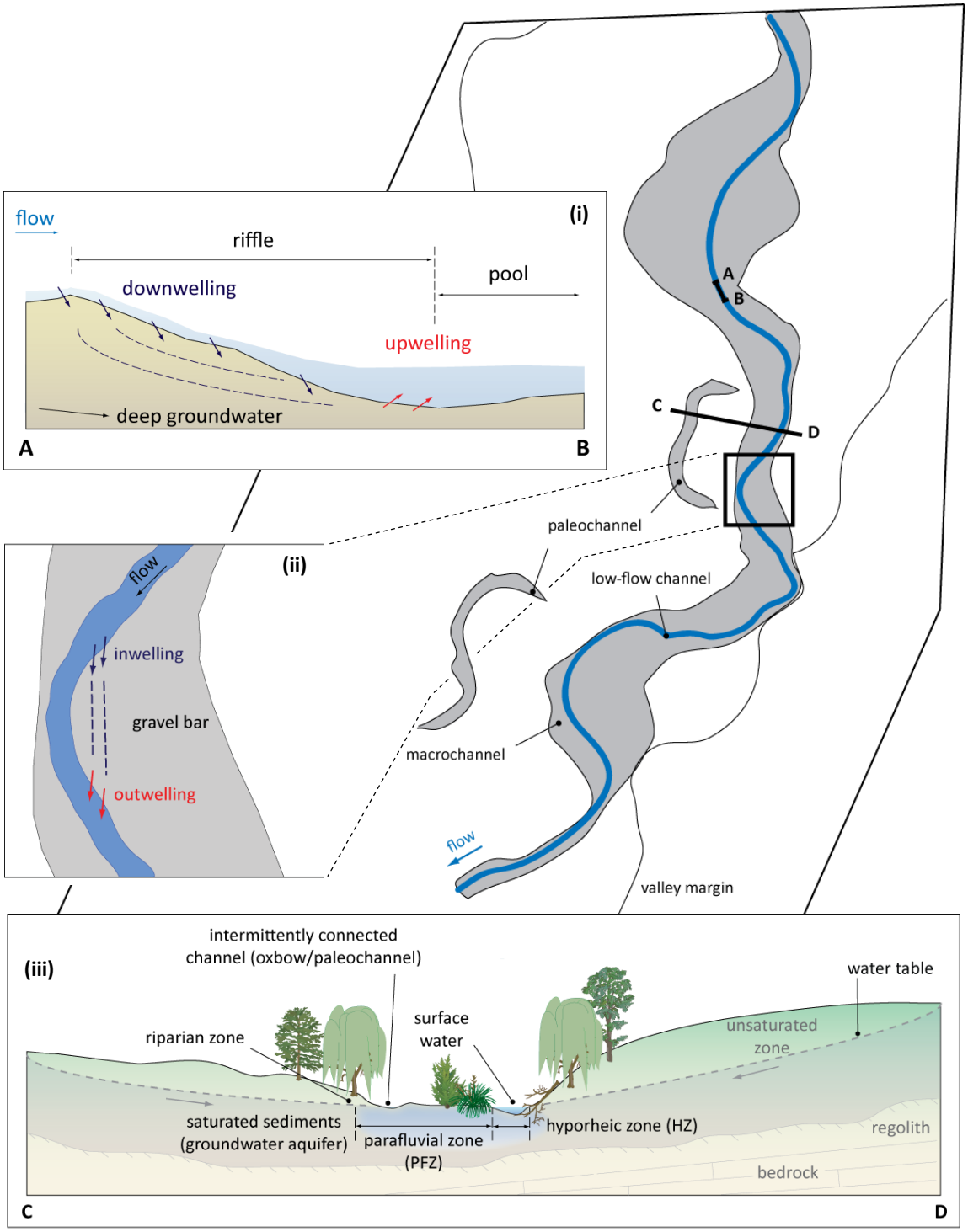

Figure 1.1 In many rivers, multiple hydrological pathways connect interdependent surface and groundwater habitats via mediating ecotones that control the direction of flow and residence time of water. **(i)** Stream water downwells into the streambed at the head and throughout most of a riffle, and interstitial water upwells at the tail of the riffle. **(ii)** At meander bends, streamwater enters the inside gravel bar (point bar), travels through the gravel and outwells at the tail of the gravel bar. **(iii)** The hyporheic zone refers to the ecotone of saturated gravel underneath the actual stream where stream water and groundwater mix and the parafluvial zone refers to the saturated sediments extending laterally from the stream. Dashed lines in (i) and (ii) represent hyporheic flowpaths.

communities in the hyporheic zone are largely heterotrophic and break down organic matter by catalyzing reduction-oxidation ('redox') reactions: organic carbon is the electron donor and is oxidized by a series of electron acceptors beginning with dissolved oxygen provided by the oxygen-rich stream water (Boano *et al.* 2010). Once aerobic respiration depletes interstitial oxygen, alternative electron acceptors are successively used during nitrification, denitrification, sulphate reduction, methanogenesis and methane oxidation (Hunter *et al.* 1998, Clilverd *et al.* 2008). Because strong redox gradients can occur across very small spatial scales (millimetres or centimetres, Morrice *et al.* 2000), organic matter can be remineralized and nutrients returned to their biologically available mineral forms ('transformed' or 'regenerated') over very small distances along the stream, resulting in 'biogeochemical hotspots' at hyporheic discharge zones (Boulton *et al.* 2010, see Section 1.4). Many studies have demonstrated that hyporheic processing strongly influences stream nutrient cycles and metabolism at the reach-scale (Triska *et al.* 1989, Fellows *et al.* 2001, Taleb *et al.* 2008).

Spatial and temporal patterns of hyporheic exchange also affect temperature dynamics in alluvial streams (Acuña and Tockner 2009). Water temperature is a critical ecological parameter (Brown *et al.* 2004), regulating the metabolic rates, physiology, distribution and abundance of aquatic biota (Arrigoni *et al.* 2008) and the rates of community processes such as nutrient cycling and productivity (Krause *et al.* 2011a). The primary external determinants of stream temperature are climatic regime (solar radiation, air temperature and wind speed), stream morphology, groundwater influx, riparian shading and the temperature of tributary inflows (Burkholder *et al.* 2008). Internal drivers of temperature, such as bed conduction and hyporheic exchange, do not add or remove heat from the river channel, but redistribute it temporally and spatially (Poole and Berman 2001). In stream reaches with active hyporheic exchange, stream water temperature both influences and is influenced by hyporheic exchange (Storey *et al.* 2003). In smaller, low-order streams, hyporheic discharge can modify stream temperature across the entire channel (Loheide and Gorelick 2006), while in larger, higher-order channels, hyporheic discharge creates thermal heterogeneity (Arscott *et al.* 2001).

There are several mechanisms by which this thermal heterogeneity occurs: stream water may be either cooled or warmed as it travels along hyporheic flowpaths (Arrigoni *et al.* 2008), be buffered in that higher temperatures are cooled and lower temperatures are warmed diurnally and seasonally (Poole *et al.* 2008, Hannah *et al.* 2009), diurnal and seasonal temperature cycles in hyporheic flowpaths may lag relative to temperature cycles in the overlying stream (Malard *et al.* 2001), or a combination of any or all of these mechanisms. Hyporheic discharge from multiple flowpaths of varying lengths, residence times and mixes of stream, hyporheic and phreatic water increases the thermal heterogeneity of alluvial reaches. In a study comparing alluvial and bedrock reaches of 1st- and 2nd-order streams in the western Cascades Range, Oregon, U.S.A., Johnson (2004) found daily maximum temperatures were buffered by up to 8.7 °C in alluvial reaches. In a study of the larger (6th-order) Clackamas River in northwest Oregon, total stream cooling was negligible (0.012 °C), but there were 40 localized patches along the 24-km reach where stream temperature differed from the reach average, and these were associated with specific geomorphic features such as gravel bars that created preferential pathways of hyporheic flow (Burkholder *et al.* 2008). In the Umatilla River in northeast Oregon, upwelling from short hyporheic flowpaths buffered the stream's diel temperature range while upwelling from long hyporheic flowpaths cooled summer and warmed winter stream temperatures (Poole *et al.* 2008).

Other studies have reported cooler water temperatures at hyporheic discharge points at the tails of riffles and gravel bars, and immediately downstream of step-pool structures (Brown *et al.* 2005, Fernald *et al.* 2006, Acuña and Tockner 2009). Because aquatic fauna have specific temperature ranges, aquatic communities are sensitive to perturbations in temperature due to climate change and human impacts (e.g. thermal pollution from dams or cooling stations). Hyporheic-induced thermal heterogeneities may buffer aquatic communities against such perturbations by creating stream and interstitial refugia and by promoting stability in fundamental community processes such as the remineralization of organic matter and nutrient regeneration (Sawyer *et al.* 2012).

Hyporheic sediments often contain a diverse invertebrate fauna composed of hyporheophiles (occasional hyporheos from benthic and phreatic zones, termed stygoxens and stygobites, respectively) and hyporheobionts (permanent hyporheos, Marmonier *et al.* 1993, Hancock *et al.* 2005). Stygophilic species inhabit the hyporheic zone during specific life-stages and/or as a refuge against adverse conditions, such as low or high flows (Brunke and Gonser 1997, 1999), or from predation as many invertebrate predator-prey interactions are based on visual cues (Franken *et al.* 2006). Hyporheic sediments have long been considered a refuge for benthic stream invertebrates ('hyporheic refuge hypothesis', Orghidan 1959, Williams and Hynes 1974) through the provision of additional colonization and incubation space for early instars, abundant food resources, greater stability of physicochemical conditions and water permanence, protection from scouring and abrasion, and reduced predation and competition pressures, especially for meiofauna (Dole-Olivier 2011); but empirical evidence is equivocal (Olsen and Townsend 2005, Stubbington *et al.* 2009, Wood *et al.* 2010). Nonetheless, studies across a range of stream types suggest that the direction of hyporheic exchange (i.e. downwelling or upwelling) creates refugia from specific hydrological perturbations (flooding or drying, respectively) for specific components of the hyporheos (benthic, phreatic or permanent hyporheos) structured within the context of spatiotemporally variable vertical connectivity at reach- and catchment-scales (Dole-Olivier *et al.* 1997, Dole-Olivier 2011, Stubbington 2012).

Hyporheic exchange zones are crucial to fish spawning, redd construction and embryo survival for salmon, trout and charr in the northern hemisphere (Soulsby *et al.* 2001, Moir *et al.* 2002, Malcolm *et al.* 2003). Very little research has been conducted into relationships between hyporheic exchange and other fish species, but similar dependencies may well be found for most lithophilic brood hiders, including Australian native fish such as freshwater catfish (Boulton *et al.* 2004). In any case, the importance of summer refugia, overwintering habitat, spawning and larval habitats, and the need for fish passage between habitats (i.e. maintenance of suitable baseflows) are common to many freshwater fish species (Power *et al.* 1999) and all rely on stream-groundwater exchange.

Groundwater comprises two-thirds of the world's fresh water resources (Freeze and Cherry 1979). In comparison, rivers contain <0.01 % of the world's fresh water (Power *et al.* 1999). Thus, in many rivers, baseflow – the component of total stream flow derived from groundwater – is such a significant proportion of the total discharge that most rivers are considered as groundwater-dependent ecosystems (GDEs, Boulton and Hancock 2006). While a small proportion of groundwater enters the channel directly via groundwater seeps or springs, the majority enters the channel via the parafluvial and hyporheic zones (Boulton and Hancock 2006, Hancock *et al.* 2009). During high flows, higher hydraulic pressures cause the river to infiltrate its banks and bed, recharging the groundwater aquifer and reducing the flood level. During periods of low surface runoff, the release of stored water over much longer temporal scales compensates for decreased stream discharge. Overall, large-scale groundwater-surface water exchange buffers stream discharge, maintaining low flows during dry periods and mitigating flood levels during wet periods (Brunke and Gonser 1997).

In summary, groundwater and stream water are intimately connected in many rivers via a spatially and temporally dynamic mosaic of biogeochemically distinct ecotonal patches knitted together by multiple, hierarchical flowpaths that also vary in space and time. The spatial and temporal configuration of vertical connectivity with its inherent variability is central to its ecological significance for river systems (Munz *et al.* 2011). Vertical connectivity promotes resilience and resistance in rivers through the storage, filtration, nutrient cycling, buffering and biological production that occur in hyporheic zones. However, in many rivers human land use has dramatically altered the spatial and temporal configuration of hyporheic exchange by disturbing the biophysical processes that drive vertical connectivity. These disturbances often act across multiple temporal and spatial scales and in synergy, reducing vertical connectivity across multiple scales or removing specific spatiotemporal scales from the mosaic. For restoration programs to be ecologically successful, they must be based on a mechanistic understanding of the ecosystem, how disturbance impairs these ecosystem processes, and how restoration works can enhance or reintroduce these processes. Given our understanding of the integral role of vertical connectivity in structuring and maintaining ecological function and resilience in alluvial rivers, the

second step in restoring vertical connectivity is to understand the actual physical processes that drive hyporheic exchange from sediment- to catchment-scales.

1.3 Processes driving vertical connectivity

Vertical connectivity occurs across a very wide range of spatial and temporal scales as systems of smaller flow cells nested inside larger flow cells (Tóth 1963, Cardenas 2007), so fine-scale drivers of hyporheic exchange are superimposed over broad-scale processes associated with catchment geology, topography and climate (Brunke and Gonser 1997, Boano *et al.* 2009). The ecological significance of specific flowpaths differs with their length. For example, very short flowpaths (sub-metre) driven by diffusion or localized topographic controls like boulders are vital for oxygenating the benthic zone (surface sediments). Likewise, biotic nutrient assimilation generally peaks at the beginning of hyporheic flowpaths, so multiple short flowpaths play an important role in nutrient turnover (Poole *et al.* 2008). Intermediate flowpaths (~10 m) such as those induced by riffles are biogeochemically influential for processes that occur at uniform rates such as the remineralization of organic material and interstitial oxygen dynamics (Findlay 1995, Poole *et al.* 2008). Long flowpaths (km) maintain baseflow and provide localized thermal refugia in many streams (Malard *et al.* 2002). Although many studies document differences in biodiversity and biogeochemical processes among patch types, sizes and shapes (see Malard *et al.* 2002 for references), the cumulative effects of multiple, sequential patches (Fisher *et al.* 1998b), and the expansion or contraction of hyporheic flow systems with stream discharge (Valett *et al.* 1996, Stanley *et al.* 1997), the ecological significance of the configuration of hyporheic patches is yet to be empirically established (Malard *et al.* 2002).

This is not a trivial concept for hyporheic restoration. Since the formulation of the Patch Dynamics Concept (Townsend 1989), hyporheic researchers have demonstrated that, despite the difficulties involved in studying patchy patterns and processes (Palmer 1993), patchiness and dynamic heterogeneity enhance biogeochemical processes (Grimm *et al.* 2005) and biodiversity in hyporheic zones (White 1990,

Boulton *et al.* 1998). Thus, embracing – not avoiding – patchiness and dynamic heterogeneity is necessary to develop our understanding of hyporheic processes (Käser *et al.* 2009). Additionally, human impacts may remove hyporheic patches (and their inherent biophysical properties and processes) at specific spatial scales (e.g. removing log steps, riffles or meanders). This alters the relative contributions of short, intermediate and long flowpaths with their differing residence times and chemical composition of exported water, with probable widespread repercussions for riverine ecosystems. Hyporheic restoration programs must consider the scalar issues and cumulative effects of impaired vertical connectivity if they are to successfully restore ecological integrity in alluvial rivers. Below, I discuss the mechanisms of and controls on vertical connectivity in rivers from fine to broad scales.

1.3.1 Fine-scale processes

Fundamentally, hyporheic exchange is driven by differences in pressure: water moves from areas of high pressure to areas of low pressure. Pressure variations at the stream-bed interface are caused by interactions among streamflow, sediment conditions and bed topography (Packman and Salehin 2003). Seven mechanisms (Hester and Doyle 2008) have been proposed to drive vertical hydrologic exchange at fine scales: (1) diffusion, (2) turbulent flux driven by the difference in velocity between stream and interstitial flow, (3) turnover exchange where water trapped in bedforms (e.g. dunes) is released as the bedforms are reworked, (4) exchange induced by turbulent streamflow over a bedform protruding into the stream (either permeable like ripples and dunes, or impermeable like boulders), (5) exchange due to heterogeneous substrates inducing localized head gradients (i.e. upwelling upstream and downwelling downstream of obstructions) within the sediment such as clay lenses or shallower bedrock, (6) exchange due to head gradients created by localized channel steepening (i.e. relative to the reach-average slope) such as riffles and steps, and (7) exchange from backwater collecting behind obstacles in the channel such as large woody debris (LWD), boulders and bars (Figure 1.2).

Clearly, multiple mechanisms of hyporheic exchange can be simultaneously induced by the same feature (Figure 1.2). For instance, a riffle induces vertical hydrologic exchange through localized channel steepening (6), but is also an area of faster flow (2), larger substrates (7), and often, layered (i.e. heterogeneous) sediments (5). While a single mechanism likely dominates total hyporheic exchange around a channel feature, the contributions of mechanisms vary with stream discharge, the dimensions of the feature, the sediment mix and time since the last bed-moving event. For example, at extreme low flows, surface flow may cease over a riffle, removing the mechanism of turbulent streamflow over a bedform (4), reducing the effects of surface velocity (2), and increasing the contribution of backwater pooling upstream of the riffle (7).

Flume experiments provide the best means of studying the basic hydrodynamic processes that control sediment-scale hydrological exchange between the stream and streambed. They permit highly controlled conditions so that individual processes can be isolated, and allow close examination of porewater flow through the bed sediment so that these processes can be visualized. Flume studies tend to focus on either sand or gravel beds, as these two types of sediment have distinctly different exchange processes. In sand beds, porewater flow is laminar with turbulent mixing restricted to a very thin surface layer (Packman and Bencala 2000). In contrast, streamflow over a gravel bed creates turbulent flow at the stream-bed interface such that turbulent flow penetrates a significant distance into the bed and influences porewater flow (Packman and Bencala 2000). In other words, interstitial water in gravel beds is more intimately associated with the overlying stream water.

Exchange across flat beds: diffusion and turbulent flow

In turbulent streamflow over flat gravel beds, pressure variations at the bed surface occur over very fine temporal and spatial scales. Two mechanisms are known to drive these pressure variations. Firstly, diffusive transport drives vertical exchange in the upper few centimetres of the bed (Packman *et al.* 2004). Secondly, the direct coupling of stream and porewater flow occurs because stream flow is turbulent and the gravel

bed is porous. The velocity of streamflow is greater than the velocity of porewater. Because the bed is porous, this creates a non-zero velocity at the very surface of the bed (called 'slip velocity'), allowing surface water to exchange momentum with the porewater (Zhou and Mendoza 1993, Higashino *et al.* 2009). This transfer of momentum causes turbulent mixing of surface water and porewater (Figure 1.2, Packman and Bencala 2000). In flat gravel beds comprising coarse sediment (d = 2-4 cm), turbulent diffusion was the dominant mechanism of solute transport (Nagaoka and Ohgaki 1990, Shimizu *et al.* 1990). This supports the theoretical analysis of Zhou and Mendoza (1993), who found that turbulent surface flow accelerated porewater velocity at the bed surface, with porewater velocity decaying exponentially with depth to a Darcy velocity driven by channel slope (Packman and Salehin 2003). In their flume study, Packman and others (2004) injected dye just below the surface of the bed and observed it migrating vertically into the stream, suggesting that turbulent mixing occurred in the upper 5 cm, or top 5-10 clasts (median grain size (d_{50}) = 6 mm) of the bed surface. Pore water velocity and subsurface transport increase with increasing stream velocity and/or increasing bed roughness (Goharzadeh *et al.* 2005, Reidenbach *et al.* 2010).

Bedform-induced exchange in gravel beds

As water flows over unconsolidated sediments it reworks these sediments, increasing the complexity of bed topography through the formation of bedforms such as ripples, dunes and antidunes (Leeder 1999). In sandy beds, the ripples and dunes themselves advect downstream, trapping and releasing porewater as they 'turn over'. In the absence of larger channel features such as pool-riffle sequences, this can be a significant mechanism of fine-scale surface-subsurface exchange. In a low-energy, sandy stream, turnover contributed 14 % of the downward and 30 % of the upward hyporheic exchange at baseflows (Mutz and Rohde 2003). However, in gravel-bed rivers, turnover exchange is significant only during bed-moving flows and only in the absence of channel features (LWD, boulders) that would block bedform movement (Hester and Doyle 2008).

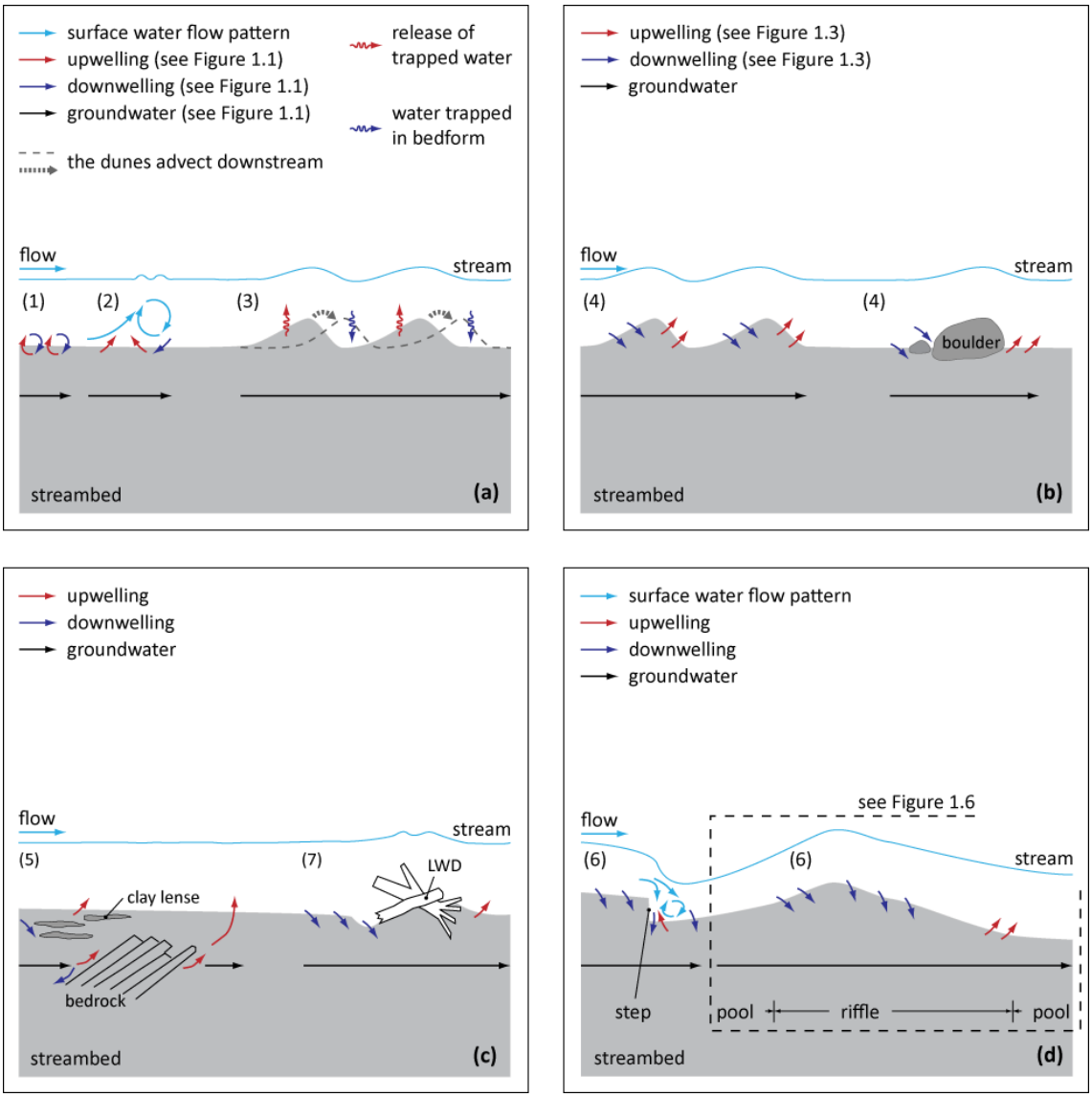

Figure 1.2 The mechanisms of fine-scale hyporheic exchange: **(a)** diffusion (1), turbulent flux (2) and turnover exchange (3); **(b)** bedform-driven exchange (4), either permeable (left) or impermeable (right); **(c)** heterogeneous substrates (5) and backwater pooling behind obstacles such as large woody debris (LWD; 7); and **(d)** localised channel steepening (6) such as steps (left) and riffles (right). Bracketed numbers refer to the mechanisms identified by Hester and Doyle (2008) on the preceding page.

Bedforms interact with turbulent streamflow to create complex patterns of turbulence, creating variations in pressure at the stream-bed interface. These variations in pressure drive surface-subsurface exchange. One of the earliest studies on the mechanisms of bedform-induced hyporheic exchange was the flume

experiment conducted by Thibodeaux and Boyle (1987). They used coarse, homogeneous gravel (d = 8 mm) with a series of triangular dunes that had shallow stoss (upstream) slopes and steeper lee (downstream) slopes. The bedforms induced complex interstitial flow to a depth five times greater than the height of the bedform. Streamwater entered the bedform along the entire stoss slope, travelled downwards at an angle of 45 ° to its final depth, and converged as it moved upwards and entered the surface stream along the lee slope (Thibodeaux and Boyle 1987).

In their mathematical modelling of bedform-induced exchange, Packman and others (2004) found that the exchange flux was a function of stream velocity, the relative roughness and wavelength of bedforms, and the hydraulic conductivity of bed sediments. The velocity of surface flow and bedform wavelength influenced hyporheic exchange much more strongly than the height of the bedform for typical triangular dunes (Packman *et al.* 2004). The height of the bedform was relevant in as much as it induced flow separation and created a lee eddy: higher bedforms did not substantially increase hyporheic exchange. This can be explained in light of later flume studies that reveal a complex relationship between turbulent streamflow, the height and steepness of the bedform, the length of the lee eddy, the pressure gradient at the stream-bed interface, and the depth and flux of the interstitial mixing zone.

As water flows over an asymmetric, triangular bedform (e.g. a dune), an eddy detaches at or near the crest of the bedform and reattaches on the stoss side of the succeeding bedform (Figure 1.3). The lee eddy controls the distribution of pressure along the stream-bed interface, and thus, exchange processes between the stream and streambed. The eddy detachment point almost always coincides with the point of minimum pressure at or near the crest of the bedform (Cardenas and Wilson 2007a). The eddy reattaches at or near the point of maximum pressure on the stoss face of the next downstream bedform (Cardenas and Wilson 2007b). As the Reynolds Number (*Re*) of streamflow increases, the eddy detachment point migrates upstream the lee slope to the bedform crest and the reattachment point migrates downstream along the stoss face of the succeeding bedform (Cardenas and Wilson 2007a). The length of the lee eddy increases asymptotically with *Re* to 4-6 times the height of the bedform in

fully turbulent flow (Cardenas and Wilson 2007b). In the flume studies of Cardenas and Wilson (2007a, 2007b, 2007c), the pressure gradient along the stream-bed interface caused stream water to downwell into the bed along the upper part of the stoss slope, and porewater to upwell along the lee face and lower part of the stoss face (Figure 1.3). Porewater flow in the deeper sediments was driven by channel slope.

Bedform geometry directly controls the length of the pressure gradient at the stream-bed interface and the latter regulates the depth of the interstitial exchange zone. As the bedform becomes steeper, the point of maximum pressure moves downstream the stoss face of the bedform, towards the minimum pressure near the bedform crest, effectively shortening the length of the pressure gradient (Cardenas and Wilson 2007b). The depth of the exchange zone is inversely related to the length of the pressure gradient: steeper bedforms have shallower exchange zones. The volumetric flux of porewater is controlled predominantly by the velocity of surface flow (Packman *et al.* 2004), although for the same stream *Re*, steeper bedforms have a smaller porewater flux than shallower bedforms (Cardenas and Wilson 2007b). The direction of porewater flow close to the stream-bed interface does not always correspond to breaks in bed topography such as troughs and crests; some flow cells cross bedforms indicating that advection through a bedform is not a closed hydrodynamic system, but rather, may be influenced by surrounding bed conditions (Cardenas and Wilson 2007a).

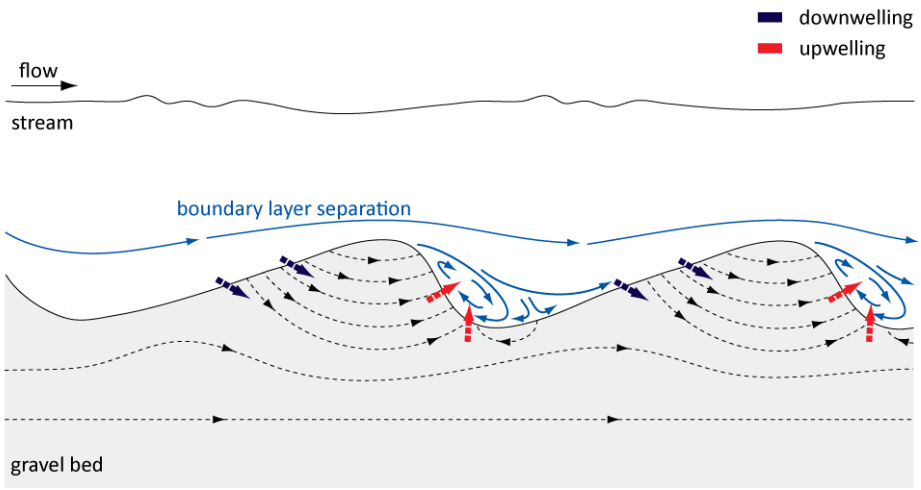

Figure 1.3 Bedforms interact with turbulent stream flow to drive surface-subsurface exchange: stream water is pushed by high pressure (downwelling) along the stoss slope of the bedform, and interstitial water is pulled from the sediment into the surface stream (upwelling) along the lee slope of the bedform.

Sediment conditions

The permeability of ecotones controls exchange processes between ecological systems. In hyporheic ecotones, permeability depends on the porosity and hydraulic conductivity of sediments (Section 1.2, Brunke and Gonser 1997). In open gravels, hydraulic conductivity is high and interstitial flow may be turbulent. Although the distribution of grain sizes and porosity are related to hydraulic conductivity, no simple empirical relationships exist among these sediment parameters (Huggenberger *et al.* 1998). The flume study of Packman and Salehin (2003) showed hyporheic exchange to be proportional to the permeability of sediments and the square of stream velocity for a range of sediment grain sizes, bed profiles and stream velocities. Where bedforms were small, hydraulic conductivity and stream velocity were the two most critical parameters for characterizing hyporheic exchange as hydraulic conductivity controlled the ability of sediments to admit any advective flux, and the coupling of streamflow and sedimentary pore water drove hyporheic exchange. In Indian Creek, an urban stream in Pennsylvania, U.S.A., groundwater flow, bed topography and sediment heterogeneity controlled the transport of solutes through bed sediments (a gravel-

cobble matrix with significant infilling of silts and sands), but heterogeneous hydraulic conductivity was the dominant controlling process (Ryan and Boufadel 2006).

The hydrogeologic history of a river determines the stratigraphy of bed sediments, in turn creating complex patterns of hydraulic conductivity (Huggenberger *et al.* 1998). Episodic scour-and-fill events may substantially rework sediment grain size distributions, organic content and bed topography to create hierarchical sedimentary units within fluvial deposits and within these units, hierarchical sets of strata. The hydrogeologic properties (including hydraulic conductivity) of these sediments are determined by grain size distributions within individual strata and by the geometry of sets of strata at microform scales (e.g. laminations), mesoform scales (e.g. crossbed sets) and macroform scales (e.g. point bar assemblages, Rubin *et al.* 2006, Sawyer and Cardenas 2009). While processes creating microforms (sediment sorting, selective transport) and macroforms (streambed stratigraphy, channel morphology) have received considerable attention, knowledge is limited at the mesoform-scale that is responsible for localized heterogeneity of hyporheic exchange (Salehin *et al.* 2004). This knowledge gap limits the success of attempts to actively restore or replicate meso-scale hyporheic structure as these hydrogeologic processes occur over long temporal scales.

A defining characteristic of fluvial sediments is their anisotropy (where characteristics are unequal in different directions) because water typically orientates sediment during the working process. Anisotropy in gravel-bed rivers occurs at multiple scales as individual clasts, strata and bedforms may be oriented with flow (Butler *et al.* 2001). In most fluvial sediments, hydraulic conductivity is anisotropic with horizontal conductivity one to two orders of magnitude greater than vertical conductivity (Huggenberger *et al.* 1998). The combination of the inherent anisotropic hydraulic conductivity and the hierarchical heterogeneous stratigraphy of natural river sediments creates complex three-dimensional networks of hyporheic exchange along preferential flowpaths (Cardenas *et al.* 2004). In a fifth-order reach of the Lahn River (Germany), the influence of sediment anisotropy on hyporheic exchange depended on the distribution of hydraulic conductivities: anisotropy increased hyporheic exchange

at low and intermediate surface flows but decreased exchange during high flows (Saenger *et al.* 2005). The distribution of hydraulic conductivities was similarly relevant for calculating hyporheic exchange in the Platte River (U.S.A.): low-conductive layers inhibited downwelling most when the layer occurred at or close to the bed surface, was less conductive, thicker, or extended further across and/or along the channel (Chen *et al.* 2008).

Several studies document a zone in the centre of the channel and aligned with flow where hydraulic conductivities were increased by a factor of two to more than an order of magnitude, likely due to increased stream velocity influencing grain size distributions in the stream centre (Storey *et al.* 2003, Cardenas *et al.* 2004, Genereux *et al.* 2008). This linkage among fluvial sedimentology, hyporheic exchange and chemical transport is ecologically noteworthy, because groundwater discharge to the stream may preferentially occur in the centre of the stream, leading to systematic differences in physicochemical and ecological attributes of hyporheic sediments between the centre and sides of the channel (Genereux *et al.* 2008).

Hydraulic conductivity varies in time as well as space. Because the viscosity and density of water are temperature-dependent properties, hydraulic conductivity varies with temperature (Brunke and Gonser 1997). In a small stream experiencing significant diurnal variations in surface water temperatures, hotter afternoon temperatures increased hydraulic conductivity, which increased downwelling and reduced stream discharge (Constanz *et al.* 1994). Temporal variability in hydraulic conductivity remains largely unexplored, but is likely to respond to variables that also vary temporally such as streambed microbial activity (through its influence on the gas and biofilm content of sediments), temperature (diurnal, seasonal and interannual cycles), bioturbation, organic content of sediments, and erosional and depositional patterns (Genereux *et al.* 2008). In a sandy North Carolinian stream (U.S.A.), temporal and spatial variability in hydraulic conductivity were controlled by vertical variability in the proportion of fine-grained sediments (silts and clays), and scour-and-fill events (Genereux *et al.* 2008).

Between bed-moving events, localized heterogeneity occurs due to differential sediment transport and grain sorting creating layers within the bed sediments (Powell 1998). Preferential removal of finer surface sediments by entrainment leaves a coarse surface layer with higher permeability than the parent material ('armouring', Figure 1.4a, Church *et al.* 1987). The thickness of the armour layer (coarse surface sediments) is usually limited to twice the size of the largest clast (operationally defined as the 90th percentile of the grain size distribution (d_{90}), Marion *et al.* 2008). Although thin, an armour layer may increase diffusive hyporheic exchange in upper sediments by an order of magnitude as diffusive exchange is proportional to the square of the grain size (Figure 1.2, Packman *et al.* 2004, Marion *et al.* 2008). This may significantly increase nutrient delivery to benthic biofilms and invertebrates (Larned *et al.* 2004). In contrast, downward coarsening of sediments occurs in bedforms such as ripples and dunes as finer clasts preferentially avalanche down the lee face of the bedforms as the bedforms migrate downstream (Figure 1.4b, Blom *et al.* 2003, Blom 2008).

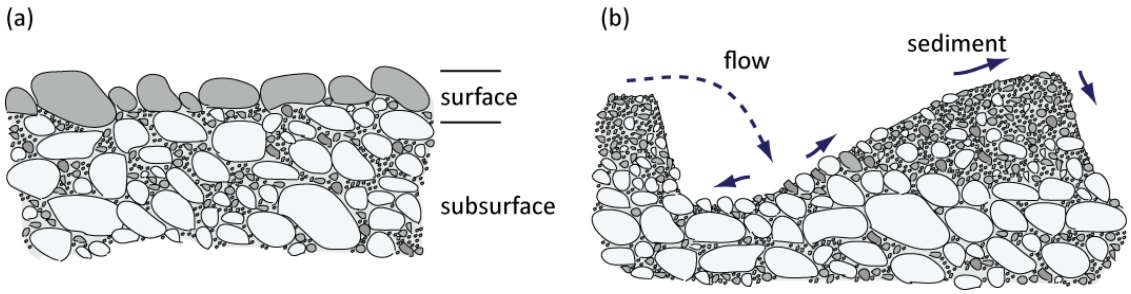

Figure 1.4 Selective transport processes that create coarse sediment layers. **(a)** Bed armouring occurs when finer sediments are entrained, leaving a residual coarse layer with permeability greater than the parent material (modified from Church *et al.* 1987). **(b)** A buried coarse layer occurs under bedforms as finer sediments are preferentially transported down the lee face of the bedforms (modified from Blom *et al.* 2003), or due to differential settling rates during floods.

Hydraulic conductivity also decreases with time between bed-moving events, as fine-grained sediments infiltrate into the sediment matrix, decreasing both pore space and the interconnectedness of voids (i.e. 'colmation', Brunke and Gonser 1999, Hancock 2002, Zimmermann and Lapointe 2005). In many rivers where low-flow conditions occur for prolonged periods, a layer of fine sediment is deposited in shallow, low-velocity habitats. For example, in the South Platte River in northeastern Colorado (U.S.A.), a layer up to 1 cm thick is deposited over much of the river bed during low flow periods, and has a hydraulic conductivity 20-25 % less than the sandy gravel bed (Cronin *et al.* 2007, Rosenberry and Pitlick 2009). Deposition of veneers of fine sediments during seasonal low flows has reportedly reduced hydraulic conductivity at the water-sediment interface by one to two orders-of-magnitude (Hatch *et al.* 2010) and up to nearly six orders-of-magnitude in instances of severe clogging (Rosenberry and Healy 2012).

Infiltration rates and variations in the grain sizes of infiltrated sediments are determined by complex interactions among sediment supply and transport processes, local hydraulics and reach morphology, and are extensively reviewed in the literature (Greig *et al.* 2007 and references within). The ratio of grain size of infiltrating fine sediments to available pore space in the receiving sediment matrix determines whether a particle is obstructed, trapped in surface sediments, or penetrates deeper into the river bed (Greig *et al.* 2007). Where fine sediments infiltrate surface sediments but are too large to penetrate subsurface layers, the pore spaces are reduced and successively finer sediments are trapped in the surface matrix. Because this surface 'seal' or 'plug' inhibits further, deeper infiltration of fine sediments, the antecedent size distribution of fine sediment in surface layers controls the amount of fine sediment that can accumulate in the river bed (Figure 1.5a, Greig *et al.* 2007).

Conversely, 'bottom-up' accumulation of fine sediments occurs when fine sediments are smaller than the pore spaces and are transported to the base of the permeable sediment layer (Figure 1.5b). Both these processes are forms of internal clogging; external clogging occurs when a layer of fine sediment (with low hydraulic conductivity) settles on the top of the streambed (Figure 1.5c, Schälchli 1992). As well

as inorganic fine sediment, fine particulate organic matter (FPOM) may infiltrate sediments and reduce hydraulic conductivity. However, the breakdown of FPOM in sediments also promotes biofilm growth, and the accumulation of biofilm extracellular polymers, bacterial cells and gaseous metabolites further reduce interstitial flow rates (Vandevivere and Baveye 1992, Battin and Sengschmitt 1999). Suspended sediments are preferentially deposited in downwelling and inwelling zones, which are proscribed by the interaction of streamflow, bed topography and sediment conditions. Thus, internal clogging of these spatially limited locations can significantly reduce hyporheic exchange throughout the whole streambed (Rehg *et al.* 2005). Despite repeated pleas over the last decade for more research into the role of hydraulic heterogeneity in structuring hyporheic exchange (Packman and Bencala 2000, Sophocleous 2002, Wagner and Bretschko 2002), it is only very recently that research is progressing in this area (Chen 2011, MacDonald *et al.* 2012, Rosenberry *et al.* 2012). Without this knowledge, it is difficult for river managers to prioritize the protection of hyporheic zones and functions.

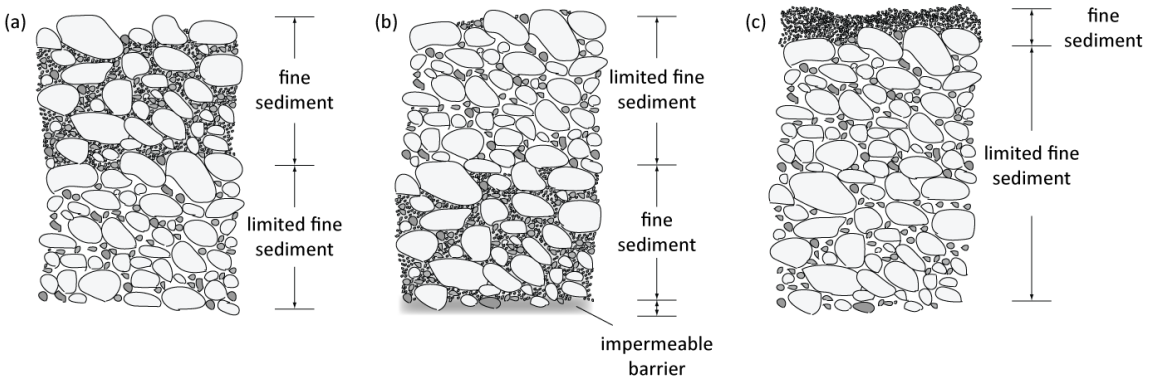

Figure 1.5 Internal and external clogging processes. **(a)** Fine sediment forms a surface 'seal' preventing further penetration of fine sediments into the streambed. **(b)** Fine sediment percolates deep into the sediment matrix until it reaches an impermeable barrier. **(c)** Fine sediment accumulates on top of the existing sediment matrix forming a barrier of low permeability on top of the streambed.

1.3.2 Reach-scale processes

Vertical hyporheic exchange

In gravel- and mixed-bed channels of low to moderate gradients, riffle-pool sequences are the characteristic reach-scale bedform and basic framework for most aquatic habitat (Clifford 1993, Thompson 2001). Riffles are topographically high (convex) areas of the channel bed that tend to fill at high flow with relatively high water-surface gradients and faster velocities at low flow; pools are topographically low (concave) areas of channel bed produced by scour at high flow with very low water-surface gradients and low velocities at low flow (Wohl *et al.* 1993, Thompson 2001). In self-formed and geomorphically forced rivers, average riffle spacing is five to seven times the channel width due to velocity reversals between riffles and pools, kinematic wave propagation, longitudinal oscillations in macroturbulent flow and the non-rhythmic distribution of channel obstructions (Yalin 1992, Knighton 1998, Hanrahan 2007). Riffle-scale hyporheic exchange has a disproportionately large significance to stream ecosystems because riffles are ubiquitous so are likely to account for more surface-subsurface interaction than longer flowpaths (Harvey and Wagner 2000). Because these interactions have intermediate residence times, relatively high concentrations of dissolved oxygen are maintained for hyporheic biota while still allowing sufficient time for biogeochemical processing (Storey *et al.* 2003).

Reach-scale hyporheic exchange is dominated by riffles forming regular breaks in streambed slope (Harvey and Bencala 1993, Kasahara and Wondzell 2003, Boano *et al.* 2006). These deviations from the reach-average slope essentially drives hydraulic gradients in riffles (Storey *et al.* 2003). The basic pattern of hyporheic exchange across a riffle-pool sequence is as follows: at the downstream end of a pool, decreasing stream depth creates a zone of high pressure at the stream-bed interface causing stream water to downwell into the streambed. This downwelling water displaces pore water, pushing it along preferential flowpaths determined by sediment stratigraphy within the riffle. At the downstream tail of the riffle, increasing stream depth creates a zone of low pressure at the stream-bed interface, pulling porewater into the surface stream (Figure 1.6, Brunke and Gonser 1997).

Hyporheic exchange through riffles is influenced by local controls affecting gradients in hydraulic head along and across the riffle, such as depth to bedrock, valley constriction, streambed stratigraphy, groundwater and stream discharge, and stream temperature (Boulton *et al.* 1998, Coulombe-Pontbriand and Lapointe 2004, Malcolm *et al.* 2004). In Girnock Burn, a semi-pristine upland stream in northeast Scotland, groundwater discharge dominated hyporheic water quality at the head and tail of a riffle, reflecting the influence of streambed stratigraphy and valley constriction (Malcolm *et al.* 2004). Groundwater discharge varies with seasonal aquifer recharge and, depending on aquifer and channel stratigraphy and channel shape, may seasonally dominate vertical or lateral hyporheic exchange (Storey *et al.* 2003, Malcolm *et al.* 2004). Stream temperature controls the viscosity of water and thus, hydraulic conductivity of sediments. In the low-gradient Speed River in Ontario (Canada), hydraulic conductivity in a riffle decreased by 40 % during lower winter temperatures (Storey *et al.* 2003).

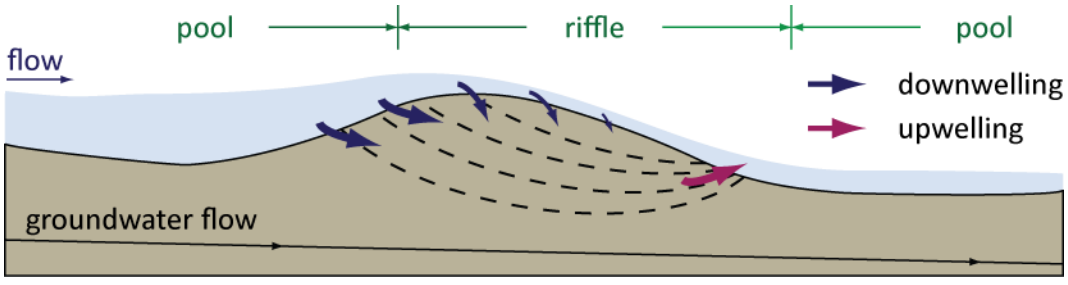

Figure 1.6 Idealized hyporheic exchange through a pool-riffle sequence. At the tail of the pool, decreasing stream depth increases pressure at the stream-bed interface, forcing stream water to downwell into the riffle, displacing porewater. Increasing stream depth at the tail of the riffle decreases pressure at the stream-bed interface and pulls porewater into the surface stream. Groundwater flow (also called 'underflow' or 'Darcy flow') is controlled by channel slope.

In pool-riffle channels, the size and three-dimensional structure of bedforms interacts with stream flow to determine the profile of the water surface. This affects the flow regime including the wetted perimeter, stream depth and near-bed hydrostatic pressure (Tonina and Buffington 2007). During low flows (or around large bedforms), the topography of the water surface varies laterally and longitudinally, increasing the spatial heterogeneity of stream-bed pressure differentials, and in turn, increasing the magnitude of hyporheic exchange. Conversely, as stream discharge increases, hyporheic exchange across riffles decreases because the effect of bed topography declines, decreasing the spatial variability in water surface topography and near-bed pressure differentials. This reduces the gradient between hydraulic heads at the head and tail of the riffle. In the Speed River, riffle-scale hyporheic exchange halved during high stream flow (Storey *et al.* 2003). This inverse relationship between stream flow and hyporheic exchange in pool-riffle channels is likely significant for many riverine ecosystems in which low flows occur for most of the year. In these systems, riffle hyporheic zones comprise a disproportionately large component of reach-scale vertical connectivity (Tonina and Buffington 2007, Wood *et al.* 2010).

Longitudinal hydraulic head gradients such as those caused by riffles and steps (transverse ribs across all or part of the channel, Comiti *et al.* 2009a) also induce lateral hyporheic flow (Harvey and Bencala 1993, Hill *et al.* 1998). Lateral exchange occurs through horizontal morphologic features such as gravel bars (Vervier *et al.* 1993), parafluvial zones (Holmes *et al.* 1996) and meander bends (Wroblicky *et al.* 1998). Interactions between vertical and horizontal morphologic features create complex flowpaths that typically increase reach-scale hyporheic exchange (Kasahara and Wondzell 2003, Wondzell *et al.* 2009).

Lateral hyporheic exchange

In higher-order streams where meanders are the prevailing river pattern, lateral exchange dominates hyporheic flux (Figure 1.1, Lautz *et al.* 2006). The longitudinal channel slope and the inclination of the water surface at bends create pressure gradients at the river banks (Revelli *et al.* 2008). In meandering rivers, these pressure

gradients develop along the relatively short distances between opposite banks of the same bend (Figure 1.7a); this 'sinuosity-driven' exchange controls the intrameander hyporheic zone (Boano *et al.* 2006, Peterson and Sickbert 2006). In Prairie Creek, a sand-and-gravel stream in Nebraska (U.S.A.), sinusoidal pressure gradients increased total hyporheic flux by a factor of two to more than an order of magnitude and decreased mean residence time (Cardenas *et al.* 2004). In the third-order Little Kickapoo Creek (Illinois, U.S.A.), 100 % of interstitial water under a meander lobe (predominantly gravel with coarse sand), was stream water with a residence time of 80-90 days (Peterson and Sickbert 2006). The hydraulic gradient of the stream around the meander was 0.003, while the hydraulic gradient across the meander neck (the narrowest part of the meander) was 0.006, creating a hydraulic potential for intrameander hyporheic flux. The longer residence times in intrameander hyporheic zones (compared with riffle hyporheic zones) provide more opportunity for interstitial water to chemically evolve and promote different biological communities (Peterson and Sickbert 2006, Van der Hoven *et al.* 2008, Boano *et al.* 2010). Hyporheic exchange similarly occurs through lateral gravel bars inset in the river channel, albeit at finer spatiotemporal scales.

Like vertical exchange, lateral hyporheic exchange is also temporally dynamic, but over longer timescales. Continuous erosion of outer banks and deposition on inner banks causes elongation and migration of meanders, increasing channel sinuosity until it is reset by a meander cutoff (Figure 1.7b). Because of the long timescales involved in meander evolution, the dynamics of intrameander hyporheic exchange are predominantly studied through mathematical modelling. As meanders elongate and migrate, the neck narrows, increasing the hydraulic gradient between the inwelling and outwelling zones (Boano *et al.* 2006). Thus, lateral hyporheic flux increases and residence time decreases across the neck of the meander as it evolves (Boano *et al.* 2006). Early flume experiments revealed that channel sinuosity, although determined by many confounding factors including sediment supply and transport, vegetation patterns and bank stability, is strongly dependent on the regional valley slope (Schumm and Khan 1971, but see Hooke 2007). Lateral hyporheic discharge through a

meander lobe becomes more sensitive to the valley slope as sinuosity and intrameander hydraulic gradients increase (Cardenas 2009a).

Although the locations of hyporheic zones differ in gaining or losing conditions, the geometry and magnitude of decreases in area, flux and residence time are similar. This also is the case for bedform-driven hyporheic zones. Likewise, small net losses or gains in streamflow reduce the area and discharge of both lateral and vertical hyporheic zones. As streamflow initially increases or decreases, hyporheic area and flux rapidly decrease; the decrease becomes more gradual and asymptotic as streamflow continues to increase or decrease (Cardenas 2009b). In bedform-driven hyporheic zones, the location of the zone becomes focused in the area where pressure gradients are largest (either the trough or crest of the bedform) which is where flux is greatest. The coupling of rapidly-reducing hyporheic area and minimally-reducing hyporheic flux significantly reduces hyporheic residence time (Cardenas and Wilson 2007d).

However, sinuosity-driven hyporheic zones are more sensitive to the magnitude of streamflow increase/decrease than bedform-driven hyporheic zones. An increase or decrease in streamflow constrains sinuosity-driven hyporheic zones to the meander apices close to the river channel (i.e. reduces the lateral extension away from the river). This is either by stream-floodplain pressures declining with decreasing river stage or by floodplain-stream pressures increasing as groundwater is recharged at high stream discharge. Unlike vertical hyporheic zones, as the areas of lateral hyporheic zones decrease, the locations of greatest hyporheic flux (meander necks) are excluded (Figure 1.7c, Cardenas 2009b). As with bedform-driven hyporheic zones, area decreases faster than flux, reducing hyporheic residence times. The process is more gradual in sinuosity-driven hyporheic zones (Cardenas 2009b), but reductions in lateral hyporheic exchange can be significant (Morrice *et al.* 1997). High stream discharge halved the area of lateral hyporheic zones in two first-order streams (Wroblicky *et al.* 1998), and similarly reduced lateral hyporheic exchange by a third in a third-order stream in the Rocky Mountains, U.S.A. (Harvey *et al.* 1996).

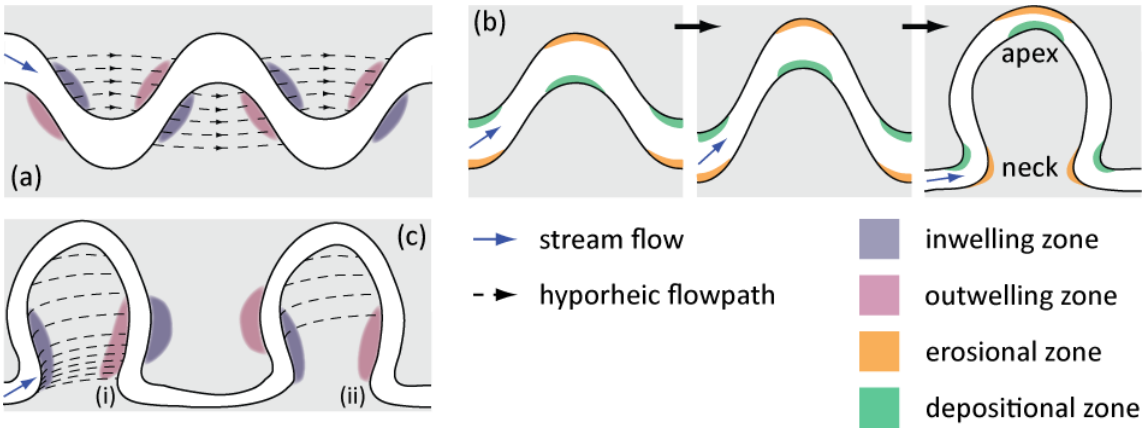

Figure 1.7 Lateral hyporheic exchange through meander bends. **(a)** Stream water inwells at the upstream side and outwells at the downstream side of the meander bend. **(b)** Meanders elongate and migrate downstream due to continuous erosion of the outer bank and deposition on the inner bank. As meanders evolve, the neck narrows, leading to increased hydraulic gradients – and hyporheic flux – through the neck. **(c)** Increase and decrease of streamflow reduces intrameander hyporheic exchange by constraining flux to the apex of meander bends and removing the zone of greatest hydraulic gradients and flux [compare (i) with (ii)].

1.3.3 Segment-scale processes

Few studies explicitly address catchment-scale controls on vertical connectivity, so the interactions of these are poorly understood (Boano *et al.* 2009). Catchment geology controls broad-scale valley and channel patterns such as valley, floodplain and channel width, alluvial thickness and geometry, the location of groundwater recharge and discharge zones, and channel curvature (D'Angelo *et al.* 1993, Wohl *et al.* 1993, Arntzen *et al.* 2006). Valley constriction affects long hyporheic flowpaths (i.e. at the scale of river segments). At the upstream end of unconstrained segments, river water infiltrates alluvial deposits in large downwelling zones. Large upwelling zones similarly occur at the downstream ends of alluvial deposits or immediately upstream of geomorphic nick points (Stanford and Ward 1993, Urbano *et al.* 2006). As rivers migrate laterally within unconstrained segments, they rework alluvial sediments into an array of channels and paleochannels, creating complex networks of high-porosity, preferential flowpaths (Stanford and Ward 1993, Takahashi *et al.* 2008). Thus, the transition from constrained to unconstrained valley segments (and *vice versa*) is a

fundamental control of vertical and lateral exchange at the scale of alluvial deposits (Dole-Olivier 2011).

Riverbed stratigraphy varies strongly at the catchment-scale as a function of stream slope and order (Coulombe-Pontbriand and Lapointe 2004). At the segment-scale, bed sediments vary in response to local changes in stream competence and local sediment inputs (e.g. from tributaries), both of which are influenced by variability in valley confinement (Rice and Church 1998, Malcolm *et al.* 2005). In the Scottish Girnock Burn, major valley constrictions reduced the channel slope immediately upstream, effectively reducing stream competence and creating large hyporheic zones as gravels accumulated in the river channel (Malcolm *et al.* 2005).

Groundwater discharge maintains baseflows in many rivers (Boulton and Hancock 2006) and occurs either diffusely or at discrete locations (Brunke and Gonser 1997). Aquifer characteristics (geology, geometry, permeability, slope, topographic variability in the water table level) influence the location, size and flux of reach-scale hyporheic exchange (Harvey and Bencala 1993, Wroblicky *et al.* 1998). The valley constrictions in Girnock Burn also forced groundwater to discharge through the river bed and banks, leading to poor water quality through these hyporheic zones, with resultant negative impacts on biota (Malcolm *et al.* 2005). Few studies have addressed the role of large-scale stream-aquifer interactions on hyporheic exchange and it remains poorly understood (Cardenas and Wilson 2006, Boano *et al.* 2008).

In summary, vertical connectivity occurs in rivers as nested flow cells (Tóth 1963), or patches, in response to interacting hydrologic and geomorphic processes that create pressure differences at multiple spatiotemporal scales. Vertical connectivity may be low at one scale while simultaneously high at another. Geomorphic features such as valley constrictions, meanders, riffles and log sills induce hyporheic flux through multiple simultaneous mechanisms, but the processes dominating the direction, magnitude and area of hyporheic exchange vary both in space and time, and fine-scale features (e.g. local differences in hydraulic conductivity) can exert significant controls. The ecological roles of flowpaths differ with their length: flowpaths with short

residence times are vital for keeping surface sediments oxygenated and for biotic nutrient assimilation; longer (intermediate) flowpaths control hyporheic oxygen dynamics, redox gradients, remineralization of organic matter and nutrient regeneration; and long flowpaths are critical for maintaining baseflows and buffering stream temperatures (Malard *et al.* 2002, Poole *et al.* 2008). However, very little is known of the additive effects (i.e. at the segment or catchment-scale) of successive hyporheic zones with their different sizes, spatial configuration and connectivity (Malard *et al.* 2002). Nonetheless, interactions between geomorphology and hydrology are suggested to peak at the same spatial scale in which geomorphic diversity peaks (Poole *et al.* 2006). In many lower-order gravel-bed rivers, riffles contribute a disproportionately large component of reach-scale hyporheic flux, while in higher-order reaches, intrameander flowpaths may dominate hyporheic flux; the combination of vertical and lateral bedforms typically increases hyporheic exchange.

Human activities have reduced vertical connectivity, impairing river function (Kondolf *et al.* 2006). These disturbances are often synergistic. To illustrate, at a catchment scale, widespread clearing of vegetation combined with clearing in the riparian zone has often accelerated stream-bank erosion, causing the channel to expand and incise (Simon and Darby 1999). This may lower the groundwater table, dewatering riparian and parafluvial zones (Hancock 2002). The increased erodibility of hillslopes in the catchment and reduced capacity of the riparian zone to buffer the stream contribute to increased suspended loads, so that fine-grained sediment clogs the interstitial pores of the river bed (Mulholland 1992), further reducing hydrological exchange between surface water and groundwater. Because the channel has expanded, connectivity with the floodplain is less frequent. The net result is that although the contribution of the hyporheic zone to stream functions such as organic matter remineralization may be proportionally much greater given the decoupled floodplain, the capacity of the hyporheic zone to perform these functions may also be significantly reduced (Mika *et al.* 2010, Appendix A).

Restoration strategies need a clear conceptual foundation based on sound ecological theory (Hobbs and Norton 1996, Ryder *et al.* 2008a). In current conceptual models of

stream ecosystems, the hyporheic zone is significant because it mediates vertical connectivity (among other crucial functions). Thus, conceptual models of hyporheic function view the hyporheic zone from the perspective of its activity and connection with the surface stream (Boulton *et al.* 1998). This is a useful perspective for underpinning hyporheic restoration strategies as most of them are driven by concerns for surface water processes and habitats.

1.4 Restoring vertical connectivity: theory and practice

Ecological restoration is defined as 'the process of assisting the recovery of an ecosystem that has been degraded, damaged or destroyed' (www.ser.org). The theoretical basis of and practical guidelines for ecological restoration have been the subject of extensive debate in the literature. Six criteria are recognized as fundamental to ecologically successful restoration: (1) a guiding image is identified *a priori* that defines the dynamic, ecologically healthy riverine ecosystem that could exist at a given reach or catchment in order to prioritize restoration activities to accomplish measurable goals that represent restoration success, (2) the mechanisms by which the intended restoration works will achieve the guiding image are defined, preferably as testable hypotheses, (3) restoration activities measurably improve ecological condition towards reference conditions or along trajectories as specified by the guiding image, (4) restoration activities increase ecosystem resilience so the system becomes more self-sustaining with a greater capacity to recover from disturbance, (5) the restoration strategies do not inflict irreparable (or unwarranted) harm such as by transferring impacts downstream, or disrupting connectivity at critical moments in breeding, spawning or migrating cycles, and (6) rigorous pre- and post-project assessments are conducted and disseminated to improve transparency, accountability and knowledge transfer (Hughes *et al.* 2005, Jansson *et al.* 2005, Palmer *et al.* 2005, Nilsson *et al.* 2007, Woolsey *et al.* 2007).

For many riverine projects, restoration goals are obvious: reduce erosion and compaction, reinstate natural flow regimes, remove or reduce exotic species, and/or

reinstate native species. However, the prioritization and achievement of these goals are complex and difficult in the face of natural variability and increasing human pressure on ecosystem components (Wohl 2005, Dufour and Piégay 2009). Furthermore, a realistic guiding image must construct biophysical restoration priorities within a framework of social and economic opportunities and constraints (Ryder *et al.* 2008a). These social and economic constraints are themselves dynamic and complex. Social disconnection with rivers often occurs during their biophysical deterioration, through the dominance of noncompatible consumptive uses, cultural change, institutional mistrust and a lack of physical or legal access (Hillman *et al.* 2008). Often, socioeconomic opportunities and constraints vary at the subcatchment scale, impeding the development of a catchment-scale vision for river restoration (Hillman and Brierley 2005).

Nevertheless, the first step in a riverine restoration project often involves the collaborative development by stakeholders of the guiding image or vision of the restored ecosystem. According to the fundamental principles of restoration, the guiding image should encompass a mechanistic understanding that specifies how the riverine ecosystem works, how it has been impaired and how on-ground strategies will move it along a restoration trajectory (Jansson *et al.* 2005). This relies on an interdisciplinary understanding of the biophysical form-function interactions (Fisher *et al.* 2007), linking geomorphology, hydrology and ecology, as well as social science and policy research. However, for projects seeking to restore vertical connectivity, it is likely that stakeholder education will precede and coincide with vision generation (exceptions may be the restoration of salmon-spawning streams or communities dependent upon groundwater extraction where awareness of the ecological and socioeconomic significance of vertical connectivity is already heightened).

By its very nature, vertical connectivity is an interdisciplinary concept (Krause *et al.* 2011b). Several disciplines have focused on different biophysical processes and, critically, different temporal and spatial scales of the same processes. Thus, our knowledge of the processes that drive vertical connectivity in rivers comprises the different perspectives of regionally-focused groundwater research (e.g. Fan *et al.*

2007), solute tracer studies that identify reach-scale surface-subsurface exchange and nutrient cycling (e.g. Wörman *et al.* 2002), ecological studies of hyporheic and benthic biota, organic matter dynamics, biogeochemistry and impacts of human land use (e.g. Boulton and Foster 1998, Olsen and Townsend 2003, Wright-Stow *et al.* 2006), through to laboratory flume studies that empirically test the mechanics of water movement through sediment (e.g. Packman and Salehin 2003). While the need to maintain and restore vertical connectivity between rivers and their alluvial aquifers has been clearly defined in the literature (Kondolf *et al.* 2006, Kasahara *et al.* 2009), significant knowledge gaps impede progress in this area (Boulton 2007). Firstly, while we know that geomorphology and hydrology control the vertical connectivity of surface water and groundwater, the mechanics of how these processes interact across multiple temporal and spatial scales to drive hydrological exchange are less clear (but see Section 1.3, Brunke and Gonser 1997, Boulton *et al.* 1998). Secondly, we understand little of how the explicit configuration of this mosaic across multiple spatial and temporal scales affects nutrient cycling, the breakdown and remineralization of organic matter and the composition of hyporheic biota (Malard *et al.* 2002). Both of these are major impediments to designing strategies to maintain and restore vertical connectivity.

Is it possible for hyporheic restoration projects to meet the criteria for ecologically-successful restoration given current knowledge gaps in hyporheic science? Currently, a number of techniques are specifically used to enhance hyporheic habitats and processes. These fall into three categories: (1) localized interventions that attempt to enhance structural attributes of vertical connectivity without addressing the disturbances that led to the impairment or the biophysical processes required to maintain these improvements, (2) reach-scale attempts to reinstate the biophysical processes the drive vertical connectivity, and (3) segment- or catchment-scale interventions that aim to reverse (at least partially) the disturbances to the biophysical processes that control vertical connectivity (Pasternack *et al.* 2004, Hancock and Boulton 2005, Kasahara and Hill 2006a, 2007a).

The first category includes gravel augmentation (i.e. creating artificial riffles) and gravel desilting (manually, or by using water jets). Typically, gravel augmentation is used to provide spawning habitat for salmonids where clogging by fine sediment has rendered the streambed unusable: success is limited in space (to the deposited gravel at best) and time (until the new gravel becomes clogged by fine sediment, Zeh and Dönni 1994, Sarriquet *et al.* 2007). Vertical connectivity may have improved in that streamwater is freely exchanging with the deposited gravel, but the original sediments remain clogged and hyporheic exchange is limited to very short, surface flowpaths (Sarriquet *et al.* 2007). These restoration activities may be appropriate as short-term measures to maintain the viability of salmonid populations while longer-term projects aimed at restoring the biophysical processes responsible for vertical connectivity are implemented, but they are not ecologically sound as stand-alone restoration projects.

The second category comprises interventions attempting to improve reach-scale biophysical processes that drive vertical connectivity such as using large wood to increase geomorphic complexity (Brown *et al.* 2004, Boulton 2007, Kasahara *et al.* 2009, Sawyer *et al.* 2011, 2012), or reconnecting meanders (Kondolf 2006, Kasahara and Hill 2007b). The third category comprises segment- or catchment-scale interventions that include dam removal, soil conservation measures and environmental flows that flush fine sediments from gravel beds (Hancock and Boulton 2005, Constantz and Essaid 2007).

While some of these strategies target the actual disturbance to hyporheic exchange (e.g. dam removal), most target the *effects* of disturbances to the processes driving hyporheic exchange (e.g. flushing interstitial silt), rather than reducing the actual causes (e.g. accelerated erosion in the catchment). Further, most of these techniques aim to increase hyporheic exchange at the reach scale. This is likely due to pragmatic constraints on what is achievable, both in the logistics of completing on-ground restoration works and in quantifying the success or otherwise of these works. However, more integrated responses that directly target disturbances to vertical exchange within a catchment context are crippled by our current limited understanding of the multiscalar biophysical interactions that drive hyporheic

exchange, and of the roles of the explicit spatiotemporal configurations of vertical connectivity in riverine processes.

Of the six criteria for ecologically-successful restoration, the first two specifically assist in restoring the biophysical processes that create and sustain vertical connectivity. Firstly, defining a guiding image of the dynamic, ecologically healthy river in the context of the catchment's history and physiography means identifying – as best as possible – the 'natural' multiscale configuration of surface water–groundwater exchange, the ecological implications of this, the disturbances that have impaired this with their spatiotemporal extents and synergisms, and possible restoration targets given irreversible thresholds crossed and current socioeconomic constraints (Kondolf 2000b, Wohl *et al.* 2005). Secondly, defining the mechanisms by which proposed restoration works will achieve ecologically sound restoration will perhaps prevent restoration efforts that clearly misunderstand the biophysical disturbances that impair vertical connectivity (such as placing a layer of coarse gravel over colmated river beds without addressing fine sediment inputs or the lack of flushing flows). A theoretical foundation for restoring vertical connectivity in rivers should integrate the mechanics of hyporheic exchange with its subsequent influence on the ecological functions of the surface stream. Although none of the several conceptual models of hyporheic ecology specifically incorporates ecological restoration theory, they do view the hyporheic zone from the perspective of its connectivity with the surface stream and biogeochemical activity (Boulton *et al.* 1998), and this is a useful perspective for underpinning hyporheic restoration strategies. It also suggests that these models can be adapted to guide restoration, by incorporating components of other conceptual models that incorporate restoration concepts, but not hyporheic ecology. I develop this approach below.

1.4.1 Ecological models of hyporheic structure and function

The study of patterns and processes in ecology are conceptualized within five general theoretical frameworks: gradient analysis, ecotones, hierarchy, connectivity and disturbance (Ward *et al.* 2002). Gradient analysis focuses on how patterns and

processes change along environmental continuums. Given that rivers are characterised by unidirectional flow, early ecological models of river function predominantly addressed longitudinal patterns and processes (Illies and Botosaneanu 1963, Vannote *et al.* 1980). Initially, paradigms of stream function focused on the physical template and used the theory of energy equilibrium to explain erosion, sediment transfer and deposition in structuring longitudinal geomorphic patterns (Leopold and Langbein 1962). Although most of this early work focused on instream processes (Leopold *et al.* 1964), lateral links between the stream and its catchment (Hynes 1975) or its groundwater (Hynes 1983), and vertical links between stream and groundwater hydrology (Freeze and Cherry 1979) were recognized to influence stream structure and function.

The River Continuum Concept (RCC, Vannote *et al.* 1980) is credited as the initial creative synthesis that linked ecological processes in rivers to the geomorphic template. The model related photosynthesis and respiration (expressed as a ratio to indicate their relative importance) to longitudinal location along the river continuum (Fisher 1997). These different sources of energy were hypothesized to have repercussions for expected proportions of functional feeding groups (e.g., shredders, collectors, grazers), thus linking longitudinal hydrologic connectivity to ecosystem processes and macroinvertebrate community composition. The RCC is now accepted as oversimplistic (Boulton and Brock 1999), in part because it did not adequately recognize the functional significance of lateral (e.g., floodplain) or vertical (e.g., hyporheic zone) connectivity in alluvial river ecosystems, despite the early acknowledgement of their existence and influence on riverine function (Mika *et al.* 2008, Appendix B).

The Hyporheic Corridor Concept (HCC, Stanford and Ward 1993) conceptualized catchment-scale hyporheic exchange from headwaters to estuary by extending the unidirectional perspective (upstream-downstream) of the RCC to include interactive pathways in lateral and vertical dimensions along the river continuum. The HCC defined an alternating sequence of constrained reaches and bounded alluvial floodplain reaches, likened to ‘beads on a string’, where longitudinal flow was

maintained along the river continuum but with the strength of lateral and vertical flow varying among reaches (Stanford and Ward 1993, Ward *et al.* 2002). Studies from the Selwyn River (South Island of New Zealand, Datry *et al.* 2007, Larned *et al.* 2008) and the Tagliamento River (Italy, Ward *et al.* 1999a) suggest that the HCC can be extended to incorporate the longer flowpaths of unbounded alluvial plains with unconfined aquifers and losing reaches analogous to the constrained-unconstrained downwelling transitions, and confined aquifers and gaining reaches analogous to the unconstrained-constrained upwelling transitions of the original HCC (Datry *et al.* 2007). Although the HCC incorporates coarse-scale vertical and lateral linkages in models of riverine ecology, the model is specific to single-thread channels and thus, does not explain vertical connectivity in braided-, or multi-channel alluvial rivers. It also has limited potential as a theoretical basis for restoration works that involve finer spatial scales.

Ecotones are defined as semi-permeable boundaries between relatively homogeneous patches; transition zones where the rates of change in ecological patterns or processes are increased relative to the surroundings (Wiens 2002). Riverine ecotones exist over wide spatiotemporal ranges. For instance, an alluvial floodplain forms a large ecotone between hillslopes and the river channel, but the floodplain itself comprises numerous smaller ecotones between surface water and groundwater, lotic to lentic transitions, riparian zones and other floodplain communities, the surface stream and groundwater, and between oxic and anoxic sediments (Ward *et al.* 2002). The ecotonal framework is central to most theories of hyporheic ecology and processes given that the hyporheic zone is itself an ecotone between surface water and groundwater (Williams *et al.* 2010).

The functional significance of any specific hyporheic ecotone is determined by its elasticity, permeability, connectivity and biodiversity (Dynamic Ecotone Model *sensu* Gibert *et al.* 1990; see review in Boulton *et al*. 2010). Elasticity refers to the extent of fluctuation in the size of the hyporheic zone in response to varying stream or groundwater discharge given the hydraulic conductivity of sediments. Permeability refers to the ease of transfer of water, solutes, particulates and organisms across the ecotone. Connectivity here refers to hydrological connectivity, the water-mediated flux

of material, energy and organisms across ecotones, between habitats and throughout the river network (Pringle 2001, Pringle 2003a, 2003b). Biodiversity encompasses structural diversity, defined as the types and spatial array of landscape units and habitat patches; functional diversity involving processes such as energy flow, nutrient cycling, disturbance and biotic interactions; and species diversity, the types and numbers of species within communities (Ward and Tockner 2001). Vervier and others (1992) demonstrated the utility of the Dynamic Ecotone Model in conceptualizing the functional significance of hyporheic zones to the surface stream by demonstrating that the permeability and connectivity of an exchange patch directly control whether the hyporheic zone acts as a nutrient 'source' (supplies nutrients to the surface stream) or 'sink' (removes nutrients from the surface stream, perhaps temporarily).

The Dynamic Ecotone Model specifically addresses boundaries – or ecotones – between patches, although concepts and measures of functional diversity also deal with biogeochemical processes within patches. It is also relevant to examine patterns and processes *within* patches. This is because patchiness is a central theme of hyporheic ecology, and patchiness and dynamic heterogeneity have been shown to enhance biogeochemical processes and biodiversity in hyporheic zones (Section 1.3; Boulton *et al.* 1998, Grimm *et al.* 2005, Käser *et al.* 2009). The patch dynamics framework comprises several fundamental principles (Townsend 1989, 1996), some of which apply to the Dynamic Ecotone Model (permeability, connectivity and biodiversity), and some are additional characteristics such as patch quality, context and spatiotemporal scale (Wiens 2002).

Habitat quality differs among patches and over time within patches. Wiens (2002) argues that this recognition is a critical step in moving from simply describing the patch mosaic to representing the spatial component of ecological processes. The critical role of hyporheic patch quality has been extensively demonstrated for lithophilic brood-hiding fish such as trout, salmon and charr, where fish do not spawn successfully in riffle sediments that are hypoxic or contain a high proportion of fine-grained sediments (Coulombe-Pontbriand and Lapointe 2004, Groves and Chandler 2005, Heywood and Walling 2007). Other studies have identified temperature (Bärlocher *et*

al. 2008), the location and quality of decaying organic matter (Boulton and Foster 1998), and the location and hydrodynamics of riffles with their high-velocity, well-oxygenated stream flow (Arnon *et al.* 2010) as determinants of patch quality for specific organisms. The quality of patches also changes over time. This may be abruptly as floods erode and deposit gravels, fine-grained sediments and organic matter, redefining the physical characteristics of existing flowpaths or reorganizing the riverscape to create new flowpaths (Poole *et al.* 2006). Conversely, changes may be gradual as interstitial stores of organic matter are depleted through remineralization, as fine-grained sediments percolate into and colmate the sediment matrix, or as surface flow declines and ceases during continued dry periods.

Patterns and processes within and between patches are affected by the spatial and temporal context of the patch (Pringle *et al.* 1988, Malard *et al.* 2002). Firstly, although ecotones have their own properties, they are largely determined by what is on either side of the boundary (Wiens 2002). For example, groundwater passes through the riparian zone as it moves from hillslope to the river channel and the hydrochemistry of the groundwater is influenced by lithology and topography (Harvey *et al.* 2008), microbial processes, and vegetation characteristics including diversity, productivity, evapotranspiration and rooting systems (Tabacchi *et al.* 1998, Ibrahim *et al.* 2010). Therefore, changes to the composition or extent of the riparian zone may profoundly alter stream hydrology and hydrochemistry (Wiens 2002). The spatial configuration of the patch mosaic also influences ecological processes such as inputs of organic material and nutrient dynamics, due to the successive effects of internal patch properties (e.g. whether the patch is a nutrient source or sink), and inter-patch boundaries (e.g. fluxes through the river network; Fisher *et al.* 1998b, Doering *et al.* 2011). The spatiotemporal context of patches may involve considerable time lags. In a study of North Carolinian streams (U.S.A.), the contemporary biodiversity of fish and aquatic macroinvertebrates was best described by catchment land use 40 years prior, rather than by current land use patterns (Harding *et al.* 1998). In the Hunter River (Australia), widespread channel incision and widening lagged 70 years after major land use changes associated with European settlement and agriculture (Spink *et al.* 2009),

as a result of interacting geologic, climatic and anthropogenic 'imprinting' upon the landscape ('landscape memory', Brierley 2010).

Patches and their characteristics of elasticity, permeability, connectivity, biodiversity, quality and context are scale-dependent. Consequently, relationships that are apparent at one scale may not be apparent or be replaced by different relationships at other scales (Wiens 2002). To illustrate, nutrient fluxes are often highly variable from small tributary basins in response to subtle changes in land use, climate and runoff, but exhibit low variability from the entire river basin (Strayer *et al.* 2003, Burt and Pinay 2005). Conversely, in a study of an agricultural catchment in Midwestern U.S.A., fish biodiversity only weakly correlated with local-scale effects of riparian vegetation, but strongly correlated with catchment-scale land use and vegetation (Roth *et al.* 1996). Typically, scale is considered either continuously (e.g. millimetres to kilometres or seconds to decades) or hierarchically (e.g. individual sediment clasts, clusters of similarly sized clasts, to hydraulic habitats incorporating specific sediment characteristics such as riffles or pools). Hence, while ecological theories of patch and ecotone dynamics are valuable for understanding patterns and processes at fine-scales, hierarchy theory is often used to conceptualize coarser scales of riverine structure and function.

Hierarchy theory conceptually deals with the complexity of ecological systems by grouping factors of interest into progressively smaller (i.e. nested) levels based on the rates of processes within these levels and their relationships with adjacent levels (Nested Hierarchical Model *sensu* Allen and Starr 1982). These nested hierarchies are defined according to the variables and hypotheses of interest, but the theory (i.e. the Nested Hierarchical Model) provides testable *a priori* predictions about relationships among levels characterized by correlations among all levels, with adjacent levels exhibiting stronger relationships than levels further apart (Smiley and Dibble 2005). The key aspect of this conceptual model is recognizing that processes structuring one hierarchical level may or may not operate at another level; that is, patterns are scale- and variable-dependent (Arscott *et al.* 2000, Ward *et al.* 2002). The Catchment Hierarchy Concept (CHC, Frissell *et al.* 1986) classifies hierarchical units from

microhabitats to catchments based on their spatial extent and temporal persistence. However, like the RCC, the CHC was based on small, intact headwater streams and does not include interactions between the stream and its floodplains or alluvial aquifers. It is not surprising that several conceptual models of hyporheic ecology incorporate principles of hierarchy theory given the early recognition of the hierarchical nature of hyporheic and groundwater flowpaths (Tóth 1963).

Findlay (1995) classified alluvial rivers into three broad classes comprising large, moderate and small ecosystem-level consequences of hyporheic exchange processes. This approach integrated the functional significance of the hyporheic zone to surface waters with the processes driving hyporheic exchange, (i.e., direction of exchange, volume of water exchanged and residence time of water within the ecotone, Figure 1.8). The purpose of Findlay's classification framework was to uncover generalities across catchments and simplify intersystem comparisons. This framework was extended by Boulton and others (1998), who showed how it might be quantified for a range of rivers (Figure 1.9). The latter conceptual model focuses on integrating reach-scale processes such as area and discharge of a given hyporheic zone, with sedimentary processes at the particle (e.g. grain size, packing, porosity, hydraulic conductivity) and reach scales (e.g. channel slope, pool-riffle sequences). As shown by their conceptual model, hyporheic contributions to riverine ecosystems are predicted to be greatest when a high proportion of total stream discharge travels at intermediate velocities through the hyporheic zone, ensuring sufficient supplies of oxygen, solutes and fine particulate organic matter (FPOM) from surface waters to the hyporheic zone. Where flowpath length and interstitial velocity result in residence times with optimal contact with interstitial microbes, biofilms and chemical microenvironments, remineralized nutrients are exported back to surface habitats. The predictions of both these conceptual models emphasize the role of hydrology in structuring hyporheic exchange and efficiency.

This framework of hierarchical hyporheic exchange patches was applied in a losing reach of Sycamore Creek, a sand- and gravel-bed desert stream in Arizona (U.S.A.) to determine nutrient retention and transport (Dent *et al.* 2001). Patch configuration and

composition influenced both the form (species) and concentrations of nutrients retained or exported, with upwelling zones generally sites of increased bioavailable nitrogen and phosphorous in the surface stream (i.e. sources). While hyporheic nutrient sources demonstrated strong seasonality, they also varied hierarchically in space. For example, as a channel unit a sand bar acted as a nutrient source, but algal-rich patches within the sand bar acted as nutrient sinks, reducing the overall magnitude of nutrient export (Dent *et al.* 2001).

The Hierarchical Patch Dynamics perspective (HPD, Wu and Loucks 1995, Poole 2002) combined aspects of both the Catchment Hierarchy Concept (Frissell *et al.* 1986) for surface waters, with hyporheic patch dynamics as propounded by Findlay (1995), Boulton and co-workers (1998), and Dent and co-workers (2001). The key premise of the HPD is the recognition that processes span spatial scales, forming *trans-scale* linkages that create, modify or remove structural or functional elements within the hierarchical patch mosaic (Pickett *et al.* 1989). 'Bottom-up' trans-scale processes are where fine-scale patch structure, function or context influence patch characteristics at coarser-scales. 'Top-down' trans-scale processes are where the structural and functional characteristics (including context) of a large patch influence patch characteristics at finer scales (Poole 2002). Experimental manipulations in streams have demonstrated that bottom-up and top-down controls co-occur either dependently or independently of each other, and that their interactions may be nonlinear and driven by abiotic and/or biotic thresholds (Forrester *et al.* 1999, Kiffney 2008). However, unlike Findlay's purpose of identifying similarities and facilitating comparisons among different systems, the HPD emphasizes the heterogeneity and thus, uniqueness of stream networks (Winemiller *et al.* 2010).

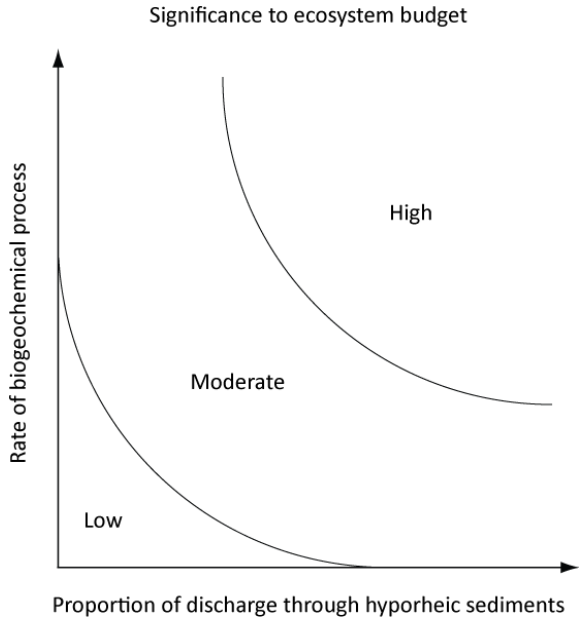

Figure 1.8 The contribution of hyporheic export to whole river nutrient budgets is hypothesized to be a function of the discharge through the hyporheic zone and the efficiency of hyporheic processing (reproduced from Findlay 1995).

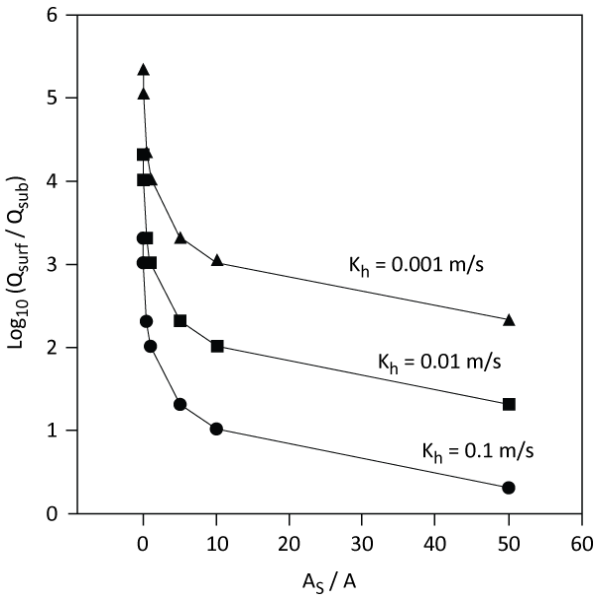

Figure 1.9 The hyporheic zone is hypothesized to influence stream function most when a relatively high proportion of total discharge travels at intermediate velocities through a relatively large hyporheic zone (reproduced from Boulton *et al.* 1998). Log_{10}-transformed ratio of surface (Q_{surf}) and subsurface (Q_{sub}) discharge where K_h is hydraulic conductivity and A_s/A is the cross-sectional area of the subsurface storage zone relative to the open channel.

The Riverine Ecosystem Synthesis (RES, Thorp *et al.* 2006) integrates concepts from patch dynamics and nested hierarchy models (e.g. the HPD framework) to view river systems as dynamic mosaics of repeatable fine-scale 'Functional Process Zones' (FPZs) within a template of large-scale hydrogeomorphic patches controlled by catchment geomorphology, climate, vegetation and flow regime. While the hydrogeomorphic patches are defined geomorphically, FPZs are defined ecologically through fundamental ecological processes such as productivity, metabolism, organic matter dynamics, nutrient dynamics and community composition (Thorp *et al.* 2006, Kobayashi *et al.* 2011). The RES emphasizes the dominance of non-equilibrial and stochastic processes in structuring FPZs, but suggests that the relative importance of deterministic and stochastic factors depends upon the structure of the large-scale hydrogeomorphic patches (i.e. is scale- and habitat-dependent). Although acknowledging the role of lateral connectivity in mediating functions such as nutrient spiralling among different FPZs, the RES does not incorporate vertical connectivity.

Connectivity theory encompasses (1) landscape connectivity referring to the degree of coupling between individual landforms such as hillslopes, floodplains and channels (Brierley *et al.* 2006); (2) sediment connectivity describing the ease of sediment moving through the catchment from production sites to downstream channel locations (Fryirs *et al.* 2007); (3) genetic connectivity reflecting the genetic variation within and among populations of organisms influenced by the position of the population within the hierarchical structure of the stream network, the geographic distance among populations, and species' life history and dispersal traits (Alexander *et al.* 2011, Wohl and Beckman in press); and (4) hydrological connectivity referring to the water-mediated flux of material, energy and organisms (especially the direction and magnitude of the flux) across ecotones, between habitats and throughout the river network (Amoros and Roux 1988, Pringle 2001, Pringle 2003b). Hydrological connectivity has long dominated models of riverine structure and function (Fisher *et al.* 2004), but the processes and linkages emphasized in these models is explicit to the specific river types for which they were developed (e.g. headwaters, alluvial rivers, floodplain rivers, Mika *et al.* 2008).

The Nutrient Spiralling Concept (NSC, Newbold *et al.* 1981) was one of the first ecological models to relate biogeochemical processing to connectivity; it is a two-component model incorporating rates of downstream transport with rates of instream uptake and remineralization. Spiralling length refers to the longitudinal (downstream) distance a particle travels before its removal from the stream's water column due to biotic assimilation, transformation or physical sorption (= uptake, Fisher *et al.* 2004). At some point after uptake, the particle is released back into the water column, and this process can be conceptualized as a spiral, oriented parallel to stream flow. While its advantages include mathematical hypotheses that quantify a variety of ecosystem processes in relation to longitudinal connectivity and directly compare across nutrients, times and streams (Minshall *et al.* 2000, Schade *et al.* 2011), it assumes streams are uniform, homogeneous, perennial and without tributaries, and does not consider the spatial heterogeneity or the configuration of subsystems or patches (Fisher *et al.* 1998a), even though the mechanisms of nutrient cycling vary as a function of hierarchical level and scale (Grimm 1994).

The Transient Storage Model (TSM, Bencala and Walters 1983, Bencala 1984) was initially a quasi-two-dimensional hydrological concept describing the temporary retention of solutes in near stationary radial zones such as floodplains, riparian zones and alluvial aquifers, and the eventual movement of these solutes into the stream channel (Stream Solute Workshop 1990). Although the TSM extends nutrient spiralling metrics (such as uptake length, uptake rate and spiralling length) to lateral and vertical linkages, TSM studies are logistically intensive and often limited to short durations and near-channel storage zones (Zaramella *et al.* 2003, Wörman and Wachniew 2007). Also, the TSM simplistically assumes a single residence time per storage zone (e.g. a hyporheic zone, Harvey *et al.* 1996). This last limitation is addressed by the General Residence Time Distribution model (General RTD, Gooseff *et al.* 2003) that specifically models the complexity of longer hyporheic flowpaths (Bencala 2005). The Hydrologic Flux Network model (HFN, Stanford and Ward 1993, Poole *et al.* 2004) more realistically encapsulates the complexity of longitudinal, lateral and vertical hydrological connections by envisioning these hydrologic vectors as having a lattice structure, thereby including longitudinal and lateral connectivity in the hyporheic zone,

and longitudinal and vertical connectivity in floodplains and riparian zones (Poole 2010). Although HFNs do not incorporate biogeochemical processes and products of connectivity, reach-scale studies are combining the modelling benefits of this approach with nutrient spiralling concepts (i.e. the Hydrological Spiralling Framework).

The Hydrological Spiralling Framework (HSF, Poole *et al.* 2008) conceptualizes hydrological connectivity as populations of individual, hierarchical, bidirectional flowpaths at multiple spatial scales and residence times that create a dynamic, patchy matrix of near-channel groundwater habitats with a wide variety of physical and biogeochemical microenvironments. Thus, even in predominantly influent or effluent reaches, the mosaic of bidirectional flowpaths means that gross hyporheic exchange is substantially greater than the net gain or loss of channel water within the reach. In an application of this framework to an unregulated reach of the anabranched, alluvial Umatilla River in northeastern Oregon (U.S.A.), discharge points for short and long flowpaths were immediately adjacent, and short flowpaths, although nested within longer flowpaths, were not always aligned with long flowpaths (Poole *et al.* 2008). While long flowpaths were driven by channel avulsions over time, medium flowpaths were driven by channel sinuosity and braiding, and short flowpaths were created by sudden steps in channel elevation from diverse bed topography such as riffles and steps (Kasahara and Wondzell 2003, Gooseff *et al.* 2006).

Applying this model to reach-scale exchange in the Umatilla River explicitly related the ecological significance of multiple, hierarchical flowpaths to the physicochemistry of stream water. For instance, short flowpaths buffered stream temperatures, while long flowpaths cooled summer and warmed winter temperatures. However, while the multitude of short flowpaths had a cumulative effect along the reach, there were fewer discharge points for longer flowpaths, so the effects of summer cooling and winter warming were constrained to localized patches (Poole *et al.* 2008). Extrapolating the pattern of hyporheic exchange to stream biogeochemistry, the model suggests that as biotic nutrient assimilation occurs most rapidly at the beginning of hyporheic flowpaths, multiple, short flowpaths distributed throughout the study reach maximize biotic uptake and turnover of nutrients. In contrast, the mineralization

of organic matter requires multiple electron receptors, each requiring specific redox conditions, and thus occurs in long flowpaths with their associated longer residence times (Findlay 1995).

Thus, the HSF explicitly acknowledges the ecological significance of the number, direction and spatial arrangement of hyporheic exchange patches, as well as the variation in flowpath lengths (Poole *et al.* 2008). However, a key premise of this model is that flowpaths are discrete. This is not always the case; scour-and-fill dynamics create complex patterns of sediment hydraulic conductivities leading to gradients in preferential flowpaths, or flowpaths of varying lengths and residence times may converge and diverge multiple times with multiple recharge and discharge points before reaching the terminal discharge point. The dynamic nature of riverine ecosystems means perturbations are a fundamental determinant of patterns and processes in communities, ecosystems and landscapes (Stanley *et al.* 2010), with scour-and-fill dynamics forming a primary mechanism of habitat disturbances in benthic and hyporheic communities (Poole *et al.* 2004, 2006, 2008).

Disturbance is defined as a damaging event in time and space that disrupts the structure of populations, communities and ecosystems, and changes the physical environment including the availability and quality of habitat and concomitant resources (Stanley *et al.* 2010). Thus, disturbance ecology is concerned with both the actual event and the ecological responses to the event (Lake 2000, 2005). Disturbances can be characterised by their duration and intensity: pulses are rapid and discrete events (e.g. floods), presses are disturbances that increase sharply and then are sustained at a constant level (e.g. dams), and ramps are where the intensity of the disturbance increases over time (e.g. droughts; Lake 2000, 2003). Early conceptual models of riverine function recognized the importance of disturbance in maintaining the ecological integrity of river systems. The Serial Discontinuity Concept (SDC, Ward and Stanford 1983) used the longitudinal gradients of the RCC as a baseline to conceptualize the upstream-downstream 'press' disruptions to abiotic and biotic patterns and processes caused by dams. However, the original SDC only considered constrained, single-thread channels, ignoring lateral and vertical linkages.

The Flood Pulse Concept (FPC, Junk *et al.* 1989) considers seasonal overbank inundation to be the key ecological determinant of river-floodplain structure and function. Thus, the ecological consequences of the 'pulse' disturbance of flooding are quantified in terms of the degree of connectivity and the exchange of matter and organisms across river-floodplain gradients (i.e. nutrient transport, storage and cycling). Later application to temperate river systems identified two different processes acting at different temporal scales that controlled connectivity within the river-floodplain landscape: erosive flooding and flow pulses (Tockner *et al.* 2000). Erosive floods create and maintain patches at a diversity of successional stages, contributing to habitat complexity and landscape permeability (Tockner *et al.* 2000). Flow pulses are in-channel spates (i.e. below bank-full discharge) that maintain connectivity among patches and enhance primary productivity (Tockner *et al.* 1999, Tockner *et al.* 2000).

Although the expanded FPC acknowledges below bank-full flows are important for autochthonous (instream) primary production, it emphasizes allochthonous (terrestrially derived) organic matter as the predominant energy basis of floodplain rivers. In contrast, the Riverine Productivity Model (RPM, Thorp and Delong 1994) emphasizes autochthonous production in riparian zones and instream shoreline habitats (littoral zones). However, conceptual models of disturbance in river systems have largely ignored the effects of catchment structure in controlling the frequency, magnitude and duration of disturbances as well as their ecological consequences. The Network Dynamics Hypothesis (NDH, Benda *et al.* 2004) argues that river network topology (the network structure and context including the location and frequency of tributary junctions) is a fundamental driver of general ecological structure and function, by directly structuring the location and extent of alluvial reaches (and thus, hyporheic zones), and partly through its influence on the frequency, spatiotemporal extent and intensity of disturbances (Jensco *et al.* 2009, Poole 2010).

The SDC was later expanded to include alluvial floodplain reaches and braided channels (Ward and Stanford 1995a, 1995b). The extended SDC incorporates concepts from the FPM and argues that connectivity is greatest in mid-catchment alluvial

floodplain reaches where a multitude of longitudinal and lateral flowpaths connect hillslopes, floodplains, riparian zones and the channel (Ward and Stanford 1995a). Dams in upland reaches decouple the linkage between the inputs of allochthonous organic matter from headwater reaches with detrital processes that would occur during downstream transport (Ward and Stanford 1995b), and desynchronize annual flow and temperature regimes. As sediments are caught within impoundments, sediment transport is truncated, degrading channels downstream of the dams and lowering the water table (Ward and Stanford 1995a), potentially dewatering riparian and parafluvial zones (Hancock 2002). Surprisingly, despite focusing on disturbances that obviously impair vertical connectivity, the extended SDC does not explicitly include vertical linkages.

The first ecological conceptual model to explicitly incorporate disturbance in vertical connectivity was the Telescoping Ecosystem Model (TEM, Fisher *et al.* 1998a), which considers the movement of materials through spatially heterogeneous subsystems (patches) and how these pathways are affected by disturbance. The TEM relates the reach-scale spatial configuration (defined as kind, size, shape, distribution, orientation, abundance and connectivity) to lateral and vertical hydrological connectivity among the surface stream and hyporheic, parafluvial and riparian zones (Figure 1.10), and can compare the functional significance of hyporheic zones among multiple river reaches over time (Boulton *et al.* 2010). The model defines flowpath length as the distance a parcel of water travels through an individual subsystem, processing length as the distance required for the uptake, transformation and release of an advected particle, and retention as input minus output for a given time period (Fisher *et al.* 1998a). The TEM explicitly includes concepts of disturbance ecology such as resistance (the capacity to withstand a disturbance) and resilience (the capacity to recover from disturbance, Lake 2000). Additionally, the TEM quantifies how these characteristics change initially in response to disturbance, and in successional time after or between disturbances. Limitations of the TEM include its linearity, treatment of subsystems as homogeneous (i.e. the model cannot consider the reach-scale effects of multiple hyporheic flowpaths), exclusion of the effects of network topology and terrestrial inputs to streams, and the inability to consider more than one nutrient (or species of

nutrient) at a time. Although not stated in the original model, the TEM has the ability to simultaneously quantify ecotonal characteristics (*sensu* the Dynamic Ecotone Model) such as elasticity, permeability, connectivity and biodiversity (i.e. functional diversity) for a number of subsystems at the reach scale (Figure 1.10).

Most conceptual models of riverine ecology consider hydrological dynamism but assume a static geomorphic template (e.g. FPM, TEM), or focus on the ecological and biological responses to the outcomes (however intermediate) of dynamic geomorphic processes such as channel braids, alluvial deposits or wood deposits. However, geomorphology should be viewed similarly to hydrology as a stochastic driver of riverine patterns and processes, albeit over different temporal scales (Lake 2000, Poole 2010). Using this approach, geomorphic adjustments are assumed to be continual, but rate-variable. Indeed, brief periods of high hydrologic and geomorphic activity are critical drivers of ecological function. Rare bed-moving floods (e.g. 1-in-100-year events) may penetrate deep into the alluvial aquifer supplying heat, oxygen, nutrients and organic carbon to hyporheic microbial and invertebrate communities (Poole *et al.* 2006) and driving microbial respiration and secondary production in the hyporheic zone for ensuing years or decades (Poole 2010). Where these hyporheic zones are nutrient sources to surface waters, the 'vertical flood pulse' may play a considerable role in maintaining stream communities over a sustained period.

Ecological models of hyporheic structure and function span the spatial and temporal scales from boundaries among temporary micro-patches, reach-scale solute transfer among flowpaths and rates of biogeochemical processing, to catchment-scale comparisons between alluvial and constrained segments. While these models incorporate the main ecological themes of gradient analysis, ecotones, hierarchy, connectivity and disturbance, few address both spatial and temporal contexts and none were specifically developed to guide restoration efforts. However, I believe that these models may be adapted to provide the theoretical foundation for hyporheic restoration programs, and demonstrate this next.

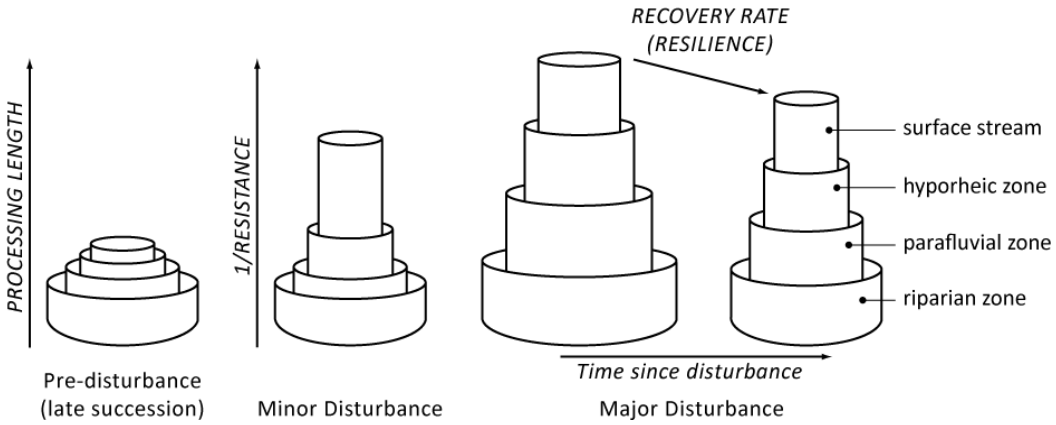

Figure 1.10 The Telescoping Ecosystem Model conceptualizes the effects of disturbance and recovery on biogeochemical processing in riverine subsystems at the reach scale (modified from Fisher et al. 1998a). The lengths of the telescoping cylinders represent processing length. Minor disturbances may affect only the least resistant subsystems while major disturbances affect biogeochemical processing in all subsystems. The horizontal extension of the cylinders measures the elasticity of the subsystems and the vertical retraction of the cylinders measures the resilience of subsystems.

1.4.2 The ecological basis of hyporheic restoration

Ideally, applicable conceptual models of hyporheic function should be useful as a tool to identify and prioritize habitats and processes to be targeted by restoration strategies (Kondolf *et al.* 2006). Such a tool should (1) illustrate the biophysical processes being manipulated by restoration strategies, thereby encouraging treatment of causes not symptoms of hyporheic degradation, (2) directly measure the effectiveness of both the changes to the process(es) under manipulation and their effects on stream function, (3) track the changes over time to identify strategies that create self-sustaining hyporheic zones and those that require continued intervention, (4) track multiple sites, rivers and restoration techniques over time, for example via the use of ratios that standardize across river size and background nutrient levels, and (5) communicate this information easily to river managers and other stakeholders.

Kasahara and co-workers (2009) present one of the earliest adaptations of an existing hyporheic model to guide and assess restoration success. They adapted Findlay's

(1995) hyporheic classification framework with its subsequent developments (Boulton *et al.* 1998, Dent *et al.* 2001, Poole 2002) to summarize the effect of gravel augmentation on vertical hydraulic gradients (VHG) in hyporheic zones of an agricultural headwater reach of the Tamoute River (France; data from Sarriquet *et al.* 2007). The model of Kasahara and co-workers hypothesizes the relationship between sediment structure and vertical hydraulic head, thereby combining measures of patch permeability and quality with connectivity (Figure 1.11). While it does not include the effects on biogeochemical processing (i.e. functional diversity), it does quantify changes in sediment structure (patch permeability) and vertical hydraulic head (patch connectivity) in response to restoration works. To improve this approach as a restoration tool, such models could include biogeochemical processes in the hyporheic zone as they relate to hydrological and/or sedimentary conditions that can be changed through restoration works (e.g. Findlay's model).

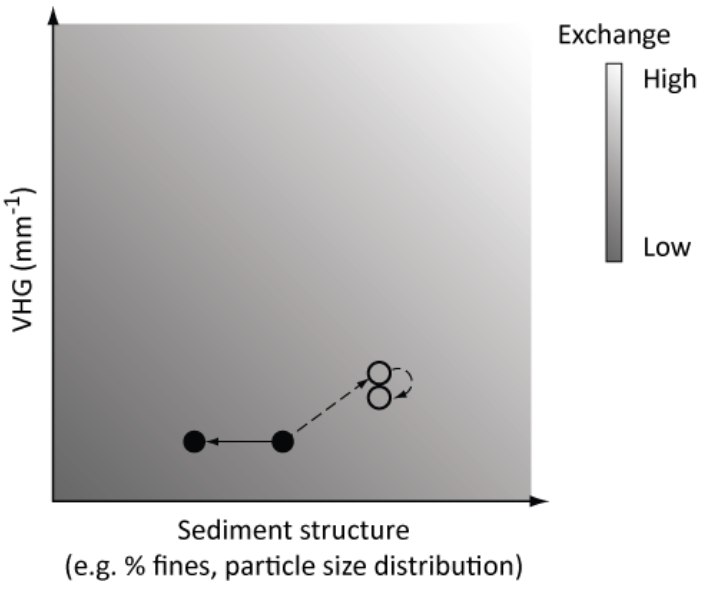

Figure 1.11 Model summarizing the effect of restoration works on vertical hydraulic gradients (VHG) in the hyporheic zone (reproduced from Kasahara *et al.* 2009). Data from the Tamoute River are from Sarriquet *et al.* (2007). Closed circles indicate the control (unrestored) reach and open circles the restored reach (gravel augmentation). The solid arrow indicates the change in state due to human-induced impacts and the dotted arrows indicate the direction and magnitude of restoration.

Ultimately, modelling approaches such as the Hydrological Spiralling Framework (Poole *et al.* 2008) offer the most detailed assessment of reach-scale hydrological connectivity and the resulting biogeochemical exchange processes among multiple, heterogeneous stream-groundwater habitats. These are data-intensive assessments that may be beyond the capabilities of many finer-scale restoration projects. However, even small projects benefit from a conceptual model that guides restoration via testable hypotheses. Findlay's (1995) framework integrates the functional significance of the hyporheic zone to surface waters with the processes driving hyporheic exchange, (i.e. the direction of exchange, the volume of water exchanged and hyporheic residence time) and provides a means of assessing the ecosystem-level consequences of hyporheic exchange processes at a reach- or channel-unit scale. Kasahara and co-workers (2009) demonstrate that this approach both clearly identifies and communicates the mechanisms and effects of restoration at the scale of a single riffle.

1.5 Research overview, objectives and thesis structure

Alluvial and semi-alluvial rivers throughout southeastern Australia underwent dramatic channel change during the 200 years since European settlement (Erskine and Bell 1982, Brooks and Brierley 2002). Similar changes were experienced in Europe and North America and a large body of research identifies the causes as the clearing of vegetation from banks and catchments coupled with the removal of large woody debris (LWD) from channels and banks (Thorne 1990, Piégay and Gurnell 1997, Montgomery *et al.* 2003).

Large wood directly and indirectly structures channels across multiple scales by influencing flow hydraulics and sediment transport (Brooks *et al.* 2003). At fine spatial scales, LWD affects channel roughness and the grain size of the bed surface (Montgomery and Piégay 2003). At the reach scale, LWD increases geomorphic complexity (defined as variation in channel morphology, flow velocity, substrate composition and vegetation characteristics, Bartley and Rutherfurd 1999) by creating inchannel features such as pools, bars and steps, and modifying channel width, lateral

channel migration and meander cutoffs. The increased geomorphic complexity of the channel influences flow velocity, discharge, shear stress, and sediment storage and transport (Mutz 2000, Montgomery *et al.* 2003). In southeastern Australia, natural LWD consisted primarily of hardwoods, up to 30 m long and several metres in diameter that could persist in the channel for thousands of years (Erskine and Webb 2003). This had profound implications for the ecological functioning of rivers by influencing nutrient dynamics and habitat availability over long temporal scales. It also likely influenced hydrologic exchange between surface and groundwater (Boulton *et al.* 2004, Scealy *et al.* 2007, Appendix C).

The loss of catchment and riparian vegetation accelerated erosion and increased sediment delivery to rivers. This was exacerbated by the removal of LWD from banks and channels leading to reduced geomorphic complexity of rivers, both longitudinally (i.e. creation and maintenance of pool-riffle and step-pool sequences) and laterally (channel width, creation and maintenance of bars and meanders). Thus, hyporheic exchange was impaired through several synergistic mechanisms. Firstly, turbulent flow over flat gravel beds drives fine-scale hyporheic exchange in the upper few centimetres of the streambed and depends on the velocity of streamflow (Section 1.3) which, in turn, is affected by channel width and longitudinal channel complexity. Secondly, bedforms create differences in pressure at the bed surface and their loss through erosion of riffles, removal of log steps and infilling of pools (Section 1.3) impaired or removed this exchange mechanism (Boulton *et al.* 2004). Thirdly, increased loads of fine-grained sediments in conjunction with reduced stream velocity, the loss of longitudinal geomorphic complexity and reduced hyporheic exchange lead to 'colmation', the process where fine-grained sediments percolate deep into the streambed and reduce sediment porosity and permeability (Section 1.3).

Fundamentally, hyporheic exchange is driven by interactions among stream flow, sediment conditions and bed topography (Packman and Salehin 2003). Restoration strategies that manipulate the processes controlling these factors are best able to treat the cause(s) of impaired vertical connectivity, but currently this is impeded by our limited understanding of the biophysical processes that create and sustain dynamic

hyporheic zones across riverine landscapes and the impacts of land use on these. Therefore, ecologically sound restoration of vertical connectivity requires that we first understand the processes driving this exchange. Chapter 1 has addressed this knowledge gap by reviewing the literature across several fields to develop an understanding of vertical connectivity that integrates geomorphological and hydrological processes. Chapter 1 has also reviewed ecological theories of riverine function to integrate restoration concepts with current conceptual models of hyporheic structure and processes.

As removal of LWD altered the drivers of vertical connectivity in many rivers, replacing large wood – including in the form of engineered log sills – may significantly improve hyporheic exchange at intermediate spatial and temporal scales (metres and days, respectively). Ideally, stream wood loadings increase naturally as native riparian trees fall into the channel (Wohl *et al.* 2005). However, this is a long-term strategy and artificially augmenting depleted wood loadings may be necessary to enhance critical processes and maintain the viability of valuable habitats and biota in the intermediate term while riparian trees mature. Overseas, the placement of large wood in streams either as fixed structures or as freely moving unattached logs has long been used to control bank and bed erosion, protect riparian revegetation areas, store sediments in low-order channels and create pool habitats for fish (Reich *et al.* 2003). However, the reintroduction of large wood to river channels is a relatively recent priority for river restoration in Australia (Erskine and Webb 2003, Brooks *et al.* 2004).

Paralleling work in Europe and North America, large wood reintroductions were designed initially to restore geomorphic structure and function by increasing bed and bank stability and re-establish pool-riffle sequences (Gerhard and Reich 2000, Abbe *et al.* 2003, Brooks *et al.* 2004). Subsequently, large wood was introduced to create or improve habitat for fish (Bond and Lake 2005, Howell 2008) and aquatic macroinvertebrates (Bond *et al.* 2006, Lester *et al.* 2007, Scealy *et al.* 2007). Most recent work has also focused on the role of large wood in ecological processes such as the retention and processing of organic matter (Brookshire and Dwire 2003, Daniels 2006, Wolfenden 2009) as well as whether reintroducing wood can restore hyporheic

exchange (Boulton *et al.* 2004, Kasahara and Hill 2006a, 2006b, Hester and Doyle 2008).

Engineered log sills (ELSs) are structures built perpendicular to flow and are commonly used to re-establish step-pools and stabilize channel beds by preventing further bed incision, such as from the upstream migration of erosion nick-points (Kasahara and Hill 2006a). Log sills increase geomorphic complexity at the reach-scale (Brooks *et al.* 2004, 2006) by increasing the topographic heterogeneity of the channel bed and this creates pressure differentials at the bed surface that induce hydrologic exchange between the surface stream and hyporheic zone (Boulton *et al.* 2004). Thus, unlike other restoration techniques that treat only the symptoms of disturbance to hyporheic function, ELSs potentially address the cause by increasing wood loadings and consequently, geomorphic complexity (Kasahara *et al.* 2009). Kasahara and Hill (2006a, 2006b) presented the first experimental investigation of the effectiveness of an ELS in enhancing hyporheic exchange in a low-order stream. However, the effectiveness of ELSs in enhancing hyporheic exchange is still in the experimental phase (Kasahara and Hill 2006a, 2006b, Sawyer *et al.* 2011, 2012), and no studies have yet documented the deployment of ELSs in management-style (and sized) restoration programs on higher-order rivers.

Predictions varied among researchers. Work by Boulton and co-workers suggests that the deposition of sediment downstream of the log sill forms a series of dunes and, in conjunction with enhanced downwelling displacing porewater, creates a zone of diffuse upwelling downstream of the scour pool (Figure 1.12a, Boulton *et al.* 2004, Boulton 2007). In contrast, Kasahara and co-workers suggest that upwelling occurs in the scour pool (Figure 1.12b, Kasahara and Hill 2006a, 2006b, Kasahara *et al.* 2009). However, although the ELS enhanced hyporheic exchange in their study, Kasahara and Hill suggest the effectiveness of the ELS was limited by the inclusion of a geotextile layer under the ELS to prevent erosion. The modelling study by Hester and Doyle (2008) suggests that downwelling peaks immediately upstream of the step with upwelling peaking downstream of the structure. However, they modelled a step, a different hydraulic structure, and did not incorporate a scour pool (Figure 1.13).

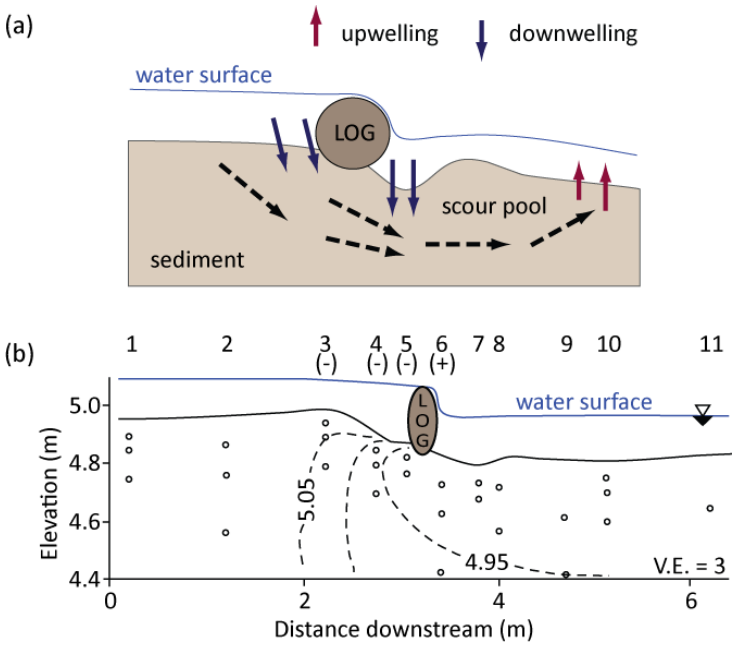

Figure 1.12 Conceptual and empirical models of log sills enhancing hyporheic exchange. Streamflow is from left to right. **(a)** Conceptual model of the effect of a log sill on hyporheic flow through a gravel bed reproduced from Boulton and others (2004). **(b)** Quantified effect of a log sill on hyporheic flow through a gravel bed reproduced from Kasahara and Hill (2006a, 2006b) and Kasahara and others (2009). Open circles indicate piezometers and bracketed symbols under the piezometer nest number indicate permanent downwelling (-) or upwelling (+). The placement of the geotextile is not indicated in the original work. V.E. is vertical exaggeration.

Despite the differences these studies found in the fine-scale spatial relationships between bed topography and direction of hyporheic exchange, the consensus is that ELSs increase hyporheic exchange – predominantly downwelling – at a local spatial scale (i.e. at the riffle scale or less). However, before hypotheses can be derived as to the specific mechanisms by which a log sill increases hyporheic exchange (addressing the second criterion for ecologically successful restoration), the geomorphic and hydrologic effects of the log sill need to be determined. The log sill obstructs flow, creating a backwater and promoting sediment deposition upstream of the log sill. The bed then aggrades, steepening the gradient of the riffle upstream of the log sill. The hydraulic step causes water to be 'rammed' into the streambed immediately downstream of the log sill, creating a plunge or scour pool. The sediment excavated from the scour pool is deposited as an unconsolidated dune downstream (Figure 1.14).

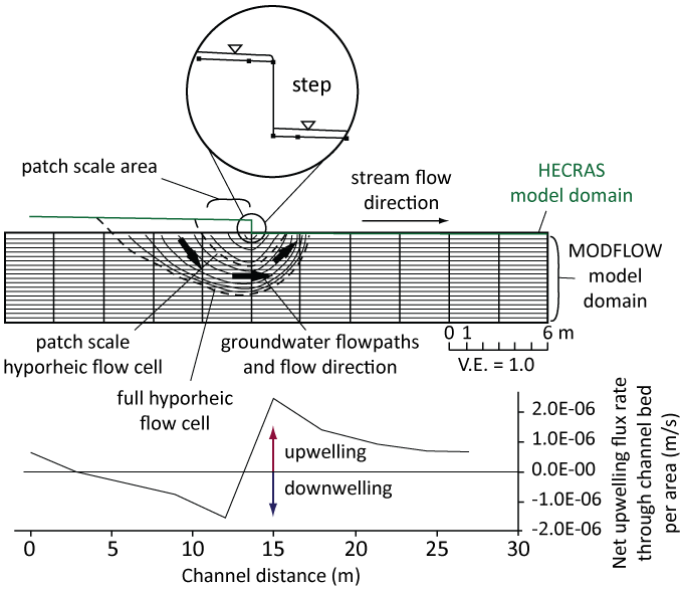

Figure 1.13 Mathematical model of the effect of a step on hyporheic flow in a gravel bed reproduced from Hester and Doyle (2008). Note the location and magnitude of downwelling and upwelling around the step. The original diagram has been modified to maintain consistency in streamflow, i.e. from left to right. V.E. is vertical exaggeration.

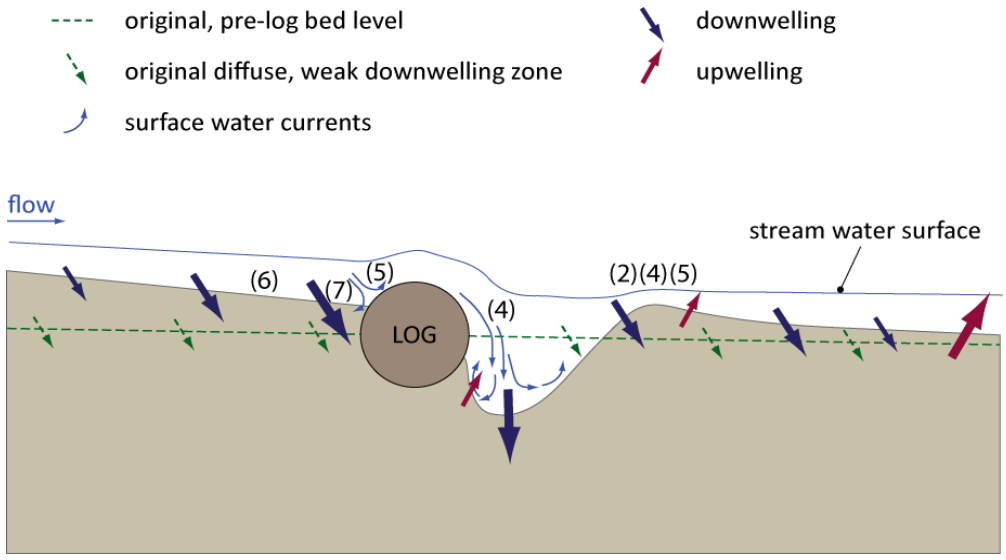

Figure 1.14 A log sill creates complex bed topography, enhancing localized hyporheic exchange through a gravel-bed. As the sill obstructs flow, sediment is deposited on the stoss (upstream) side of the log. This steepens the bed gradient, inducing downwelling that intensifies close to the log. A scour pool forms on the lee (downstream) side of the log, inducing highly localized zones of upwelling and intense downwelling. Sediment eroded from the scour pool is deposited as an unconsolidated dune downstream, also causing localized zones of downwelling and upwelling. Bracketed numbers refer to the seven mechanisms identified in Section 1.3.1.

In Section 1.3.1, I reviewed the seven mechanisms (Hester and Doyle 2008) suggested to drive vertical hydrologic exchange at fine scales: (1) diffusion, (2) turbulent flux, (3) turnover exchange, (4) turbulent streamflow over a bedform protruding into the stream, (5) heterogeneous substrates, (6) localized channel steepening, and (7) backwater collecting behind obstacles in the channel. Using this framework, I hypothesize that a log sill induces hyporheic exchange through multiple mechanisms (Figure 1.14): localized channel steepening upstream of the sill (6), backwater pooling upstream of the sill (7), the sill creating an impermeable obstacle within the sediment (5), turbulent flux (2), turbulent streamflow over the sill (4), and turbulent streamflow over the downstream dune (4). The contributions of these different mechanisms likely vary with stream discharge, the dimensions of the feature, the sediment mix and time since the last bed-moving event. For example, at extreme low flows, a log sill may completely obstruct surface flow, removing the mechanism of turbulent streamflow over a bedform (4), reducing the effects of stream velocity (2), and increasing the contribution of backwater pooling behind the sill (7).

Process-oriented hyporheic restoration is in its infancy and few studies of hyporheic restoration measures have been conducted in rivers (as opposed to flumes), especially in higher-order, degraded rivers that are the traditional realm of restoration works by river management agencies. To address this major knowledge gap and mismatch in spatial sale, I examined the effectiveness of ELSs in enhancing hyporheic exchange in two degraded gravel-bed rivers in New South Wales. The log sills presented here are large, multi-log structures representative of log sills installed by local catchment management agencies to promote bed and bank stability. My conceptual model of hyporheic exchange around a log sill placed within a riffle (Figure 1.14) integrates the work of Boulton and others (2004), and Kasahara and co-workers (2006a, 2006b, 2009) and is applied to these two field-scale restoration projects to test three broad hypotheses:

(1) Log sills increase topographic complexity at the riffle scale.

(2) Increased topographic complexity increases vertical hydrologic exchange.

(3) Enhanced vertical hydrologic exchange increases nutrient processing in the hyporheic zone, and for some nutrients, export to the surface stream.

Chapters 2 and 3 discussing the two restoration projects are structured according to these three broad hypotheses. Chapter 2 addresses the first two hypotheses, quantifying the changes in geomorphic complexity and sediment characteristics and the resulting increases in vertical hyporheic exchange after the installation of four log sills in the Hunter and Williams Rivers, New South Wales, Australia. After describing the catchment and sites, Chapter 2 explains the specific restoration strategy for each site, including the design and construction of the log sills. The key point to take from the descriptions of the restoration strategy is the scale of and disturbance associated with the installation of log sills as management-style intervention measures. Typically, experimental log-sills have not been as large or involved as much site disturbance as these ELSs, and this limits the ability of these experiments to accurately inform river managers of the benefits and costs of these types of restoration works.

I use Findlay's (1995) classification scheme as a theoretical model for identifying the mechanisms of hyporheic exchange that are targeted by the ELSs and the biogeochemical effects of these four log sills at the channel unit (i.e. riffle) scale. In Chapter 2, the model relates increases in vertical hydrologic exchange to changed sediment characteristics. Chapter 3 focuses on hyporheic oxygen and nutrient dynamics, and here the model relates the increases in vertical hydrologic exchange to hyporheic nutrient processing and export.

The findings from the two field experiments are synthesized in the context of my conceptual model of the mechanisms by which log sills enhance hyporheic exchange in degraded gravel-bed rivers and the utility of Findlay's conceptual model of hyporheic function and export as a tool to guide, explain and communicate hyporheic restoration projects (Chapter 4). Finally, I revisit the published hyporheic ecological models and show how current ecological theory can be extended to explicitly guide reach-scale hyporheic restoration via hypotheses generated directly from a hybridized theoretical model (Chapter 4).

Chapter 2

Log sills increase local topographic complexity and vertical hydrologic exchange in riffles

2.1 Introduction

Riffle-pool sequences are the characteristic reach-scale bedform and basic geomorphic template for most instream habitat in gravel- and mixed-bed channels of low to moderate gradients (Clifford 1993, Thompson 2001). In these reaches, hyporheic exchange is dominated by the localized channel steepening associated with riffles (Kasahara and Wondzell 2003, Boano *et al.* 2006). Riffle-scale hyporheic exchange is disproportionately important to these stream ecosystems because the ubiquity of riffles likely accounts for more surface-subsurface interaction than longer flowpaths (Harvey and Wagner 2000), the magnitude of riffle hyporheic exchange is greatest during low flows, which may occur for most of the year (Tonina and Buffington 2007, Wood *et al.* 2010), and riffle hyporheic flowpaths generally have intermediate residence times ensuring relatively high concentrations of dissolved oxygen for hyporheic biota as well as sufficient time for biogeochemical processing (Chapter 1, Storey *et al.* 2003).

Although catchment context (geology, topology, depth of alluvium), riffle topography and sedimentology, and stream discharge determine the area, magnitude and direction of hyporheic exchange through a riffle, riffle hyporheic exchange often follows a general pattern (Chapter 1). In brief, decreasing stream depth at the downstream end of a pool creates a high pressure zone, forcing stream water to downwell at the head of the riffle. The downwelling displaces pore water, pushing it along preferential flowpaths within the riffle. At the tail of the riffle, increasing stream depth creates a low pressure zone at the stream-bed interface, pulling porewater into the surface stream (Figure 1.6, Franken *et al.* 2001).

Catastrophic channel change caused by deforestation, clearing of riparian vegetation and the removal of instream large wood ('desnagging') occurred in many alluvial and semi-alluvial rivers worldwide (Brooks and Brierley 2002, Erskine and Webb 2003). Generally, river channels widened and incised, and longitudinal channel complexity was lost through erosion, smothering of riffles and infilling of pools (Brooks *et al.* 2003, 2006). These changes in channel morphology likely impaired reach-scale hyporheic exchange by reducing bedform-driven exchange (Wondzell *et al.* 2009), as well as reducing the hydraulic conductivity of bed sediments (and therefore, turbulent flux) by the storage of fine sediments (i.e. siltation, smothering and colmation, Figure 1.5; Packman and Bencala 2000, Boulton *et al.* 2004).

Bed sills are commonly used by river management agencies to reintroduce longitudinal profile, and manage sediment supply and transport through river reaches (Brooks *et al.* 2004, 2006, Comiti *et al.* 2009b). Reach-scale hyporheic exchange is sensitive to changes in wood loadings (Andreoli *et al.* 2007), and field experiments and modelling studies suggest log sills increase hyporheic exchange both through the increase in topographic complexity and the downward hydraulic jet effect of the log sills (Section 1.5). However, the specific mechanisms by which log sills increase hyporheic exchange are yet to be elucidated or empirically documented for large-scale riverworks in high-order degraded rivers.

This study investigated the effectiveness of four engineered log sills (ELSs) in increasing localized hyporheic exchange in riffle zones of two degraded gravel-bed rivers in south-eastern Australia. To test my conceptual model of the mechanisms by which log sills increase vertical hyporheic exchange (Chapter 1, Figure 1.14) derived from previous descriptions of the mechanisms of fine-scale hyporheic exchange (Hester and Doyle 2008) and the topographic changes induced by log sills (Boulton *et al.* 2004, Kasahara *et al.* 2009), I measured changes in the reach geomorphology, sediment properties and vertical hydraulic gradients over time using repeated, high-resolution topographic surveys, freeze-cores and instream piezometers.

I hypothesized (1) that topographic complexity at the riffle scale increases after the installation of the log sills, and (2) that increased topographic complexity increases vertical hydrologic exchange. From my tests of these hypotheses, I intend to show how the theoretical ecological model of the functional significance of hyporheic exchange to surface streams as developed by Findlay (1995, Figure 1.8) and subsequent authors (Boulton *et al.* 1998, Dent *et al.* 2001, Kasahara *et al.* 2009) can be used to directly guide restoration efforts and assess whether restoration has been successful.

2.2 Study area, experimental design and methods

2.2.1 Study area

General description of the Hunter catchment

The Hunter River is a warm temperate, sand- and gravel-bed river that drains 22,000 km^2 to the eastern coast of New South Wales (Figure 2.1). The Hunter catchment is divided into two geologically-distinct zones by the inactive Hunter-Mooki Fault. Northeast of the fault, New England Fold Belt units form rugged and hilly country with a high proportion of mudstones (Cook *et al.* 1988, Fryirs *et al.* 2007). Tributaries in the northeast originate from elevations ≅ 1200-1500 m above sea level, have relatively high gradients with fast flow, and supply gravels and cobbles to the Hunter River (Raine 2000, Schneider 2007). In contrast, the western side of the catchment comprises Sydney Basin units of sedimentary rocks (shales, sandstones, conglomerates and coal, Fryirs *et al.* 2007) with deeply dissected tributary valleys of highly erodible sandy soils (Schneider 2007). Tributaries originate from elevations ≅ 800-1000 m above sea level, have lower gradients (Fryirs *et al.* 2007) and supply sand to the Hunter River (Raine 2000). To the northwest, tributaries draining the Liverpool Ranges and Merriwa Plateau are characterized by basaltic gravel and cobble streambeds, and high concentrations of dissolved salts and minerals (Schneider 2007). Overall, a third of the catchment (≈7,300 km^2) is classified as mountainous (>15 ° slope), including the sub-alpine areas in the northern highlands (ANRA 2008a). Approximately half of the catchment (≈10,200 km^2) is classified as undulating and less

than one-quarter (≈4,400 km^2) is classified as flat (<3 ° slope), including the large alluvial floodplain (ANRA 2008a).

Annual catchment rainfall ranges from 600-1400 mm (Figure 2.1, Raine 2000). Coastal and lower sub-catchments receive the highest annual rainfall, generally in January-March, with an irregular smaller peak in mid-winter (ANRA 2008b). The western regions of the catchment are the driest, receiving their peak rainfall in December-January (ANRA 2008b). Average yearly runoff is 1,800,000 ML, approximately 12.5 % of the total catchment rainfall (DLWC 2000). However, this is not distributed evenly across the catchment. For example, the Paterson, Allyn and Williams Rivers drain 10 % (2,230 km^2) of the Hunter catchment, yet contribute 42 % of the total river flow (760,000 ML $year^{-1}$, DLWC 2000). The Hunter Valley has experienced significant droughts and floods (Erskine and Warner 1988), leading to extensive flood mitigation and impoundment works throughout the catchment (Figure 2.1, ANRA 2008b).

The Hunter River is regulated for 250 km from Glenbawn Dam to the tidal limit at Maitland (DIPNR 2004). Eight major structures regulate flow in the catchment (Figure 2.1). Glenbawn Dam (870,000 ML capacity), 11 river-kilometres upstream of Aberdeen, captures runoff from 30 % of the Hunter catchment and traps 98.9 % of the total sediment load (Erskine 1985, 1992). It was completed in 1958 for flood mitigation and provides water for irrigation, industry (coal mining and power generation) and domestic use. Glenbawn Dam reduces the size and frequency of small to medium spates, maintains increased low flows, reverses the seasonality of flows and causes cold-water pollution for 30 km downstream (Chessman *et al.* 1997).

At the time of European settlement, the mid- to upper Hunter was characterized by a narrow but dense riparian zone dominated by river oaks (*Casuarina cunninghamiana*) and river red gums (*Eucalyptus camaldulensis*), while the alluvial floodplain supported dense grasslands with scattered river red gums, forest red gums (*E. tereticornis*) and yellow box (*E. melliodora*) (Peake 2003). Most native vegetation was cleared soon after European settlement (Mika *et al.* 2010). Today, the riparian vegetation is dominated by introduced willows (*Salix* spp.) with scattered stands of river oaks (Scealy *et al.* 2007,

Appendix C). The lack of riparian vegetation along many streams leading to bed and bank instability is a management priority for the catchment (Raine 2000). Only 13 % of native riparian vegetation in the catchment is protected and 44 % of streams have unstable banks and/or beds (H-CRCMA 2007). Virtually all large woody debris were cleared from the banks and channels in the lowland reaches of the catchment (Erskine and Webb 2003). The loss of riparian vegetation and unstable channels led to accelerated erosion and sedimentation, loss of pool-riffle sequences, lowered groundwater tables causing dewatering of riparian zones, increased nutrient loads from nonpoint sources, and reduced shading leading to increased surface water temperatures (Wolfenden *et al.* 2005, H-CRCMA 2007). Concentrations of nitrogen and phosphorus in streams of the Hunter catchment are greater than the Australian median, and are predominantly associated with fine sediments (Hancock 1997, ANRA 2008c). These nutrients are retained within the river system and do not reach the estuary, as nutrient loads entering the Hunter estuary are lower than the Australian median (ANRA 2008c).

The settlement history of the Williams catchment is similar to that of the Hunter. Land surveys began in the mid-1820s and widespread clearance of floodplains and hillslopes occurred soon after (Ford 1995 in Brooks *et al.* 2004). Like the rest of the Hunter, the loss of vegetation increased runoff and peak flood discharges (Erskine 1998). Flood mitigation and 'river training' works began the mid 1950s; works included extensive desnagging (i.e. removal of instream wood from bars, bed (e.g. log steps, Brooks *et al.* 2004) and banks). In the Williams River study reach (Figure 2.2), desnagging began in March 1966 (Erskine 1998). A comparison of historic aerial photographs shows that the channel dramatically expanded in the 1960s when desnagging coincided with a series of large floods (Erskine and White 1996). Engineering works were initiated to combat the resulting bank and bed instability, and these included channel realignment, removal of the gravel armour and boulders from riffles, installation of wire mesh and/or steel cable fences, and planting exotic trees in the riparian zone (mostly willows, Brooks *et al.* 2004). While the riverworks improved bank stability, bed instability is still a management priority

for the Williams catchment, particularly the erosion of riffles and infilling of low-flow pools (Erskine 1998, Brooks *et al.* 2004).

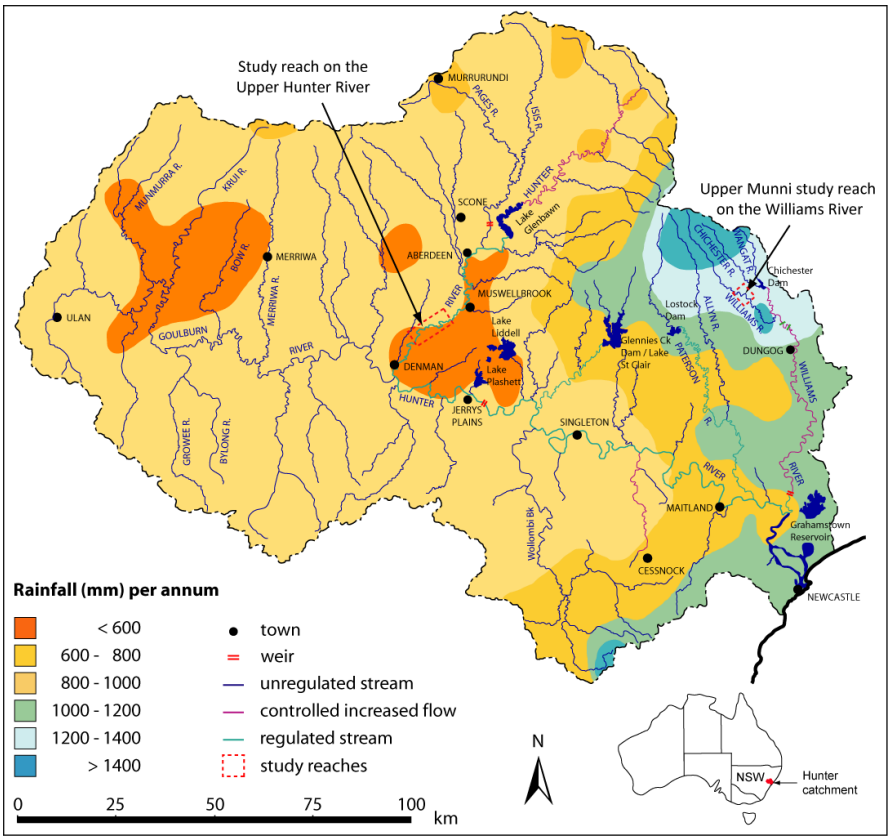

Figure 2.1 Rainfall, stream channels and impoundments in the Hunter catchment. Rainfall data sourced from DLWC (2000). Extent of unregulated, controlled and regulated flow sourced from Ryder and others (2008b).

Study reaches

The study reach on the degraded, fourth-order Hunter River is 5 km southwest of Muswellbrook (32°17'S, 150°50'E), approximately 20 km downstream of Glenbawn Dam (Figure 2.1). The 10-km reach has a catchment area of 4,220 km^2 and is characterized as a low-to-moderately sinuous (sinuosity ≈ 1.3), passively meandering gravel-bed river with an average bed gradient of 0.001 m m^{-1} (Hancock 2006, Hoyle *et al.* 2008a). The floodplain and banks of the reach comprise fine sands, silts and clays

(5-8-m deep, Hoyle *et al.* 2008a), and localized erosion of these fine-grained sediments contributes to the river's suspended load during high flows (Scealy *et al.* 2007). In contrast, the channel bed consists of noncohesive sand and gravel (Hoyle *et al.* 2008a) where pebble-cobbles dominate riffle substrates and pool substrates contain substantial silt loads (Scealy *et al.* 2007).

Average bankfull discharge is 150,000 ML day^{-1} or ≈1,736 m^3 s^{-1} (1:14 annual recurrence interval), but low-flows (i.e. <1,000 ML day^{-1} or <11.57 m^3 s^{-1}) occur for more than 90 % of the time (Hoyle *et al.* 2008b). Riffles support extensive beds of water milfoil (*Myriophyllum verrucosum*) (Scealy *et al.* 2007). Pools contain low background loads of large instream wood (willows and river oaks) owing to the long history of de-snagging (Erskine and Webb 2003). The riparian vegetation is dominated by river oaks and exotic species such as willows and balloon vine (*Cardiospermum grandiflorum*. Land use along the study reach includes dairying, lucerne cropping and improved pastures, horse and cattle studs, viticulture and open-cut coal mining.

Within the Hunter River reach, the treatment site 'Goat Bar' (HGB), is 1.3 river-km downstream of Keys Bridge, the upstream extent of the study reach (Figure 2.2). The low-flow channel splits around an island and most flow travels down the right arm. At baseflow, the right arm is 10 m wide, and the riffles have an average depth of 26 cm and flow at 0.69 m sec^{-1} (Scealy *et al.* 2007). The control site 'Sandwich Bar' (HSB), is 1.8 river-km downstream of HGB (Figure 2.2) and also has a low-flow channel that splits around an island with most flow travelling down the 10-m right arm. Average water depth and velocity along the riffle at baseflow are 29 cm and 0.49 m sec^{-1}, respectively (Scealy *et al.* 2007). At both sites, the substrate is dominated by pebbles and cobbles. The location of the control site downstream of the treatment site was constrained by the absence of suitable riffle sites upstream of the riverworks.

On the Williams River, the study reach at 'Upper Munni' (WUM) drains a catchment of approximately 185 km^2 (Figure 2.3). The river is a discontinuous-floodplain gravel-bed river with an average bed slope of 0.002 m m^{-1} along the 150-m reach (Brooks *et al.* 2004). The floodplain and banks of the reach comprise basaltic silts and clays while the

bed is dominated by cobbles, with localized sand drapes deposited in pools. Average bankfull discharge is 800 m^3 s^{-1} (>100-yr recurrence interval). The mean annual flood is 170 m^3 s^{-1}, estimated from the flow gauge at Tillegra Bridge (catchment area 194 km^2), 5.3 river-km downstream of WUM (Brooks *et al.* 2004). The low-flow channel splits around a central island. Most surface flow travels down the right arm which is 5 m wide, averages 20 cm deep and flows at 0.24 m sec^{-1} at baseflow. Riparian vegetation is dominated by native species such as river oaks. The land use along the reach is beef production.

Restoration works

Previous work demonstrated that engineered log jams (ELJs) successfully re-established geomorphic variability in Stockyard Creek, a sand-bed tributary of Wollomi Brook in the southeast of the Hunter catchment. Based on the success of these trials, 20 ELJs were installed along 1,100 m in the Williams River, downstream of the Upper Munni site. Monitoring of this reach found increased sediment storage and bed complexity five years later (Brooks *et al.* 2004, 2006). Given these successes, similar ELJs were installed at Upper Munni to counteract: (1) the loss of a pool-riffle sequence via erosion of the riffle and infilling of the downstream pool, (2) excessive bed instability and high sediment flux, and (3) localized bank erosion that was perceived to threaten a bridge. Installation first involved damming the upstream riffle. The river bed was excavated (Plate 2.1) and an engineered log sill (ELS) constructed that anchored in to the right bank, spanned the right arm of the low-flow channel and anchored in the central island (Plate 2.2). Steel cables were used as additional support. The ELJs were then backfilled with native gravel. This was repeated downstream and the dam then removed.

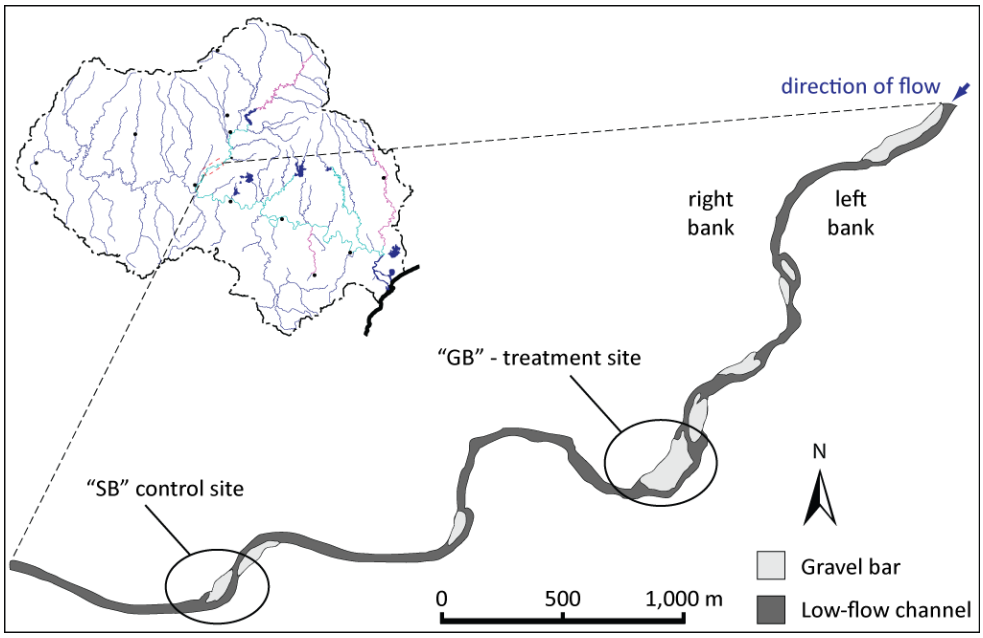

Figure 2.2 The study reach on the Hunter River showing the location of the treatment site "HGB" and the control site "HSB". Direction of flow is from right to left.

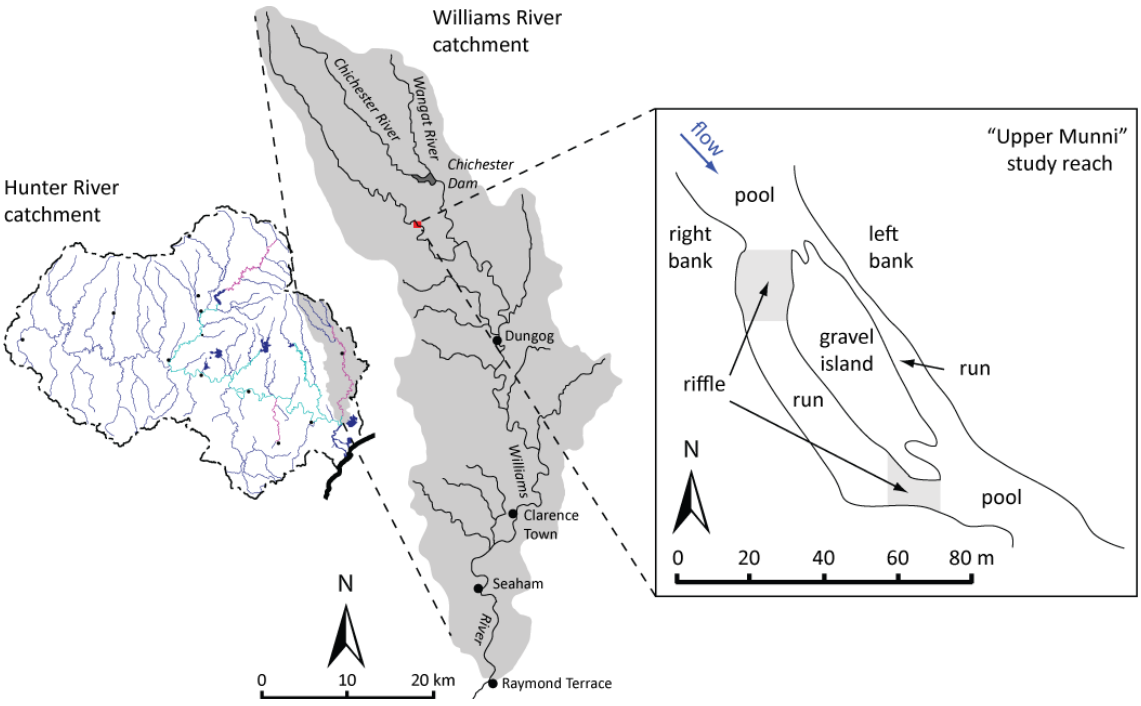

Figure 2.3 The study reach at Upper Munni in the Williams River catchment. The Williams River is a tributary of the Hunter River.

On the Hunter River, a combined research and restoration project (2003-2007) aimed to produce both a community resource and a model for future restoration efforts by creating an ecologically sustainable riparian plant community dominated by endemic species and reintroducing instream wood to provide habitat for native aquatic biota (Keating *et al.* 2008, Mika *et al.* 2010). The restoration component included planting 53,400 native trees and shrubs in riparian and floodplain habitats as well as installing 33 ELJs throughout the reach (Keating *et al.* 2008). Two of the ELJs were log sills spanning the width of the main channel and placed within a single site comprising two riffles, HGB (Figure 2.3). These two log sills were designed to increase the hydraulic and geomorphic variability within the river bed by creating hydraulic steps with their associated localized erosion and deposition.

The right (main) channel was dammed upstream of the first riffle (Plate 2.3), diverting flow to the left channel (Keating *et al.* 2008). The upstream log sill was constructed by excavating a trench 1.2-m wide and 1.2-m deep across the whole width of the right channel. Logs were placed into the trench in a pyramid three layers high and secured by piles and cables (Figure 2.4). Three abutment jams were constructed parallel to flow on the downstream side of the log sill, one built into the right bank, one in the middle and one into the central island (Plate 2.4). The structure was backfilled with native gravel so that the ELS protruded about 0.1 m from the channel bed (Plate 2.5). A similar process was repeated for the downstream log sill. A large “bank deflector jam” was built into the right bank 50 m upstream of the first ELS (Plate 2.6) to prevent high flows from outflanking the log sills (Figure 2.4).

2.2.2 Experimental design

The site at Upper Munni on the Williams River (WUM) was included opportunistically, limiting the experimental design to two riffles within a single treatment site (Figure 2.4). While this is a weak experimental design, very few projects of this scale have been undertaken worldwide, and far fewer have been monitored. To date, the only published empirical field study on the use of log sills to restore hyporheic function is that by Kasahara and Hill (2006a, 2006b), in a second-order stream in Canada. Thus, despite the limitations inherent in conducting research alongside management interventions (Michener 1997), my opportunistic sampling provided a valuable opportunity to evaluate log sills in a larger river as well as testing field and laboratory sampling methods prior to commencing work in the Hunter River. Most significantly, it revealed the extent of site disruption during installation, particularly the damming and excavation of the river channel (Plate 2.4). Post-ELS sampling at WUM identified significant bed compaction in the area between log sills where heavy machinery repeatedly traversed the bed during construction. This enabled the experimental design for the Hunter River restoration project to be modified to include a machinery-exclusion zone.

Plate 2.1 Constructing the ELJ that anchored the upstream log sill into the right bank at WUM. Note that the channel was dammed upstream of the riffle and the river bed excavated to place the logs.

Plate 2.2 Native gravel was used to backfill the log structures. The photo was taken looking upstream from below the second (downstream) log sill.

Plate 2.3 The riffle on the right channel at HGB. The photo was taken looking upstream from the right bank.

Plate 2.4 The upstream log sill at HGB. Note the right channel has been dammed to the right (upstream) of the ELS. The ELS consists of the cross-spanning logs, the supporting abutment jams and the piles. Photo was taken from the central island looking towards the right bank.

Plate 2.5 The finished log sill immediately after the dam was removed. Note that about 10 cm of the log sill is above the river bed. The wetted channel is 10 m wide.

Plate 2.6 The 'bank deflector jam' on the right bank upstream of the first log sill. Its purpose is to deflect flow from the head of the gravel bar on the right bank to prevent the upstream log sill from being outflanked during high flows.

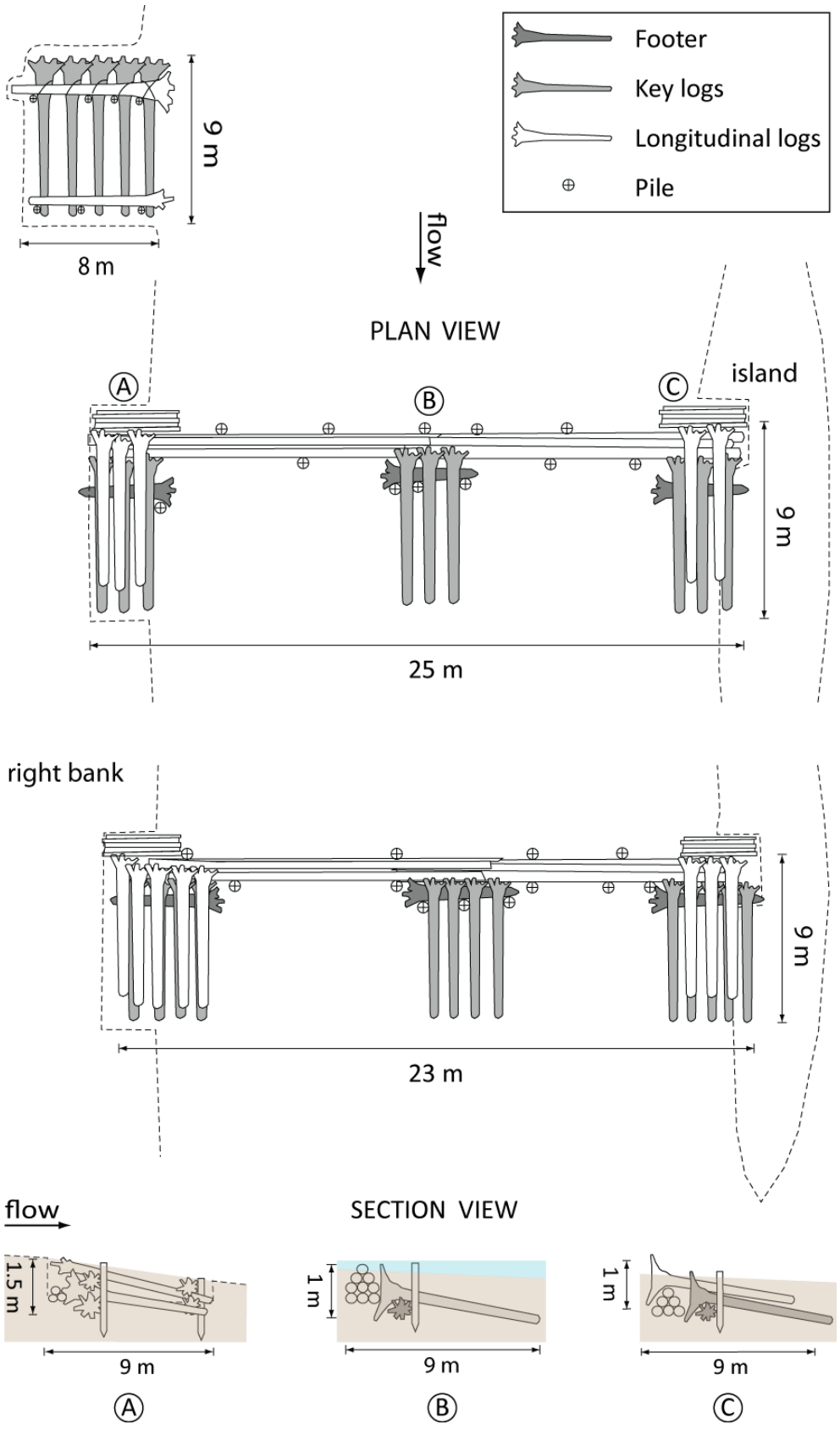

Figure 2.4 Plan and section views of the two log sills and upstream deflector structure built in the right channel at the treatment site HGB. Native gravel was used to backfill over the structures so that only the top 10 cm was left exposed. Diagram not to scale. Modified from Keating and others (2008).

The mean daily low flow during the study was 4.77 $m^3 s^{-1}$ in the Hunter River (Muswellbrook gauge) and 0.93 $m^3 s^{-1}$ in the Williams River (Tillegra gauge, Figure 2.5). The log sills were installed at WUM in October 2003. A flood in late March 2004 (peaking at 73.09 $m^3 s^{-1}$, Figure 2.5a) reworked the low-flow channel, shifting it from the right margin to the left margin of the macro-channel (*sensu* van Niekerk *et al.* 1999), removing surface flow from over the log sills (Plate 2.7). As a result, the 12 months post-wood-installation samples could not be taken. Log sills were installed at HGB in late September 2004. Dam releases were reduced prior and during the installation work (Figure 2.5b). Although this did not prevent the collection of pre-installation data, it did mean that data were collected as the riffles at HGB began dewatering.

At the treatment sites on the Hunter and Williams Rivers (HGB and WUM, respectively), high-resolution topographic surveys were taken prior to the installation of log sills and the associated site disruption. Surveying was repeated one month, six months, and (at HGB) 12 months after the log sills were installed. Vertical profiles of sediment mix were collected using freeze-cores, by burying a metal standpipe in the streambed and using CO_2 gas to freeze sediment to the outside of the standpipe (Section 2.2.3). Hollow polyvinyl chloride rods ('wells') were inserted into the streambed and hyporheic water was pumped out to sample physico-chemical parameters (Section 3.2). Mini piezometers were inserted into the wells and the difference between the surface of the stream and the water level in the piezometer estimated vertical hydraulic gradients (Section 2.2.5). At HGB, sediment conditions were quantified using triplicate freeze-cores one month before and after construction, and six and 12 months post-construction. The same sampling design was used at WUM, but the 12 months post-wood freeze-cores were not collected due to the relocation of the low-flow channel (Plate 2.7). Freeze cores were collected near wells (that collected interstitial water for physico-chemical analyses, Chapter 3) and care was taken not to resample exact core locations to avoid sampling interference (Figure 2.6). Vertical hydraulic head was measured in wells prior to the extraction of freeze-cores (Section 2.2.5).

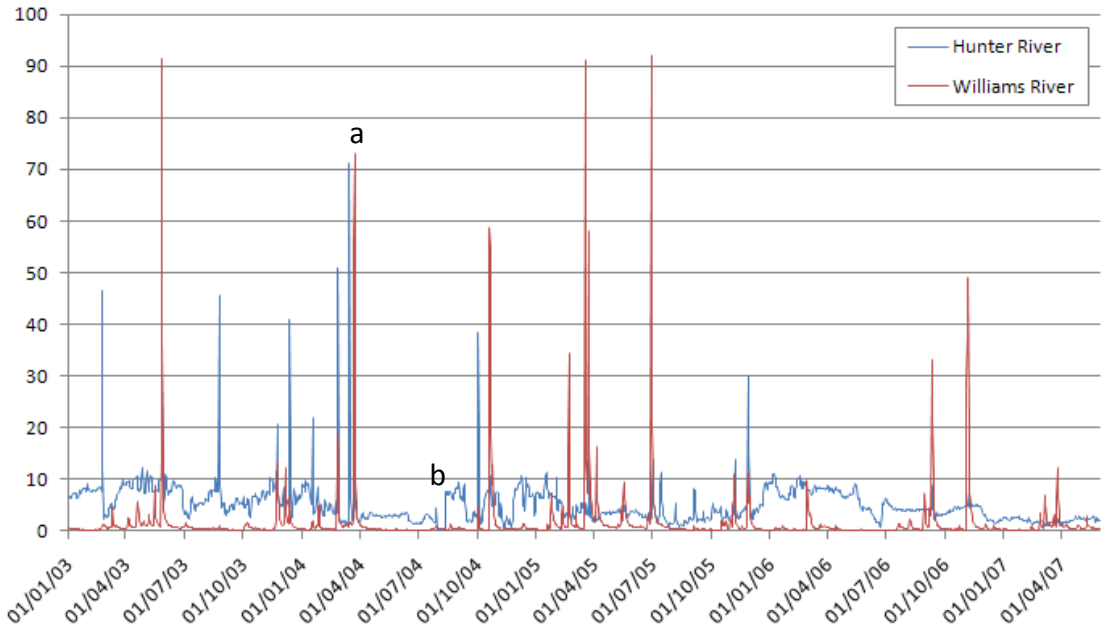

Figure 2.5 Mean daily discharge ($m^3 s^{-1}$) in the Hunter and Williams Rivers between January 2003 and May 2007 (data from NSW Office of Water). **(a)** The flood in the Williams River in March 2004 that realigned the low-flow channel at WUM (Section 2.2.1). **(b)** Immediately prior to the installation of log sills in the Hunter River, flow decreased such that the treatment site (HGB) ceased to flow (Section 2.2.1).

Plate 2.7 After the March 2004 flood in the Williams River, surface flow at WUM was down the left channel (to the right of the photo), dewatering the right channel. The photo was taken looking upstream with the downstream log sill in the foreground. The broken upstream log sill can be seen in the background.

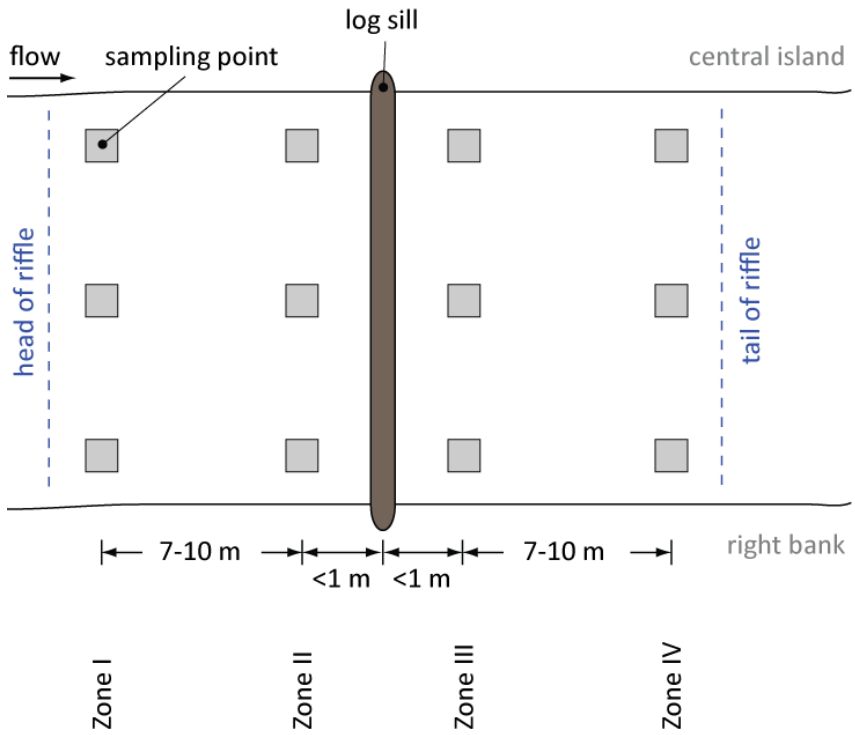

Figure 2.6 Design of triplicate sampling points (wells and freeze-cores) in the four Zones around log sills embedded in riffles in the sites WUM (Williams R.) and HGB (Hunter R.). Two log sills were installed in each site, separated by a run (50 or 20-m long, respectively. The same sampling design was used at the control site HSB (Hunter R.). Zone I is at the head of the riffle, Zone II is immediately upstream of the log sill, Zone III is immediately downstream of the log sill and Zone IV is at the tail of the riffle.

2.2.3 Streambed topography

Field and DEM processing methods

High-resolution, quantitative topographic data were acquired using a Leica TC 805 electronic total station (theodolite and reflector-prism) before and 1-, 6- and 12 months after the log sills were installed following the methods of Kail (2003) and Wheaton and co-workers (2010a). Reach surveys exceeded densities >1 point m^{-2} and were feature-based with point densities increasing in topographically complex terrain (Wheaton *et al.* 2010b). Surveyed points comprised cross-sections with point densities >1 point m^{-2}; topographic breaks in slope (e.g. top-of-bank, toe-of-bank, pool and riffle extent, nick-points, dunes and scour pools around log sills) to ensure these were not missed in the cross-sectional surveys; water's edge for bathymetry and discharge

calculations; boundaries of log sills; and locations of sampling points (e.g. freeze-cores, wells, piezometers).

High-resolution, three-dimensional terrain models were computed from the raw survey data using ArcGIS Version 9.3.1 (ESRI, U.S.A.). DEM (digital elevation model) surfaces were computed in the 3D Analyst module of ArcMap (ESRI, U.S.A.) using triangulated irregular networks (TINs) following Keim and co-workers (1999) and Wheaton and co-workers (2010a). TIN algorithms assume that survey points are on breaks of slope and that no breaks of slope occur between any points. As such, local elevation minima and maxima are measured in the field and not interpolated by the algorithm. TINs are computationally efficient, able to capture fine-scale topographic complexity through the direct measurement of breaks-of-slope and return lower elevation errors in comparison to other interpolation methods for meso-scale geomorphological change estimation (Heritage *et al.* 2009, Milan *et al.* 2011). During construction of the TINs, a hard-clip polygon was drawn around the surveyed points constraining the TINs to prevent spurious interpolation beyond surveyed areas (Wheaton *et al.* 2010b). TINs were rasterized using 3D Analyst (ESRI, U.S.A.) to compute DEMs with a resolution of 5 cm. This was an iterative process to eliminate any erroneous elevations from the datasets.

DEMs of Difference were derived following the methods of Wheaton and co-workers (2010a, 2010b) by subtracting the original DEM surface from each successive DEM surface (i.e. each DEM of Difference is relative to the original reach DEM) to compute spatial patterns (area and volume) of erosion and deposition. To quantify changes in topographic complexity, bed roughness or rugosity was measured by calculating the unitless topographic roughness index (TRI) for the baseflow channel (i.e. wetted area) for each DEM surface following Stambaugh and Guyette (2008). The TRI is the proportion of 3-dimensional surface area to planimetric (or 2-dimensional) area where a TRI ≈ 1 indicates a 'flat' topography and TRI > 1 indicates increasingly complex topography. Long sections (the thalweg up- and down-stream of the log sills) were extracted from DEM surfaces in ArcGIS.

2.2.4 Sediment characteristics

Field and laboratory methods

Sediment core samples were collected using the freeze-core technique of Marchant and Lilywhite (1989). A metal standpipe (internal diameter = 50 mm) was sunk 50 cm into the sediments. The top of the standpipe was covered in plastic to prevent water entering the standpipe, and a, stilling dam, was placed around the standpipe to prevent flow around the standpipe from hindering the freezing process (Plate 2.8). Sediment cores were frozen to the outside of the standpipe by pumping CO_2 gas into the standpipe for eight minutes. Using a tripod and block-and-tackle, the frozen sediment core was winched from the streambed and taken to the bank where it was photographed (Plate 2.9), sectioned into 10-cm intervals (i.e. 0-10, 10-20, 20-30, 30-40 and 40-50 cm) and placed into separate, doubled, preweighed, resealable, plastic bags for transport to the laboratory.

In the laboratory, bags were weighed ('wet weight'). These were then air-dried for several weeks to a constant weight ('dry weight'). Porosity was calculated as the percentage of free interstitial water (by volume) to the total sample volume (Stocker and Williams 1972, Hancock 2004). Samples were then wet-sieved through a nest of sieves (16, 8, 4, 2, 1, 0.5, 0.25, 0.125, 0.063 and <0.063 mm). These fractions were air-dried to a constant weight and weighed (± 0.01 g). The finer fractions (0.250, 0.125, 0.063 and <0.063 mm) were ashed in a muffle furnace at 500 °C for three hours, then reweighed to give the ash-free dry mass (AFDM) for each fraction. The difference between dry weight and AFDM was used to estimate fine benthic organic matter (FBOM), here restricted to ≤ 0.250 mm.

Determining sediment variables

To compare grain size distributions, several statistics are commonly visually interpolated from cumulative size-distribution curves (Kondolf 2000a). The most common statistic is the median particle diameter, d_{50}. Sediment sorting, referring to the degree fluvial processes have collected similar-sized particles together, may be assessed by calculating a sorting coefficient such as the inclusive graphic standard

deviation (σ_I) which spans over 90 % of the sediment distribution (Folk and Ward 1957):

$$\sigma_I = \frac{\phi 84 - \phi 16}{4} + \frac{\phi 95 - \phi 5}{6.6} \quad \ldots \quad \text{(Equation 2.1)}$$

where phi (ϕ) refers to Wentworth units. However, visually interpolating percentiles from a cumulative distribution graph is both inefficient (particularly with many samples) and potentially inaccurate. Thus, I developed a novel mathematical method for calculating these percentiles. Cumulative grain size distributions are approximated by individual straight lines between consecutive size fractions (Hartwig 1973), meaning the relationship between any two consecutive size fractions can be described by a straight line having a beginning point P_1 and an end point P_2, with coordinates x_1 y_1 and x_2 y_2, respectively (Figure 2.7). The straight line between P_1 and P_2 is described by the equation:

$$y = m\,x + b$$

where m is the slope of the line and b is the y-intercept. From this, y_1 and y_2 are derived:

$$y_1 = m\,x_1 + b \quad \ldots \quad \text{(Equation 2.2)}$$

$$\text{and } y_2 = m\,x_2 + b\,. \quad \ldots \quad \text{(Equation 2.3)}$$

The value of x_1 is the grain size (in ϕ) of the fraction described by P_1, and the value of y_1 is the cumulative percentage of that fraction plus the coarser fractions preceding it (Figure 2.7). Likewise, x_2 is the grain size (in ϕ) of the fraction described by P_2, and y_2 is the cumulative percentage of that fraction plus the coarser fractions preceding it. Since x_1 y_1 and x_2 y_2 are known, m and b can be calculated. Subtracting Equation 2.3 from Equation 2.2 gives:

$$y_2 - y_1 = m\,(x_2 - x_1)$$

$$\text{and } m = \left(\frac{y_2 - y_1}{x_2 - x_1} \right). \quad \ldots \quad \text{(Equation 2.4)}$$

Plate 2.8 Freeze-coring at the downstream log sill at WUM on the Williams River. The stilling dam is the cylindrical metal object at the base of the tripod. A plastic flange at the base of the stilling well prevents near-bed flow from dissipating the effects of the freezing. Stream flow is from right to left.

Plate 2.9 A frozen core from the downwelling zone at the head of the upstream riffle at WUM prior to cutting into 10-cm sections (black lines on the ruler).

Substituting Equation 2.4 into Equation 2.2 gives:

$$y_1 = \left(\frac{y_2 - y_1}{x_2 - x_1} \right) x_1 + b$$

$$\text{and } b = y_1 - \left(\frac{y_2 - y_1}{x_2 - x_1} \right) x_1 . \quad \ldots \quad \text{(Equation 2.5)}$$

Substituting Equation 2.4 and Equation 2.5 into the general equation of a straight line gives:

$$y = \left(\frac{y_2 - y_1}{x_2 - x_1} \right) x + y_1 - \left(\frac{y_2 - y_1}{x_2 - x_1} \right) x_1 . \quad \ldots \quad \text{(Equation 2.6)}$$

Thus, y can be calculated directly from the two points $x_1\ y_1$ and $x_2\ y_2$, where $x_1 \leq x \leq x_2$; and more usefully, x can be calculated directly from the two points, $x_1\ y_1$ and $x_2\ y_2$, for any given y-value where $y_1 \leq y \leq y_2$:

$$x = \frac{y - y_1 - \left(\frac{y_2 - y_1}{x_2 - x_1}\right) x_1}{\left(\frac{y_2 - y_1}{x_2 - x_1}\right)} \quad . \qquad \ldots \quad \text{(Equation 2.7)}$$

If m and b are calculated separately (using Equations 2.4 and 2.5, respectively), the equations for x and y can be simplified to:

$$y = m\,x + b\ , \qquad \text{where } x_1 \leq x \leq x_2 \qquad \ldots \quad \text{(Equation 2.8)}$$

$$\text{and } x = (y - b) / m, \qquad \text{where } y_1 \leq y \leq y_2\ . \qquad \ldots \quad \text{(Equation 2.9)}$$

Using this novel approach, median particle size (d_{50}) and the inclusive graphic standard deviation (σ_I) were calculated for each depth interval of each core. The proportion of fine sediment (≤ 1 mm) and the organic proportion of sediment ≤ 250 µm were also calculated for each depth interval of each core. Porosity (θ) was calculated for each core section as the percentage of the volume of free interstitial water to the total sample volume. These five parameters are used to characterize changes in sediment conditions induced by the installation of log sills.

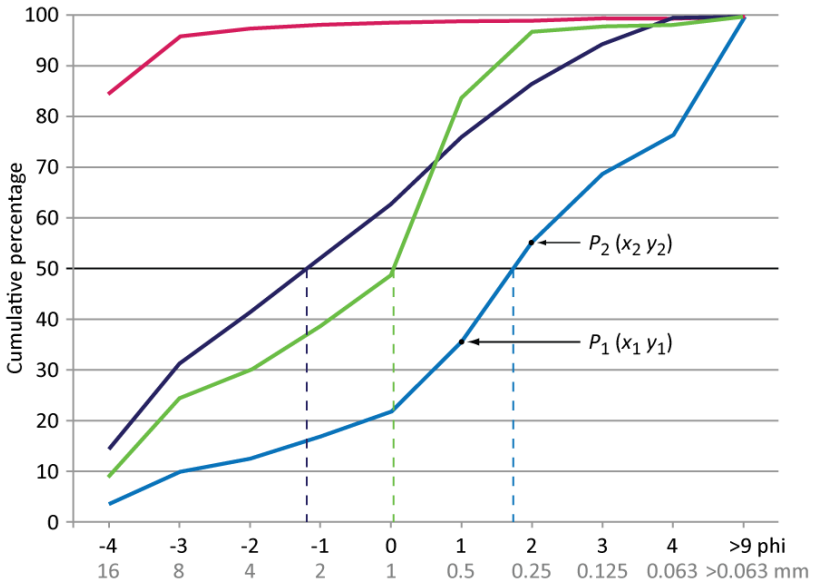

Figure 2.7 Illustrative granulometric curves and median grain sizes (d_{50}, broken lines) of four substrates. The Wentworth scale (phi, ϕ) is used because it gives equidistant intervals between size classes. Phi = -(log x (mm)) / (log 2). The equivalent grain size in mm is provided for clarity.

Statistical analyses

To determine whether the installation of engineered log sills (ELS) were associated with changes in sediment conditions, I used three-factor, fixed-effects analyses of variance (ANOVAs) to test for differences in sediment variables at the two treatment sites (WUM and HGB) and the control site, HSB (Table 2.1). Analyses of log sills were conducted separately because log sills cannot be assumed to be independent within a site given their proximity to each other. Including both log sills (even nested within Site) in a single model commits pseudoreplication (Hurlbert 1984) at the log-sill level. Thus, the three fixed factors in the ANOVA model were *Time* (with a = 3 (WUM) or 4 (HGB and HSB) levels, namely one month pre-ELS, one month post-ELS, six months post-ELS and, for the sites on the Hunter River, 12 months post-ELS); *Zone* (with b = 4 levels, comprising (I) head of riffle/far upstream, (II) immediately upstream, (III) immediately downstream, and (IV) tail of riffle/far downstream of the log sill, see Figure 2.6); and *Depth* (with c = 5 levels being 0-10, 10-20, 20-30, 30-40 and 40-50 cm deep).

Prior to ANOVA analyses, data were tested for normality (Shapiro-Wilk test) and equality of variances ('heteroscedasticity', Levene's test). Where heteroscedastic factors were significant in the ANOVA models, nonparametric Kruskal-Wallis tests were used to validate ANOVA results. If the multivariate Kruskal-Wallis test did not support the ANOVA results, I took the conservative approach of dismissing significant ANOVA results. This occurred in only a few instances and the outcomes are reported with the relevant ANOVA results.

Post hoc tests were used to identify significantly different levels within the factors of Time, Zone and Depth and their interactions, as these directly relate to the hypothesized changes in each of the four zones around the log sills (Section 2.1). *Post hoc* pairwise comparisons of means were performed using either Tukey's HSD test for significant factors with equal variances or Games-Howell tests for significant heteroscedastic factors as the latter test does not assume equal variances among groups and uses separate variance error terms for each group. 'Variance components'

were calculated using the formula of Winer and others (1991: 125) for fixed factors. The 'variance component' for fixed factors is not strictly a measure of component of variance, but represents variation among the population means of fixed-factors (Quinn and Keough 2002). 'Variance components' are expressed as percentages with negative values adjusted to zero. All statistical analyses were computed using SYSTAT Version 12 (SYSTAT Software Inc., San Jose, U.S.A.).

Table 2.1 Statistical design of the fixed-effects ANOVA model that tested for differences in sediment variables around log sills at WUM, HGB, and the control site HSB. Time has a = 3 (WUM1, WUM2) or a = 4 (HGB1, HGB 2, HSB) levels, Zone has b = 4 levels and Depth has c = 5 levels. N = 180 (WUM1, WUM2) or N = 240 (HGB1, HGB2, HSB), and n = 3 for all sites.

Source of variation	Degrees of freedom			Multipliers				Estimated mean square
		df [1]	*df* [2]	j	k	l	r	
1. Time [T_j]	a-1	**2**	**3**	0	b	c	n	$bcn\sigma^2_j + \sigma^2_n$
2. Zone [Z_k]	b-1	**3**	**3**	a	0	c	n	$acn\sigma^2_k + \sigma^2_n$
3. Depth [D_l]	c-1	**4**	**4**	a	b	0	n	$abn\sigma^2_l + \sigma^2_n$
4. T*Z_{jk}	(b-1)(a-1)	**6**	**9**	0	0	c	n	$cn\sigma^2_{jl} + \sigma^2_n$
5. T*D_{jl}	(c-1)(a-1)	**8**	**12**	0	b	0	n	$bn\sigma^2_{kl} + \sigma^2_n$
6. Z*D_{kl}	(c-1)(b-1)	**12**	**12**	a	0	0	n	$an\sigma^2_{jk} + \sigma^2_n$
7. T*Z*D_{jkl}	(c-1)(b-1)(a-1)	**24**	**36**	0	0	0	n	$n\sigma^2_{jkl} + \sigma^2_n$
8. Error [E_r]	abc(n-1)	**120**	**160**	1	1	1	1	σ^2_n

[1] Degrees of freedom for WUM1 and WUM2 analyses. The error term (Term 8) with 120 degrees of freedom, is the denominator for Terms 1-7.

[2] Degrees of freedom for HGB1, HGB2 and HSB analyses. The error term (Term 8), with 160 degrees of freedom, is the denominator for Terms 1-7.

2.2.5 Vertical hydrologic exchange

Field methods

Vertical hydraulic gradients (VHG) indicate the strength and direction of surface water-groundwater exchange. They are determined from hydraulic head measurements in the streambed and calculated by $\Delta h\ \Delta l^{-1}$, where Δh is the elevation difference of the water tables observed at the inside and outside of the piezometer and Δl is the well depth (Dahm and Valett 1996, Krause *et al.* 2011a). VHG ($cm_{head\ difference}\ cm_{well\ depth}^{-1}$) was measured by inserting a polyvinyl chloride well (internal diameter = 16 mm) 20 cm

(shallow) or 40 cm (deep) into the streambed. Samples of 6 L were collected from the well using a hand-operated bilge pump and processed for chemical analyses (Chapter 3). Once the well was recharging freely, VHG was measured by inserting a clear, Plexiglass mini-piezometer into the well, slowly removing the well, pumping water through the mini-piezometer to ensure it recharged freely and taking several readings. The piezometer was not screened but had several small holes (3 mm diameter) drilled into the bottom 5 cm. VHG ($cm_{head\ difference}\ cm_{well\ depth}^{-1}$) was calculated as the difference between the water level in the mini-piezometer and the adjacent river after Dahm and Valett (1996).

Statistical analyses

I tested whether the installation of log sills enhanced hyporheic exchange across riffles using the three-factor, fixed-effects ANOVA model described in Section 2.2.4, comprising the factors *Time*, *Zone* and *Depth*. The only difference with this model is that here Depth has (c = 2) with the levels 20 cm or 40 cm (Table 2.2). Prior to ANOVA analyses, data were tested for normality (Shapiro-Wilk test) and equality of variances (Levene's test). VHG data were heteroscedastic for all factors at all sites (Table 2.6). Because magnitude and direction are critical parameters of VHG, the data were not transformed. However, multivariate tests were used to validate significant ANOVA results as described in Section 2.2.4 above. Where factors were significant in the ANOVA models, *post hoc* Games-Howell tests were performed using the same approach as described above (Section 2.2.4). All statistical tests were computed using SYSTAT Version 12 (SYSTAT Software Inc., San Jose, U.S.A.).

Table 2.2 Statistical design of the fixed-effects ANOVA model that tested for differences in VHG around log sills at WUM, HGB, and the control site HSB. Time has *a* = 4 (WUM1, WUM2) or *a* = 5 (HGB1, HGB 2, HSB) levels, Zone has *b* = 4 levels and Depth has *c* = 5 levels. *N* = 96 (WUM1, WUM2) or *N* = 120 (HGB1, HGB2, HSB), and *n* = 3 for all sites.

Source of variation	Degrees of freedom			Multipliers				Estimated mean square
		df [1]	*df* [2]	j	k	l	r	
1. Time [T_j]	a-1	**3**	**4**	0	b	c	n	$bcn\sigma^2_j + \sigma^2_n$
2. Zone [Z_k]	b-1	**3**	**3**	a	0	c	n	$acn\sigma^2_k + \sigma^2_n$
3. Depth [D_l]	c-1	**1**	**1**	a	b	0	n	$abn\sigma^2_l + \sigma^2_n$
4. T*Z_{jk}	(b-1)(a-1)	**9**	**12**	0	0	c	n	$cn\sigma^2_{jl} + \sigma^2_n$
5. T*D_{jl}	(c-1)(a-1)	**3**	**4**	0	b	0	n	$bn\sigma^2_{kl} + \sigma^2_n$
6. Z*D_{kl}	(c-1)(b-1)	**3**	**3**	a	0	0	n	$an\sigma^2_{jk} + \sigma^2_n$
7. T*Z*D_{jkl}	(c-1)(b-1)(a-1)	**9**	**12**	0	0	0	n	$n\sigma^2_{jkl} + \sigma^2_n$
8. Error [E_r]	abc(n-1)	**64**	**80**	1	1	1	1	σ^2_n

[1] Degrees of freedom for WUM1 and WUM2 analyses. The error term (Term 8) with 64 degrees of freedom, is the denominator for Terms 1-7.

[2] Degrees of freedom for HGB1, HGB2 and HSB analyses. The error term (Term 8), with 80 degrees of freedom, is the denominator for Terms 1-7.

2.3 Results

2.3.1 Streambed topography

The installation of log structures induced substantial geomorphological change in the WUM study reach (Figure 2.8). One month after the ELJs were installed, a pool approximately 1.4 m deep had scoured next to the bank-attached log jam, but only minor erosion had occurred around both the log sills (Figure 2.8c). Also, a large area of the bed surface of the reach (2528.45 m^2) was slightly lower than the original reach surface, likely due to compaction from the heavy machinery in traversed areas and settling of unconsolidated material in the reworked areas (Figure 2.8c, Table 2.3). The substantial increase in the surface elevation of the right bank was due to backfilling around the log structures (Figure 2.8c). Overall, there was a net increase in reach-scale sediment storage (281.51 m^3) one month after riverworks (Table 2.3).

In contrast, after six months the scour pool around the bank-attached ELJ had filled in, but there was substantial scour around both ELSs and much of the left-hand channel such that most of the surface water flowed down the left channel (Figure 2.8d). While

some of the exported gravel was deposited within the reach – particularly on the central island (Figure 2.8d) – the reach was a net source of sediment with 447.46 m^3 of gravel exported from the reach (Table 2.3). Erosion of the upstream riffle had clearly begun (Figure 2.8d), and continued so that by 12 months after riverworks, enough sediment had eroded to cause structural failure of the upstream ELS (Plate 2.7). Although shallower, the pool extended downstream, scouring both the riffle and head of the central island (Figure 2.8b-d). Long profiles of the thalweg of the right channel demonstrate the increased topographic complexity around the log sills (Figure 2.9). Wetted channel area (at baseflow) decreased initially but then increased to greater than original area (Table 2.4). Although the TRI increased from 1.011 pre-wood to 1.022 six months post-ELJs, this was a small increase of 1.09 % (Table 2.4).

Table 2.3 Area and volume of reach-scale scour and fill at WUM, HGB and the control site HSB one, six and (for Hunter River sites) 12 months after engineered log sills were installed.

Site		Scour		Fill		Net volumetric change (m^3)
		Area (m^2)	Volume (m^3)	Area (m^2)	Volume (m^3)	
WUM	1mo post-ELS	2528.45	374.20	2665.00	655.71	+281.51
	6mo post-ELS	2685.52	871.44	2420.90	705.49	-165.95
HGB	1mo post-ELS	4231.34	401.52	3250.26	147.38	-254.14
	6mo post-ELS	3767.16	447.67	2570.30	140.87	-306.80
	12mo post-ELS	3587.31	447.45	2187.21	143.57	-303.88
HSB	1mo post-ELS	1063.57	1.39	1052.97	1.43	+0.04
	6mo post-ELS	1070.82	7.57	1045.72	6.80	-0.77
	12mo post-ELS	1073.98	8.89	1042.56	6.55	-2.34

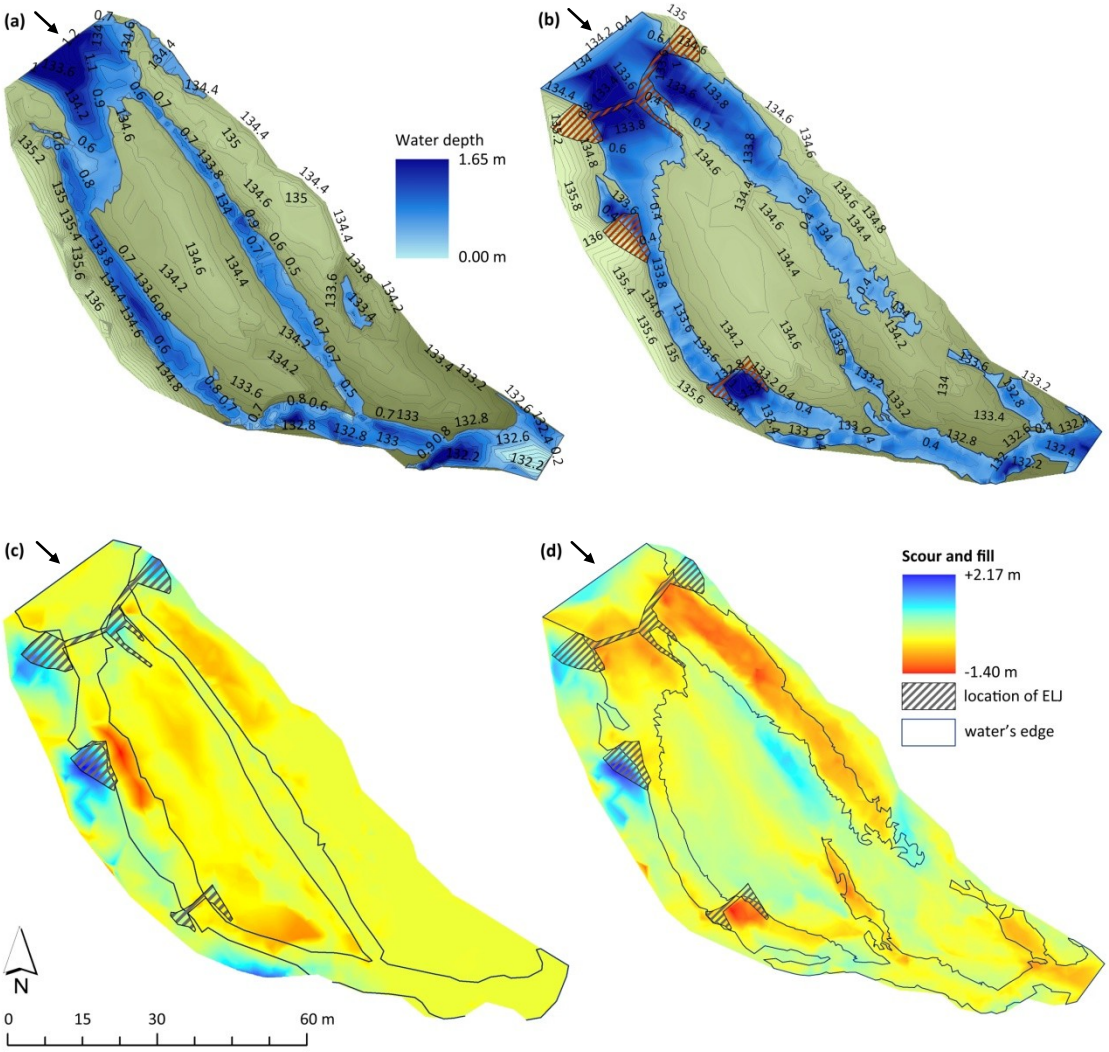

Figure 2.8 Topographic change at the site WUM (Williams R.): **(a)** the DEM of the original reach topography, **(b)** the DEM of the final reach topography (at six months post-ELJ), and the DEMs of Difference at **(c)** one month and **(d)** six months post-ELJ. The arrows show the direction of streamflow through the reach; (a) and (b) share the same scale of water depth, and (c) and (d) share the same scale of scour and fill. DEMs of Difference are comparisons with the original (pre-ELJ) reach topography.

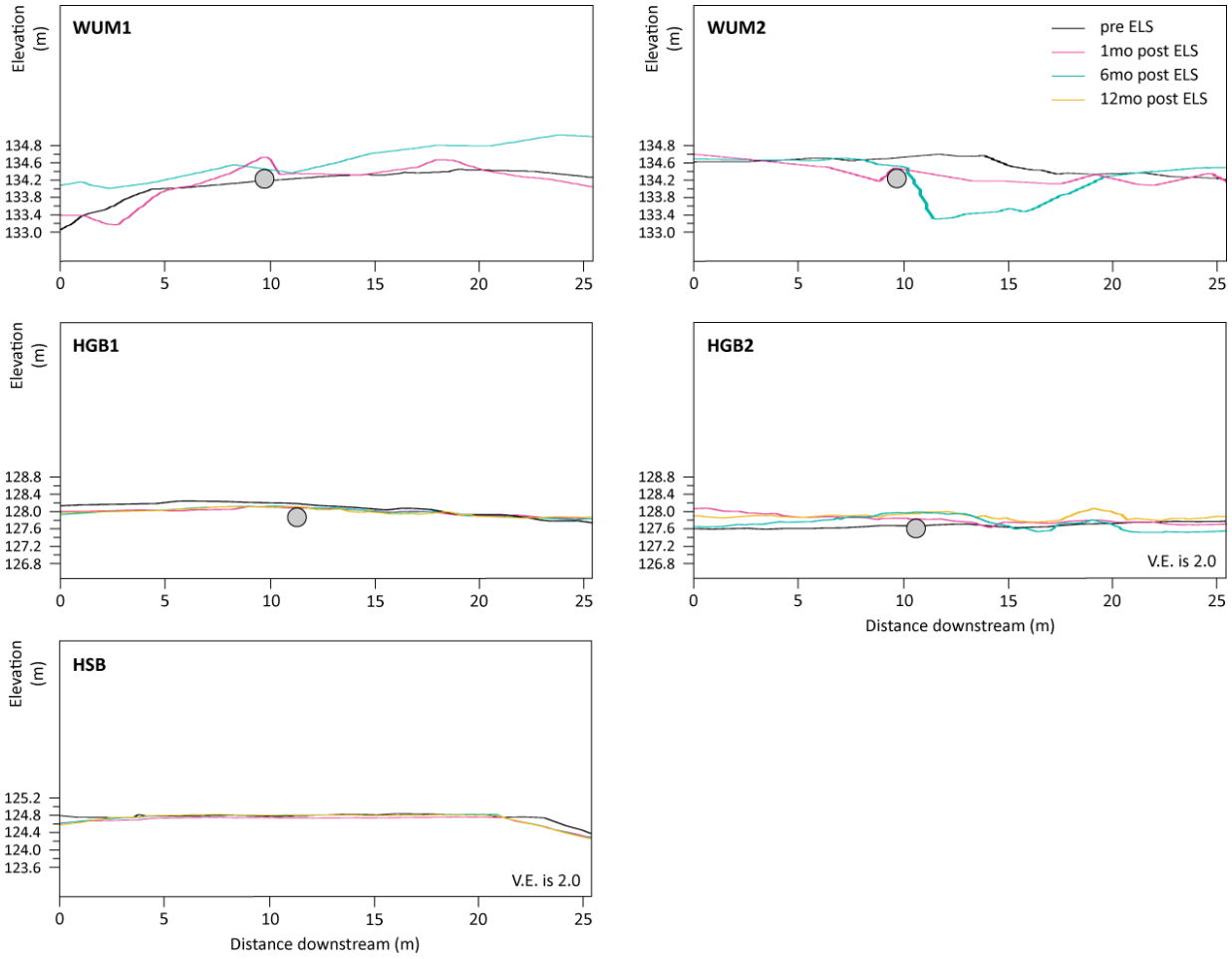

Figure 2.9 Long profiles of the thalwegs of the riffles before and after log sills in the Williams River and Hunter River, and the control riffle in the Hunter River (HSB). V.E. is vertical exaggeration.

Table 2.4 Planimetric and surface area of the wetted channel at baseflow at the two treatment sites WUM and HGB, and the control site HSB, before and after the installation of log sills. The topographic roughness index is the ratio of surface area to planar area and is a measure of roughness or rugosity.

Site	Time	Planimetric area (m^2)	Surface area (m^2)	Topographic roughness index	% increase in TRI from Pre-ELS
WUM	Pre-ELS	1752.35	1771.50	1.011	
	1mo post-ELS	1498.27	1521.88	1.016	0.50
	6mo post-ELS	1883.33	1925.53	1.022	1.09
HGB	Pre-ELS	2559.22	2571.11	1.005	
	1mo post-ELS	2543.61	2583.85	1.016	1.09
	6mo post-ELS	2548.09	2585.49	1.015	1.00
	12mo post-ELS	2553.53	2587.46	1.013	0.80
HSB	Pre-ELS	879.98	889.49	1.011	
	1mo post-ELS	879.73	890.59	1.012	0.10
	6mo post-ELS	879.85	890.86	1.013	0.20
	12mo post-ELS	879.92	891.56	1.013	0.20

Morphological changes were more subtle in the lower gradient Hunter River (HGB, Figure 2.9). At one month after the installation of ELJs, sediment was deposited primarily along the right bank and the riffle downstream of the riverworks (Figure 2.10c). Although scour occurred immediately downstream of the log sills, the plunge pools were narrower and shallower than those that developed in the Williams River. Overall, the Hunter reach was a source of sediment, exporting 254.14 m^3 (Table 2.3). Six months post-ELJs, the unconsolidated sediment at the downstream riffle had been eroded, along with the unconsolidated deposits along the right bank (Figure 2.10d). The lowered bank surface at the bank-attached structure (Figure 2.10d) was likely due to settling rather than scour given the low flows experienced during the study period (Figure 2.5). Both log sills were buried by a shallow layer of sediment and this remained at 12 months post-ELJs (Figure 2.9). Very little sediment was exported from the reach in the six-month period: a net export of 52.66 m^3 (Table 2.3).

There was very little difference at a reach scale between the six and twelve month post-ELJ sampling periods (Figure 2.10d-e). The downstream riffle continued to erode slightly and there was minor erosion around the bank-attached structure (Figure 2.10e). Overall though, the reach stored 2.92 m^3 of gravel (306.80 – 303.88 m^3, Table 2.3). Similar to the Williams River reach, the morphological changes associated with the ELJs resulted in more of the surface flow travelling down the left channel; but there was also a small reduction in wetted area in the Hunter River reach (at baseflow, Table 2.4). Although the installation of ELSs increased the TRI of the channel (from 1.005 to 1.016), this was a very small increase of 1.09 % (Table 2.4). Subsequent erosion and deposition reduced the channel roughness; the 12 month post-ELJ TRI of 1.013 was an increase of 0.80 % from the original channel roughness. However, this increase equalled the TRI at the Hunter control reach, HSB (Table 2.4). Morphological change in HSB was restricted to minor deepening of the thalweg (Figures 2.9, 2.11). At one month post-upstream-ELJs, HSB had a net storage of 0.04 m^3 (Table 2.3); but, six and 12 months after, the control reach exported small amounts of sediment (Table 2.3).

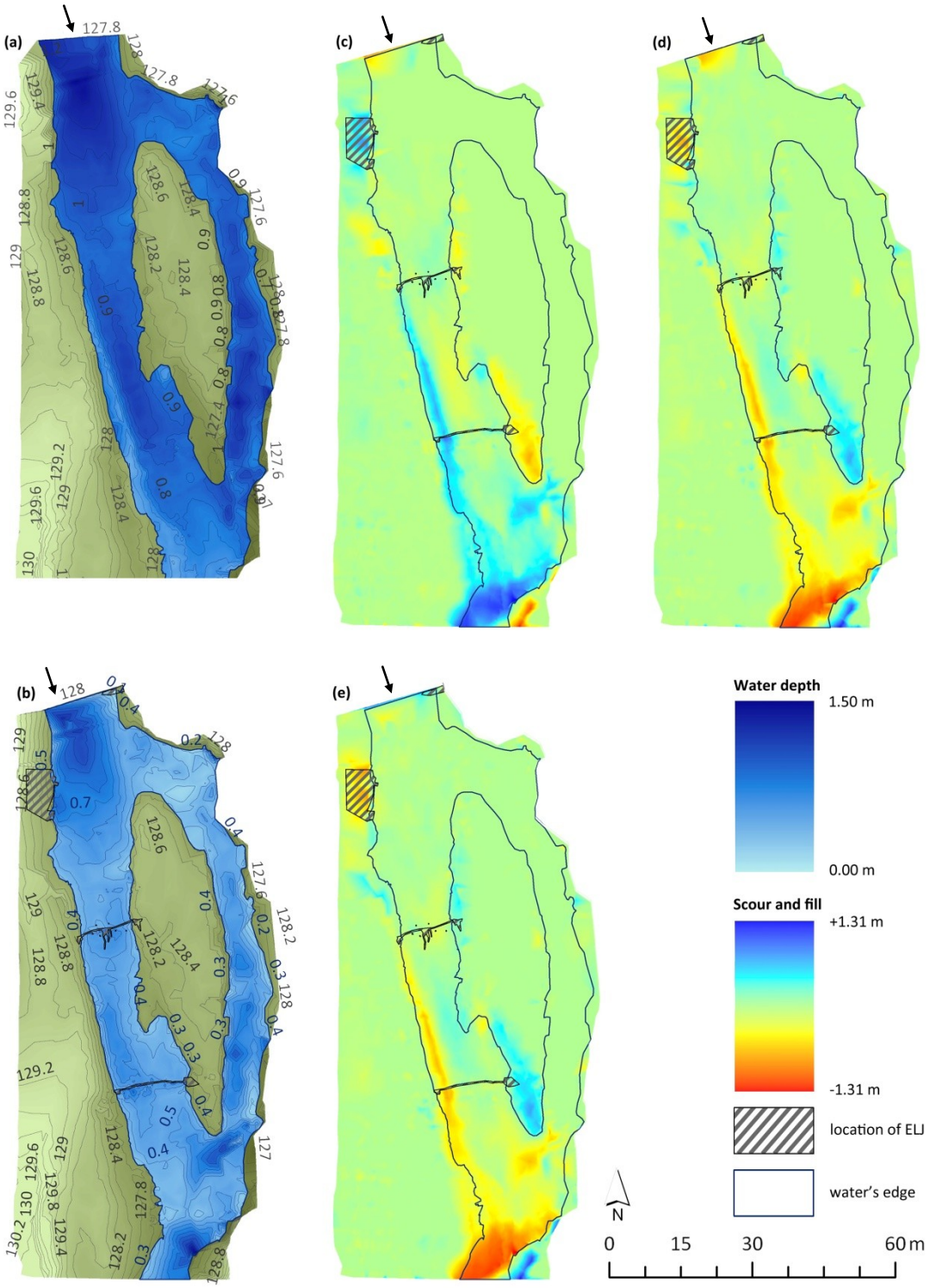

Figure 2.10 Topographic change at the site HGB (Hunter R.): **(a)** the DEM of the original reach topography, **(b)** the DEM of the final reach topography (at 12 months post-ELJ), and the DEMs of Difference at **(c)** one month, **(d)** six months, and **(e)** 12 months post-ELJ. The arrows show the direction of streamflow through the reach; (a) and (b) share the same scale of water depth, and (c), (d) and (e) share the same scale of scour and fill. DEMs of Difference are comparisons with the original (pre-ELJ) reach topography.

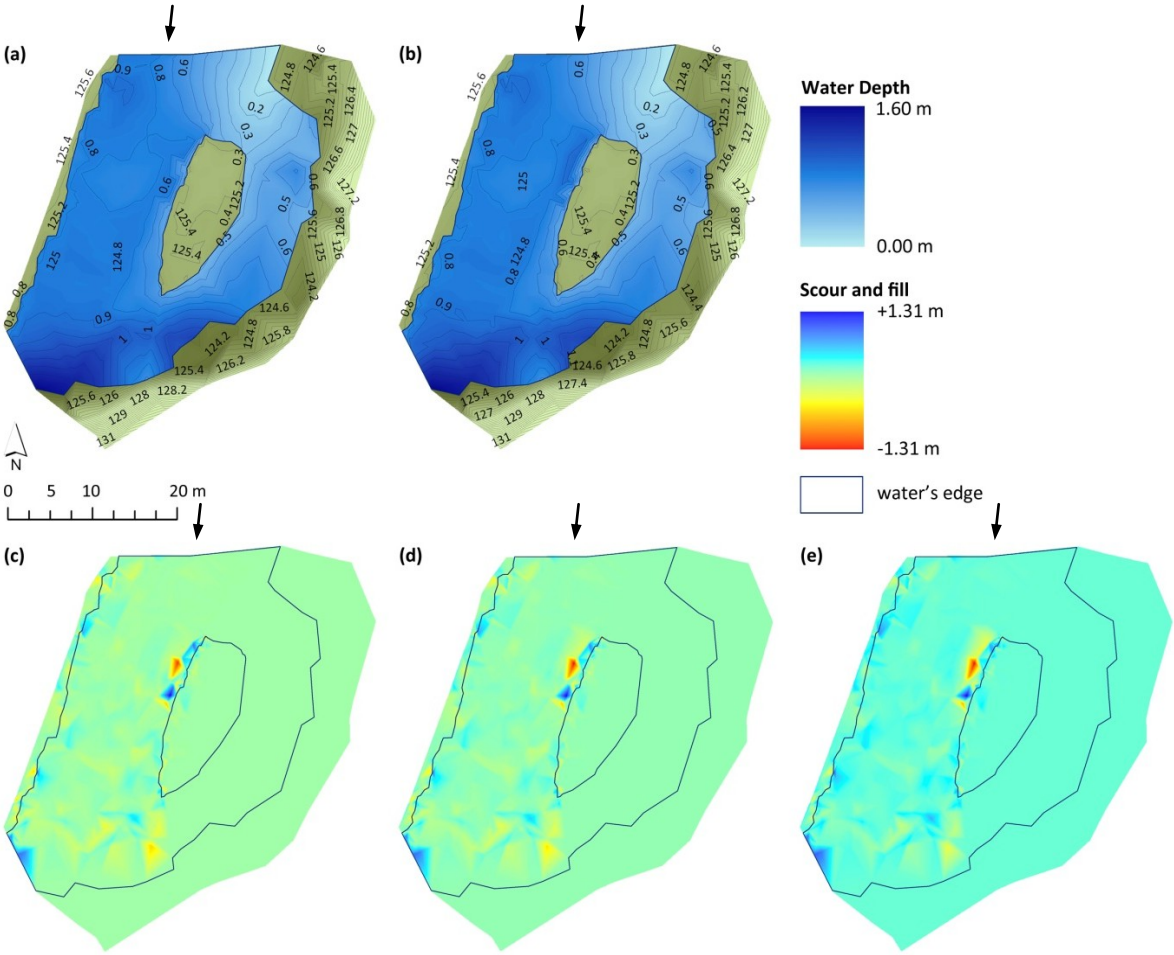

Figure 2.11 Topographic change at the control site HSB (Hunter R.): **(a)** the DEM of the original reach topography, **(b)** the DEM of the final reach topography (at 12 months post-ELJ), and DEMs of Difference at times equivalent to **(c)** one month, **(d)** six months, and **(e)** 12 months post-ELJ at the treatment site (HSB). The arrows show the direction of streamflow through the reach; (a) and (b) share the same scale of water depth, and (c), (d) and (e) share the same scale of scour and fill. DEMs of Difference were calculated using the original (pre-ELJ) reach topography.

2.3.2 Sediment characteristics

The loss of the armour surface layer was the most striking change in sediment characteristics after the installation of log sills at Upper Munni on the Williams River (WUM, Figure 2.12). Along most of the upstream riffle, the cobble armour layer comprised the top 10-cm (the exception was Zone II, where it extended 0-20 cm). Along the downstream riffle, the armour layer increased to 20-cm deep towards the tail of the riffle (i.e. Zones III and IV, Figure 2.12). Before the onset of riverworks, there was clear vertical fining of sediment from cobbles to coarse gravel along both riffles (Figure 2.12). Consequently, Time and Depth explained most of the variance in the ANOVA models of sediment characteristics (Table 2.5).

At the upstream log sill, WUM1, initial d_{50} (mean = 167 mm) was greater than six months post-ELS (mean = 39 mm) which was greater than one month post-ELS (mean = 22 mm, *post hoc* Tukey HSD tests at $p \leq 0.001$). The d_{50} of the surface layer (0-10 cm, mean = 190 mm) was larger than for the subsurface sediment (i.e. 10-50, mean = 42 mm, Table 2.5; *post hoc* Games-Howell tests confirmed 0-10 cm > 10-50 cm and 10-20 cm (mean = 67 mm) > 30-40 cm (mean = 37 mm) at $p \leq 0.05$). However, these ANOVA results must be interpreted within the context of significant Time*Depth and Zone*Depth interactions, both of which confound temporal and depth patterns. *Post hoc* Games-Howell tests (at $p \leq 0.05$) suggest that the significant Time*Depth interaction (Table 2.5) was largely explained by the loss of the armour layer from the bed surface (0-10 cm) with the installation of the log sill, and by the relatively large d_{50} 20-30 cm deep after the installation of the log sill (i.e. one month and six months post-ELS, Figure 2.12). Similarly, the loss of the armour layer explained most of the significant pairwise comparisons of the Zone*Depth interaction (Table 2.5); in most zones, the armour layer extended 0-10 cm, but in Zone II, it extended 0-20 cm.

Clearly, d_{50} is affected by the coarsest fractions (i.e. d_{90}) as well as the finer fractions (i.e. d_{10}). Not surprisingly, ANOVA results were similar for proportions of fine-grained sediment (≤ 1 mm). The proportion of fine-grained sediment increased dramatically one month after the log sill was installed and although levels of fine sediment

decreased afterwards, they still remained above initial levels six months after the installation of the log sill (Table 2.5; Games-Howell tests confirm initial fine sediment (mean = 0.083) was less than six months post-ELS (mean = 0.154) which was less than one month post-ELS (mean = 0.206) at $p \leq 0.05$). With the exception of the coarse 0-10 cm surface layer, the proportion of fine-grained sediment did not differ with depth (Table 2.5). As with d_{50}, interactions among Time, Zone and Depth were significant; however, these explained substantially more of the modelled variance in fine-grained sediment, largely due to the coarser substrate that extended 0-20 cm deep before the onset of riverworks, and the increased fine sediment that was present after the riverworks, particularly at 10-20-cm deep at the head of the riffle and 30-40-cm deep away from the head of the riffle (Table 2.5).

Initial bed sediments were poorly sorted at the surface (0-10 cm layer, mean σ_I = 1.985) and subsurface sediments were very poorly sorted with sorting decreasing with depth (subsurface 10-50 cm, mean σ_I ranged 2.796 at 10-20 cm to 3.141 at 40-50 cm). Although ANOVA results found no significant difference among Times, Zones or Depths, the Time*Depth and Zone*Depth interactions were both significant and explained most of the modelled variance (Table 2.5). *Post hoc* Tukey HSD pairwise comparisons of the Time*Depth interaction (Table 2.5) found only three significant pairs: the initial 30-40-cm layer was more poorly sorted than the initial armour layer (0-10 cm, $p = 0.016$), and the 20-30-cm layer one month ($p = 0.049$) and six months ($p = 0.008$) after the log sill was installed. Although the Zone*Depth interaction (Table 2.5) explained 41.3 % of the modelled variance, only one pairwise comparison was significant: sediments were more poorly sorted at 40-50 cm than at 0-10 cm in Zone I (Tukey HSD $p = 0.035$).

Hyporheic sediments were most porous six months after the ELS were installed (mean = 30.3 %) at WUM1 (Figure 2.13, Table 2.5). Interestingly, the riverworks initially decreased porosity (i.e. one month post-ELS mean = 21.6 % compared with initial mean of 24.2 %), but this was not statistically significant. *Post hoc* Tukey HSD tests found only that porosity six months post-ELS was less than initial porosity ($p = 0.022$) and one-month post-ELS ($p = 0.001$). Porosity did not change with distance along the

flowpath (i.e. Zones, Table 2.5), or depth, although the latter was confounded by a significant Time*Depth interaction that explained most of the modelled variance (52.2 %, Table 2.5). *Post hoc* Tukey HSD pairwise comparisons suggest this was due to the high porosity at 40-50 cm one month after the log sill ($p \leq 0.05$), particularly in Zones I and III (Figure 2.13), and high porosity at 0-10 cm six months after the log sill ($p \leq 0.05$), particularly in Zones I, II and IV. However, these results must be interpreted cautiously given the significant Time*Zone*Depth interaction (Table 2.5).

Although the surface armour layer comprised less fine sediment than subsurface sediment, more of the fine sediment in the surface armour layer was organic (i.e. FBOM, Figure 2.14, Table 2.5; Tukey HSD tests confirm 0-10 cm (mean = 0.637) > 10-50 cm (mean = 0.279) at $p \leq 0.001$). FBOM differed along the riffle flowpath (Table 2.5), with greater FBOM in Zones II and IV (means = 0.440, 0.408) than Zones I and III (means = 0.284, 0.271, respectively; Games-Howell tests at $p \leq 0.05$).

Similar to WUM1, the surface armour layer was disrupted by the installation of the log sill in the downstream riffle WUM2 (Figure 2.12). Median grain size (d_{50}) decreased one month after the log sill was installed (mean = 28 mm), but increased six months post-ELS (mean = 57 mm); however, the final d_{50} was much smaller than before the onset of riverworks (initial mean = 283 mm, Table 2.5; Games-Howell tests confirm initial d_{50} > six months post-ELS > one month post-ELS at $p \leq 0.001$). The armour layer extended 0-10 cm in Zones I and II, increasing to 20-cm deep in Zones III and IV; this pattern was responsible for significant Zone, Depth and Zone*Depth differences. *Post hoc* Tukey HSD tests confirm d_{50} in Zone I (mean = 53 mm) was smaller than in Zone III (mean = 102 mm, $p = 0.001$) and Zone IV (mean = 91 mm, $p = 0.009$; Table 2.5). Generally, d_{50} decreased with depth (Table 2.5); *post hoc* Tukey HSD pairwise comparisons confirm that d_{50} at 0-10-cm deep (mean = 352 mm) was coarser than 10-50-cm deep (mean = 52 mm, $p < 0.001$), and the 10-20-cm layer (mean = 80 mm) was coarser than 20-30 cm (mean = 57 mm, $p = 0.013$) and 40-50 cm (mean = 26 mm, $p = 0.005$). Although the Time*Depth interaction was statistically significant, it explained none of the modelled variance (Table 2.5), and *post hoc* Games-Howell pairwise comparisons confirm that the initial coarse armour layer extending 0-10 cm in Zones I

and II, and 0-20 cm in Zones III and IV explained all significant pairs. The significant Zone*Depth interaction (Table 2.5) was due to coarser d_{50} at 0-10 cm across all zones and finer d_{50} at 40-50 cm in Zones II, III and IV (Tukey HSD tests at $p \leq 0.05$).

Proportions of fine-grained sediment (≤ 1 mm) partly explained the trends seen in d_{50} at WUM2; fine sediment peaked one month post-ELS (mean = 0.174, Figure 2.12), then decreased at six months post-ELS (mean = 0.143), but remained more than twice initial levels (mean = 0.055, Table 2.5; Games-Howell pairwise comparisons confirm initial fine sediment < one month post-ELS and six months post-ELS with $p \leq 0.001$). The proportion of fine sediment increased with depth from 0.065 in the armour layer to 0.191 at 40-50 cm deep (Table 2.5). *Post hoc* Games-Howell tests confirm that the armour layer contained significantly less fine sediment than all deeper layers, and that the 40-50 cm layer contained more fine sediment than the 10-40-cm layers ($p \leq 0.001$). Although zonal differences were statistically significant in the ANOVA model (Table 2.5), *post hoc* Tukey HSD tests found no significant differences among comparisons of pairs. The significant Zone*Depth interaction (Table 2.5) likely masked differences among Zones, and was explained by more fine sediment in subsurface sediments (40-50 cm) than all surface sediment (0-10 cm), and most 10-30-cm deep sediment (Games-Howell tests at $p \leq 0.05$).

Overall, sediments were more poorly sorted at the downstream riffle than the upstream riffle. Sediments were very poorly sorted at WUM2, and sorting decreased more after the installation of the log sill (Table 2.5; Tukey HSD tests confirm the initial σ_I (mean = 3.031) and one month post-ELS (mean = 3.077) < six months post-ELS (mean = 3.344) with $p \leq 0.05$). Most of the modelled variance in sediment sorting was explained by the Time*Depth interaction (Table 2.5), and this is due to the initial surface armour layer (0-20 cm) having a smaller range of grain sizes (i.e. better sorted) than either the initial deeper sediments, or all sediments after the installation of log sills (Games-Howell tests with $p \leq 0.05$).

Hyporheic sediments at WUM2 were slightly less porous than at WUM1 (Figure 2.13). However, as with WUM1, porosity declined immediately after riverworks (mean one

month post-ELS = 20.7 %), and then increased to above initial porosity (mean = 22.8 %) six months post-ELS (mean = 27.7 %, Table 2.5; Games-Howell tests confirm six months post-ELS > one month post-ELS with $p \leq 0.001$). Porosity declined rapidly along the riffle flowpath (Table 2.5); with Zone I (mean = 29.5 %) more porous than Zones II, III or IV (means = 21.8, 20.8, and 22.6 %, respectively; Tukey HSD tests with $p \leq 0.05$). Porosity also decreased with depth (Table 2.5), with 0-10 cm (mean = 28.8 %) more porous than 10-50 cm (means ranging 25.8 – 15.7 %; Tukey HSD tests with $p \leq 0.05$). Although the Time*Depth interaction was statistically significant, it explained very little of the modelled variance (Table 2.5).

Like the upstream riffle, FBOM (≤ 0.250 mm) decreased rapidly with depth (Figure 2.14, Table 2.5). This explained most of the modelled variance (81 %) and *post hoc* Tukey HSD tests confirm that FBOM at 0-10 cm (mean = 0.688) was higher than in 10-50 cm (mean ranges 0.240 – 0.323, $p \leq 0.001$). Although these results must be interpreted cautiously in light of the significant Time*Depth interaction, this interaction term explained little of the modelled variance (Table 2.5). There was also a higher FBOM in Zone I (mean = 0.427) than in Zone II (mean = 0.277; Tukey HSD p = 0.001, Table 2.5).

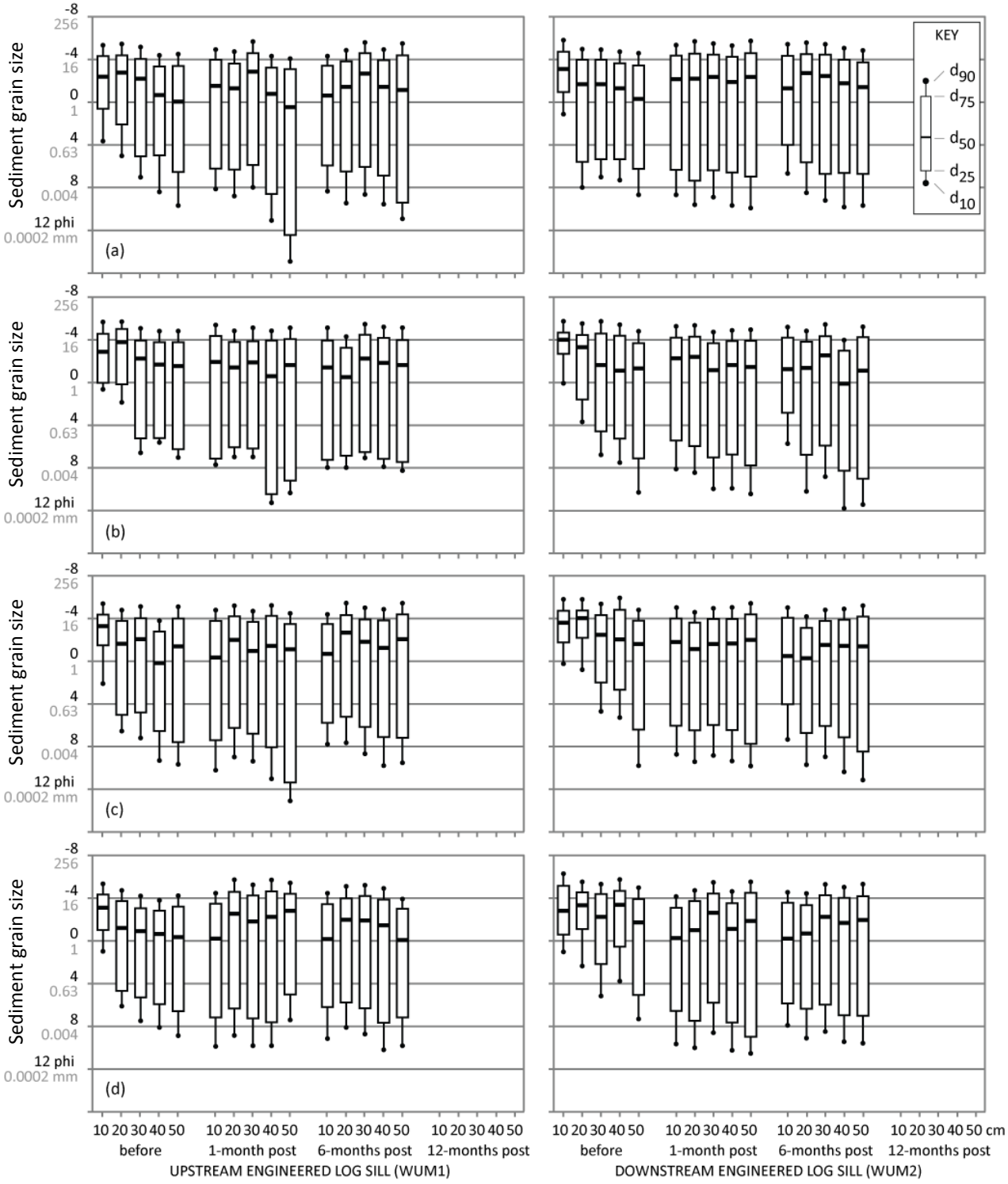

Figure 2.12 Sediment grain size distributions at WUM at five depths (0-50 cm) before and after the installation of engineered log sills. **(a)** Zone I, far upstream of the log sills, **(b)** Zone II, immediately upstream of the log sills, **(c)** Zone III, immediately downstream of the log sills, and **(d)** Zone IV, far downstream of the log sills. Each box-and-whisker combination is the mean of three cores and represents specific grain size fractions as specified in the key, e.g. d_{10} is the grain size at which 10 % of the sample is finer.

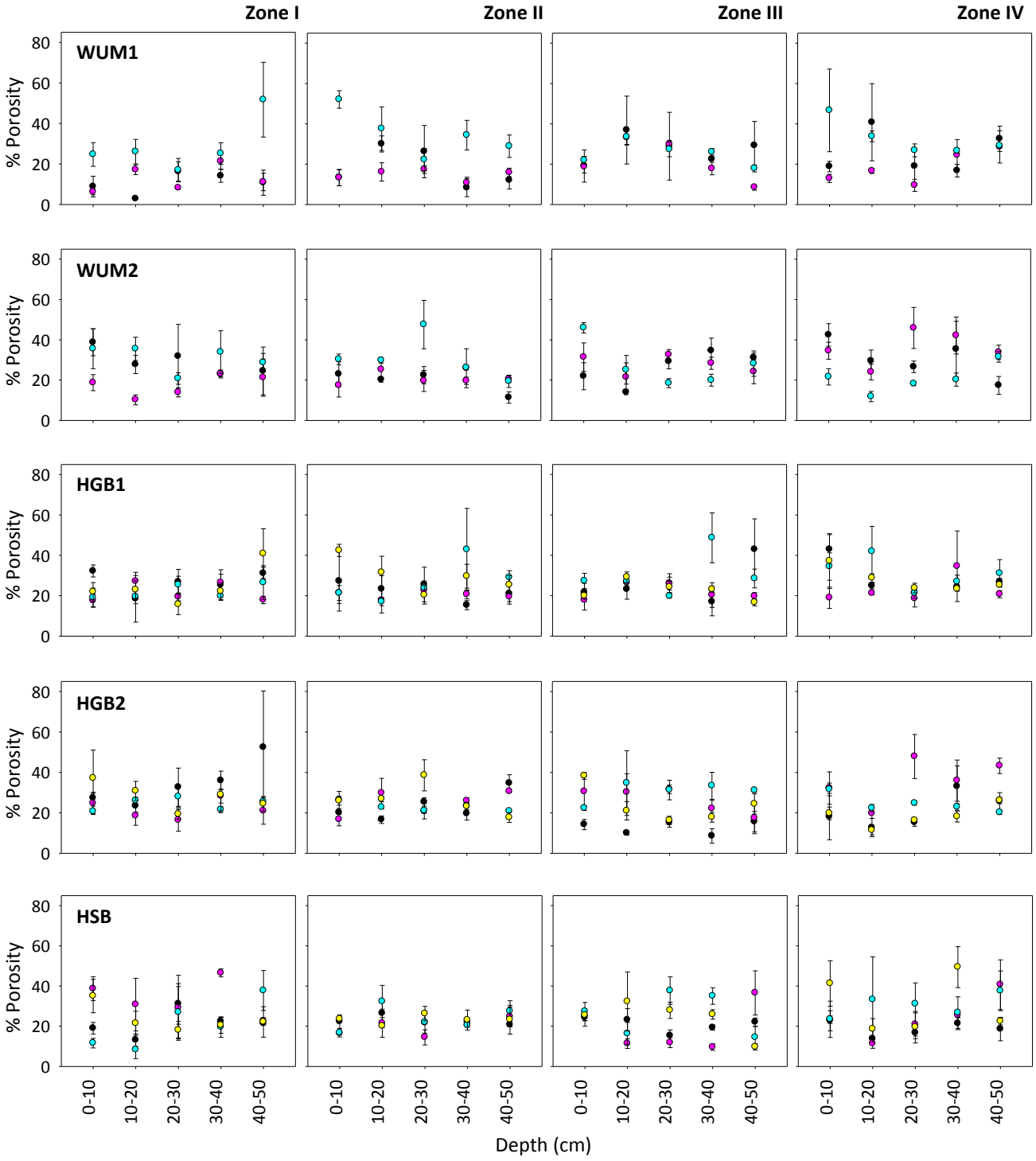

Figure 2.13 Porosity (%, mean ± SEM) at five depths (0-50 cm) before and after the installation of log sills at WUM and HGB, and the control site HSB. Zones I, II, III and IV are far upstream, immediately upstream, immediately downstream and far downstream of the log sills, respectively, or equivalent locations at HSB. Sites are organised along rows and Zones along columns. Freeze-cores were taken before (black fill), and one month (magenta), six months (cyan) and at HGB and HSB, 12 months (yellow) after the installation of log sills or equivalent times at HSB.

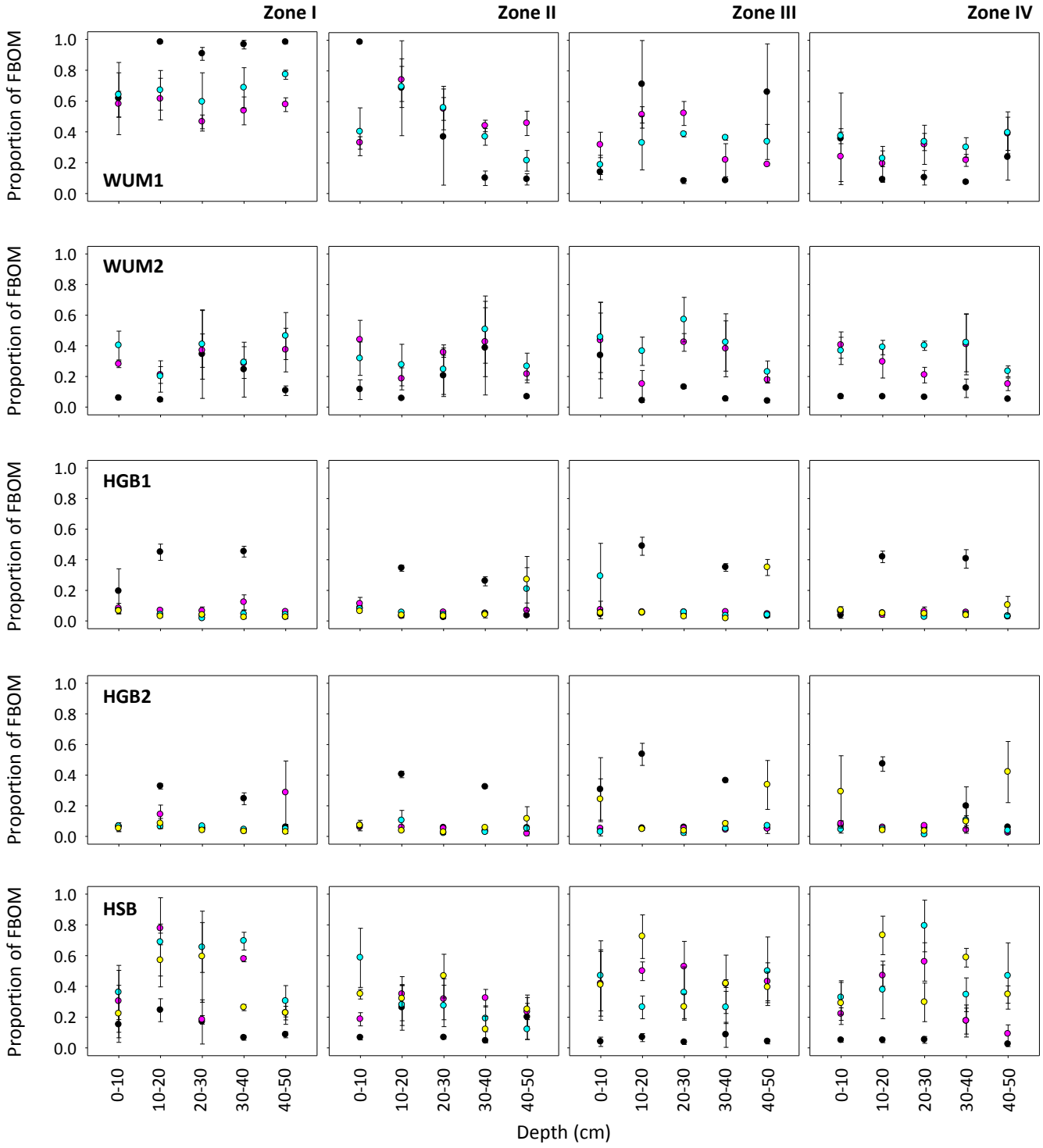

Figure 2.14 The organic proportion (FBOM) of fine sediment ≤ 0.250 mm (mean ± SEM) at five depths (0-50 cm) before and after the installation of log sills at WUM and HGB, and the control site HSB. Zones I, II, III and IV are far upstream, immediately upstream, immediately downstream and far downstream of the log sills, respectively, or equivalent locations at HSB. Sites are organised along rows and Zones along columns. Freeze-cores were taken before (black fill), and one month (magenta), six months (cyan) and at HGB and HSB, 12 months (yellow) after the installation of log sills or equivalent times at HSB.

Table 2.5 ANOVA results of the sediment variables median grain size (d_{50}), proportion of fines, sorting coefficient, porosity, and the proportion of FBOM upstream and downstream of log sills at WUM on the Williams River. VC is variance components (%) and *df* is degrees of freedom. Normality was assessed by the Wilk-Shapiro test (*W*) and equality of variances by Levene's test (*H*, see notes below). Significant *p*-values are bold: all significant *p*-values of heteroscedastic factors (see Notes 2 and 4, below) were supported by nonparametric Kruskal-Wallis tests.

	Source	*df*	-- Median Grain Size (d_{50}) --			---- Proportion of Fines ----			---- Sorting Coefficient -----			---------- Porosity ----------			--- Proportion of FBOM ---		
			F	*p*-value	VC	*F*	*p*-value	VC	*F*	*p*-value	VC	*F*	*p*-value	VC	*F*	*p*-value	VC
WUM1	Time	2	103.165	**<0.001**	47.9	28.119	**<0.001**	38.1	0.980	0.378		7.743	**0.001**	18.7	2.949	0.056	4.8
	Zone	3	2.392	0.072	1.0	1.663	0.179	1.5	0.200	0.896		0.502	0.682		5.314	**0.002**	15.9
	Depth	4	37.940	**<0.001**	34.7	11.975	**<0.001**	30.9	2.229	0.070	15.0	0.758	0.555		15.345	**<0.001**	70.3
	Time*Zone	6	0.901	0.497		0.628	0.708		1.065	0.387	1.2	1.006	0.425	0.1	0.323	0.924	
	Time*Depth	8	3.952	**<0.001**	5.5	2.071	**0.044**	6.1	2.554	**0.013**	38.0	5.707	**<0.001**	52.2	1.615	0.127	6.0
	Zone*Depth	12	4.857	**<0.001**	10.9	3.752	**<0.001**	23.4	2.126	**0.020**	41.3	1.474	0.143	7.9	0.615	0.826	
	Time*Zone*Depth	24	0.857	0.658		0.875	0.634		1.060	0.399	4.4	1.636	**0.044**	21.2	1.105	0.349	3.0
	Error	120									0.1						

	Source	*df*	-- Median Grain Size (d_{50})--			---- Proportion of Fines ----			----- Sorting Coefficient -----			---------- Porosity ----------			---- Proportion of FBOM ----		
			F	*p*-value	VC	*F*	*p*-value	VC	*F*	*p*-value	VC	*F*	*p*-value	VC	*F*	*p*-value	VC
WUM2	Time	2	132.373	**<0.001**	51.4	78.381	**<0.001**	56.8	5.375	**0.006**	14.7	7.088	**0.001**	18.7	5.937	**0.003**	5.6
	Zone	3	6.097	**0.001**	3.0	1.010	0.391		1.287	0.282	1.5	6.563	**<0.001**	25.6	4.985	**0.003**	6.8
	Depth	4	51.192	**<0.001**	39.3	25.740	**<0.001**	36.3	2.337	0.059	9.0	8.285	**<0.001**	44.7	36.864	**<0.001**	81.0
	Time*Zone	6	1.234	0.294	0.3	1.444	0.204	0.9	1.958	0.077	9.7	0.509	0.801		1.867	0.092	3.0
	Time*Depth	8	5.553	**<0.001**		1.514	0.159		4.717	**<0.001**	50.1	3.683	**0.001**		6.489	**<0.001**	3.0
	Zone*Depth	12	3.593	**<0.001**	6.1	2.382	**0.009**	6.0	1.742	0.066	15.0	0.913	0.537		1.436	0.159	
	Time*Zone*Depth	24	1.006	0.465		0.562	0.948		0.844	0.674		1.302	0.177	11.1	0.584	0.936	
	Error	120															0.6

Note 1. No variables were normally distributed at WUM1: **Median Grain Size (d_{50})** $W = 0.982$, $p = 0.021$; **Proportion of Fines** $W = 0.818$, $p < 0.001$; **Sorting Coefficient** $W = 0.974$, $p = 0.002$; **Porosity** $W = 0.888$, $p < 0.001$; and **Proportion of FBOM** $W = 0.868$, $p < 0.001$.

Note 2. Equality of variances at WUM1 were tested using Levene's (*H*) test. The following are the significant *p*-values: **Median Grain Size (d_{50})** $p = 0.004$ (Depth); **Proportion of Fines** $p = 0.016$ (Time) and $p = 0.002$ (Depth); and **Proportion of FBOM** $p = 0.025$ (Zone).

Note 3. No variables were normally distributed at WUM2: **Median Grain Size (d_{50})** $W = 0.945$, $p < 0.001$; **Proportion of Fines** $W = 0.942$, $p < 0.001$; **Sorting Coefficient** $W = 0.977$, $p = 0.004$; **Porosity** $W = 0.945$, $p < 0.001$; and **Proportion of FBOM** $W = 0.908$, $p < 0.001$.

Note 4. Equality of variances at WUM2 were tested using Levene's (*H*) test. The following are the significant *p*-values: **Median Grain Size (d_{50})** $p = 0.009$ (Time); **Proportion of Fines** $p = 0.026$ (Time) and $p = 0.048$ (Depth); **Sorting Coefficient** $p = 0.015$ (Depth); and **Porosity** $p = 0.007$ (Time).

The riffles at the treatment site in the Hunter River, HGB, were comprised of very coarse gravel fining with depth to medium gravel (Figure 2.15). Unlike the two riffles in the Williams River, the riffles at HGB lacked an armour layer (Figure 2.15). However, both riffles were characterized by horizontal stratification, driven primarily by the proportion of fine sediment (i.e. d_{10}), rather than the proportion of coarse sediment (i.e. d_{90}; Figure 2.15). These layers were typically around 10 cm in depth.

At the upstream riffle HGB1, the median grain size d_{50} decreased one month post-ELS (mean = 11 mm), but then increased back to the initial d_{50} (mean = 22 mm at 12 months post-ELS compared to initial mean = 20 mm; Table 2.6,Tukey HSD tests confirm d_{50} one month post-ELS > initial d_{50}, six months- and 12 months post-ELS at $p \leq 0.001$). The significant Time*Zone interaction (Table 2.6) was due to relatively fine sediment (d_{50} mean = 7 mm) in Zone I one month post-ELS and coarse sediment (d_{50} mean = 36 mm) in Zone IV 12 months post-ELS, relative to the overall temporal trend (Tukey HSD tests at $p \leq 0.05$). Most of the modelled variance was explained by the vertical fining of sediment (Table 2.6), and *post hoc* Games-Howell pairwise comparisons confirm that d_{50} at 0-10 cm (mean = 38 mm) was coarser than 10-30 cm (mean = 21 mm) which was coarser than 40-50 cm (mean = 10 mm, at $p \leq 0.05$). However, these results must be interpreted within the context of significant interaction terms. The Time*Depth interaction (Table 2.6) explained 16.0 % of the modelled variance and *post hoc* Games-Howell pairwise comparisons confirm this was due to the presence of a coarse surface layer (mean d_{50} = 66 mm at 0-10 cm) before and six months post-ELS, and relatively fine sediment 30-40 cm and 40-50 cm deep one month post-ELS (mean d_{50} = 7 and 3 mm, respectively). The Zone*Depth interaction (Table 2.6) suggests that differences between Zones were more marked at the head of the riffle (Zone I) due to coarser surface sediment (0-10 cm, mean d_{50} = 49 mm) and relatively finer deep sediment (40-50cm, mean d_{50} = 5 mm).

The influence of fine sediment on the median grain size at HGB1 is demonstrated by the similarity between ANOVA results of d_{50} and the proportion of fine-grained sediments. Fine sediments peaked one month post-ELS (mean = 0.260, Table 2.6). However, it is interesting to note that the proportion of fine sediments decreased six

months post-ELS (mean = 0.155), and final proportions (mean = 0.178) were less than initial proportions (mean = 0.218). *Post hoc* Games-Howell tests confirm more fine sediment was present one month post-ELS than six months and 12 months post-ELS, and that fine sediment at six months post-ELS was less than initial proportions ($p \leq 0.05$). The proportion of fine sediment increased with depth from 0.122 at 0-10-cm deep, to 0.286 at 40-50-cm deep (Table 2.6). *Post hoc* Games-Howell tests confirm less fine sediment at 0-10 cm (mean = 0.122) than 10-50 cm, and less fine sediment at 10-20 (mean = 0.192) and 20-30 cm (mean = 0.187) than 40-50 cm (mean = 0.286, $p \leq 0.05$). However, this must be interpreted cautiously, as the significant Time*Depth interaction may have confounded general patterns (Table 2.6). *Post hoc* Games-Howell tests identified significant pairwise comparisons were due either to relatively low proportions of fine sediment at 0-10 cm initially and 12 months post-ELS, or relatively high proportions of fine sediment initially at 30-40 cm and at 40-50 cm one month post-ELS. *Post hoc* Games-Howell tests identify less fine sediment in surface layers and a high proportion of fine sediment 40-50 cm at the head of the riffle (Zone I), as reasons for the significant Zone*Depth interaction (Table 2.6).

Sediments were very poorly sorted at HGB1, but sorting increased after the installation of the log sill (Table 2.6; Games-Howell tests confirm initial sorting (mean = 2.939) < six months post-ELS and 12 months post-ELS (means = 2.577 and 2.615, respectively, $p \leq 0.05$). Sediment sorting peaked in Zone 1 (mean = 2.471), with sediments better sorted in Zone I than Zone II (mean = 2.743) and Zone III (mean = 2.942; Tukey HSD tests at $p \leq 0.05$, Table 2.6). However, the significant Time*Zone interaction likely confounded patterns and was driven by sediments 20-30 cm deep that were particularly poorly sorted initially (mean = 3.383) and one month post-ELS (mean = 3.226). Sediment sorting decreased with depth, with *post hoc* Tukey HSD tests confirming that sediments were better sorted at 0-10 cm (mean = 2.475) than 20-30 cm (mean = 2.804, $p = 0.031$) and 40-50 cm (mean = 2.901, $p = 0.002$).

Porosity ranged from 15.3 – 40.8 % at HGB1, but only temporal differences were statistically significant (Figure 2.13, Table 2.6), with porosity at one month post-ELS (mean = 21.7 %) less than six months post-ELS (mean 27.6 %, Tukey HSD test p =

0.019). The proportion of FBOM (≤ 0.250 mm) decreased after the riverworks (Figure 2.14, Table 2.6; Games-Howell tests confirm that initial FBOM (mean = 0.189) > one month, six months, and 12 months post-ELS (means = 0.062, 0.066, 0.071, respectively, $p < 0.001$). Interestingly, the strata that contained the most fine sediment (10-20 and 30-40 cm) also contained the highest proportions of FBOM (means = 0.141 and 0.127, respectively, Table 2.6; Games-Howell tests confirm FBOM at 10-20 cm and 30-50 cm > 20-30 cm (mean = 0.041), and 10-20 cm > 0-10 cm (0.089) and 40-50 cm (mean = 0.086, $p \leq 0.05$). However, the differences between the horizontal strata were more pronounced before the riverworks (Table 2.6), with almost all significant *post hoc* Games-Howell tests due to the high organic content initially at 10-20 cm and 30-40 cm (means = 0.425, 0.367, respectively, $p \leq 0.05$). The Time*Zone and Zone*Depth interactions were also statistically significant, but explained very little of the modelled variance (Table 2.6).

Initially, the median grain size (d_{50}) was finer at the downstream log sill HGB2 (mean = 15 mm), than the upstream log sill HGB1 (mean = 20 mm). Sediment was slightly coarser one month post-ELS at HGB2 (mean = 16 mm), with coarser sediments at the downstream than upstream riffles (mean = 11 mm). However, median grain size equalized 12 months post-ELS (mean d_{50} = 22 mm at both riffles). At HGB2, sediments were coarser at 12 months post-ELS than initially ($p = 0.005$) or at six months post-ELS (Tukey HSD tests at $p < 0.001$, Table 2.6). Median grain size increased along the riffle flowpath except for the tail of the riffle (Zone IV mean = 12 mm), which was finer than Zone III (mean = 24 mm; Games-Howell test at $p = 0.001$, Table 2.6). However, most the modelled variance in d_{50} was explained by the horizontal layering of coarse and medium gravels (Table 2.6). *Post hoc* Games-Howell tests confirm d_{50} at 0-10 cm (mean = 28 mm) was coarser than sediments at 10-20 cm (mean = 14 mm, $p < 0.001$), 30-40 cm (mean = 12 mm, $p < 0.001$) and 40-50 cm (mean = 13 mm, $p < 0.001$), and that d_{50} at 20-30 cm (mean = 21 mm) was coarser than 10-20 cm ($p = 0.012$), 30-40 cm ($p = 0.001$) and 40-50 cm ($p = 0.004$). However, these results must be interpreted cautiously in the context of significant Time*Depth and Zone*Depth interactions. *Post hoc* Games-Howell tests of the Time*Depth interaction (Table 2.6) identify all significant pairwise comparisons occur due to four groups; most occur due to the

relatively large d_{50} initially at 20-30 cm (mean = 31 mm) and at 0-10 cm 12 months post-ELS (mean = 88 mm), but a few are due to the relatively small d_{50} initially at 30-40 cm (mean = 8 mm) and the relatively coarse d_{50} at 20-30 cm one month post-ELS (mean = 30 mm). The significant Zone*Depth interaction (Table 2.6) was due to three specific combinations: the relatively large d_{50} 0-10 cm in Zone III (mean = 46 mm), and the relatively small d_{50} in Zone IV at 30-40 cm and 40-50 cm (means = 4 and 7 mm, respectively; Games-Howell tests with $p \leq 0.05$).

In contrast to the upstream riffle HGB1, the proportion of fine sediment (≤ 0.250 mm) at HGB2 was remarkably stable through time, only decreasing 12 months post-ELS (Table 2.6; Tukey HSD tests confirm 12 months post-ELS < initial and one month post-ELS at $p \leq 0.05$). The decrease in fine sediment 12 months post-ELS was most marked in surface sediments (0-10 cm, mean = 0.054, Table 2.6), but proportions of fine sediment varied with depth (Table 2.6), and patterns followed the horizontal layering suggested by median grain size. There was less fine sediment at 0-10 cm (mean = 0.155) than 10-20 cm (mean = 0.216, Tukey HSD test $p = 0.008$), 30-40 cm (mean = 0.250, $p < 0.001$) and 40-50 cm (mean = 0.225, $p = 0.001$), and less fine sediment at 20-30 cm (mean = 0.190) than 30-40 cm ($p = 0.009$). The significant Time*Zone interaction was due to the relatively low proportion of fine sediment initially in Zone III (mean = 0.161) and the relatively high proportion of fine sediment in Zone IV at six months post-ELS (mean = 0.276, *post hoc* Tukey HSD tests of the significant Zone*Depth interaction, Table 2.6) identify the high proportion of fine sediment in Zone IV occurred at 30-40 cm and 40-50 cm depths (means = 0.319, 0.304, respectively).

Sediments were very poorly sorted at HGB2 and although sorting improved after the riverworks, 12 months post-ELS sorting was comparable with initial levels (Table 2.6); *post hoc* Tukey HSD tests confirm sediments initially and at 12 months post-ELS (mean $\sigma_I = 2.971$ and 2.777, respectively) were more poorly sorted than at one month and six months post-ELS (mean $\sigma_I = 2.458$ and 2.496, respectively; $p \leq 0.05$). Sediments were better sorted towards the tail of the riffle i.e. Zones III and IV (means = 2.664 and 2.419, respectively, Table 2.6); and *post hoc* Games-Howell tests confirm sediments

were more poorly sorted in Zone I (mean = 2.717) than Zones II (mean = 2.902, $p < 0.001$) and III ($p < 0.001$), and more poorly sorted in Zone II than Zone IV ($p = 0.023$).

Porosity ranged from 8.5 – 52.4 % at HGB2, but most of the modelled variance was explained by a relatively high initial porosity of 34.4 % at the head of the riffle (Zone I), and one month post-ELS at Zone IV (mean = 35.8 %), and by very low porosity (12.7 %) initially in Zone III (Figure 2.13, Table 2.6). FBOM (≤ 250 μm) declined after the riverworks (Figure 2.14, Table 2.6), and *post hoc* Games-Howell tests confirm that the initial proportion of FBOM (mean = 0.192) was greater than all other times ($p \leq 0.05$, Figure 2.14). Overall, FBOM was constant with depth with the exception of the 20-30 cm layer which, as well as having very little total fine sediment, had relatively less FBOM (Table 2.6, Games-Howell tests confirm 20-30 cm (mean = 0.044) < 10-20 cm or 30-50 cm with $p \leq 0.05$). The Time*Zone and Time*Depth interactions (Table 2.6) provide additional detail on how temporal patterns differed with depth and along the riffle flowpath. FBOM was initially concentrated in Zones II and III, particularly at 10-20 cm and 30-40 cm, but final proportions of FBOM were also high in the deep sediments (40-50 cm) of Zone IV (all *post hoc* Games-Howell tests with $p \leq 0.05$).

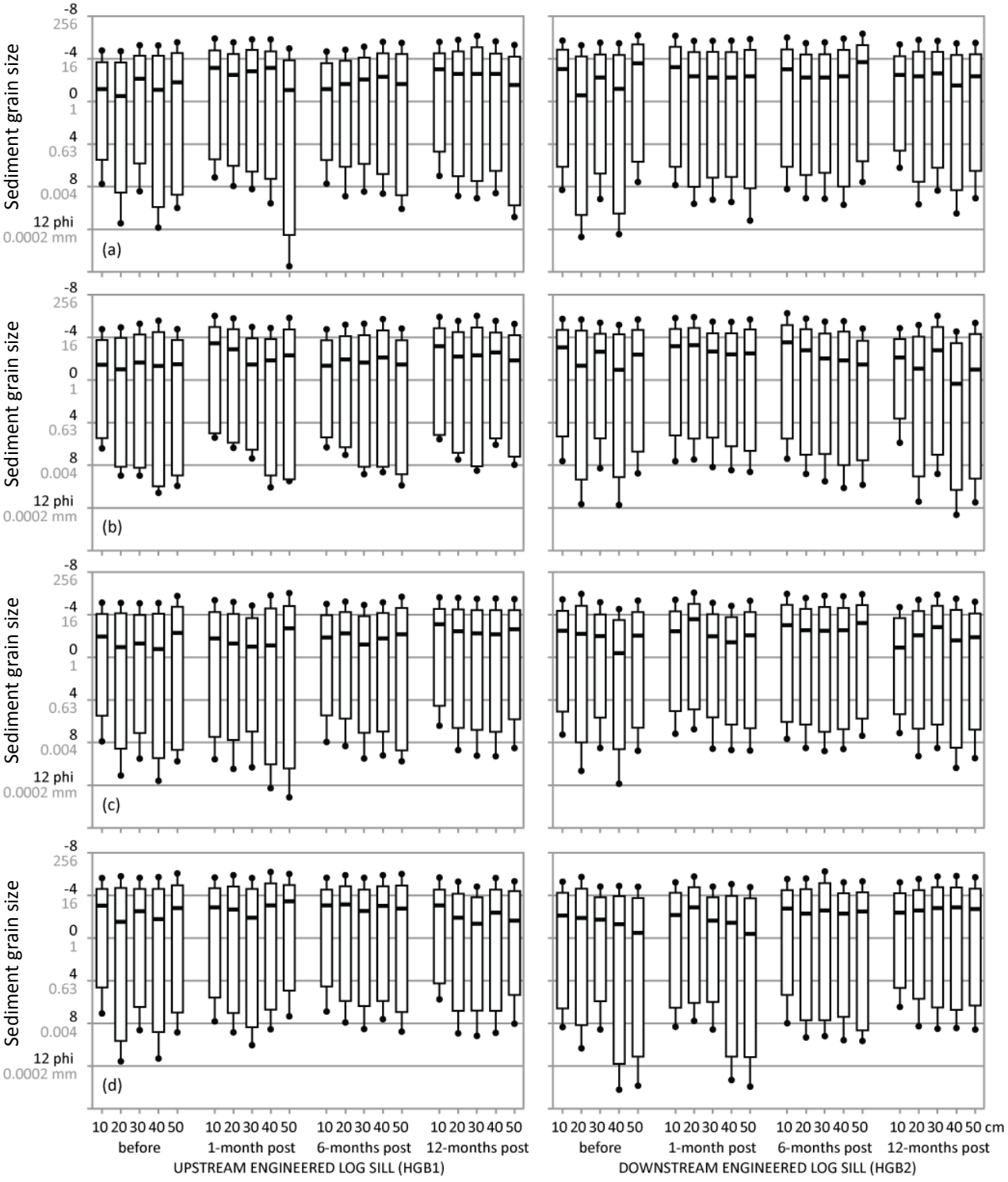

Figure 2.15 Sediment grain size distributions at HGB at five depths (0-50 cm) before and after the installation of engineered log sills. **(a)** Zone I, far upstream of the log sills, **(b)** Zone II, immediately upstream of the log sills, **(c)** Zone III, immediately downstream of the log sills, and **(d)** Zone IV, far downstream of the log sills. Each box-and-whisker combination is the mean of three cores. See Figure 2.12 for the key to box-and-whisker combinations.

Table 2.6 ANOVA results of the sediment variables median grain size (d_{50}), proportion of fines, sorting coefficient, porosity, and the proportion of FBOM upstream and downstream of log sills at HGB on the Hunter River. VC is variance components (%) and *df* is degrees of freedom. Normality was assessed by the Wilk-Shapiro test (*W*) and equality of variances by Levene's test (*H*, see notes below). Significant *p*-values are bold; the underlined *p*-value was not supported by a nonparametric Kruskal-Wallis test ($H = 5.180$, $p = 0.269$, $df = 4$; see Notes 2 and 4, below).

	Source	*df*	-- Median Grain Size (d_{50}) --			---- Proportion of Fines ----			----- Sorting Coefficient -----			--------- Porosity ---------			---- Proportion of FBOM ----		
			F	*p*-value	VC	*F*	*p*-value	VC	*F*	*p*-value	VC	*F*	*p*-value	VC	*F*	*p*-value	VC
HGB1	Time	3	10.443	**<0.001**	13.4	12.877	**<0.001**	19.1	5.118	**0.002**	18.3	3.134	**0.027**	27.4	40.855	**<0.001**	23.8
	Zone	3	0.362	0.780		1.693	0.171	1.1	7.283	**<0.001**	27.9	1.140	0.335	1.8	1.240	0.297	0.1
	Depth	4	26.288	**<0.001**	47.9	19.975	**<0.001**	40.8	3.969	**0.004**	17.6	1.110	0.354	1.9	13.206	**<0.001**	9.7
	Time*Zone	9	3.118	**0.002**	9.0	1.907	0.054	4.3	3.463	**0.001**	32.8	1.018	0.428	0.7	2.149	**0.028**	1.9
	Time*Depth	12	3.825	**<0.001**	16.0	4.275	**<0.001**	21.1	0.777	0.674		1.687	0.074	35.2	25.960	**<0.001**	59.7
	Zone*Depth	12	3.404	**<0.001**	13.7	2.204	**0.014**	7.7	1.164	0.314	2.9	0.976	0.474		2.096	**0.020**	2.5
	Time*Zone*Depth	36	0.827	0.745		1.308	0.133	5.8	1.011	0.462	0.6	1.215	0.207	33.1	1.392	0.086	2.3
	Error	160															
	Source	*df*	--- Median Grain Size (d_{50}) ---			---- Proportion of Fines ----			----- Sorting Coefficient -----			--------- Porosity ---------			---- Proportion of FBOM ----		
			F	*p*-value	VC	*F*	*p*-value	VC	*F*	*p*-value	VC	*F*	*p*-value	VC	*F*	*p*-value	VC
HGB2	Time	3	7.620	**<0.001**	10.8	3.173	**0.026**	4.8	12.563	**<0.001**	45.4	1.962	0.122	4.1	22.499	**<0.001**	28.0
	Zone	3	12.162	**<0.001**	18.2	2.629	0.052	3.5	8.476	**<0.001**	29.3	1.483	0.221	2.1	1.964	0.122	1.2
	Depth	4	13.785	**<0.001**	27.7	7.781	**<0.001**	19.7	2.724	0.031	9.0	1.244	0.295	1.4	7.368	**<0.001**	11.0
	Time*Zone	9	1.199	0.299	1.0	2.594	**0.008**	10.5	1.681	0.098	8.0	6.317	**<0.001**	68.0	2.913	**0.003**	7.4
	Time*Depth	12	4.204	**<0.001**	20.9	4.713	**<0.001**	32.4	1.400	0.171	6.3	1.560	0.108	9.5	10.437	**<0.001**	49.1
	Zone*Depth	12	3.417	**<0.001**	15.7	2.726	**0.002**	15.1	1.132	0.338	2.1	1.047	0.409	0.8	0.543	0.884	
	Time*Zone*Depth	36	1.292	0.144	5.7	1.509	**0.045**	13.4	0.913	0.614		1.276	0.156	14.1	1.236	0.188	3.3
	Error	160						0.6									

Note 1. No variables were normally distributed at HGB1: $\boldsymbol{d_{50}}$ $W = 0.909$, $p < 0.001$; **Proportion of Fines** $W = 0.780$, $p < 0.001$; **Sorting Coefficient** $W = 0.954$, $p < 0.001$; **Porosity** $W = 0.856$, $p < 0.001$; and **Proportion of FBOM** $W = 0.601$, $p < 0.001$.

Note 2. Equality of variances at HGB1 were tested using Levene's (*H*) test. The following are the significant *p*-values: $\boldsymbol{d_{50}}$ $p = 0.015$ (Depth); **Proportion of Fines** $p < 0.001$ (Time) and $p < 0.001$ (Depth); **Sorting Coefficient** $p = 0.002$ (Time); and **Proportion of FBOM s** $p < 0.001$ (Time) and $p = 0.003$ (Depth).

Note 3. No variables were normally distributed at HGB2: $\boldsymbol{d_{50}}$ $W = 0.888$, $p < 0.001$; **Proportion of Fines** $W = 0.873$, $p < 0.001$; **Sorting Coefficient** $W = 0.942$, $p < 0.001$; **Porosity** $W = 0.866$, $p < 0.001$; and **Proportion of FBOM** $W = 0.582$, $p < 0.001$.

Note 4. Equality of variances at HGB2 were tested using Levene's (*H*) test. The following are the significant *p*-values: $\boldsymbol{d_{50}}$ $p = 0.005$ (Zone) and $p = 0.022$ (Depth); **Sorting Coefficient** $p = 0.001$ (Zone) and $p = 0.015$ (Depth); **Porosity** $p = 0.005$ (Time); and **Proportion of FBOM** $p < 0.001$ (Time) and $p = 0.009$ (Depth).

Unlike either of the two treatment riffles on the Hunter River, the control riffle HSB, was characterized by an armour surface layer of cobbles (0-10 cm, mean = 127 mm) overlying coarse gravel (Figure 2.16, Table 2.7, Games-Howell tests confirm d_{50} at 0-10 cm > 10-50 cm with $p < 0.001$). Median grain size increased towards the tail of the riffle, with d_{50} in Zones I (mean = 21 mm) and II (mean = 20 mm) finer than Zones III (mean = 41 mm) and IV (mean = 51 mm; Tukey HSD tests at $p \leq 0.05$, Table 2.7). These two trends – a surface cobble layer and sediment coarsening at the tail of the riffle – explain the significant Zone*Depth interaction (Table 2.7); *post hoc* Games-Howell tests found significant pairs were due to the surface armour layer of cobbles in Zones II, III and IV (means = 120, 232 and 102 mm, respectively), very fine sediments at 30-50 cm in Zone I (mean = 11.5 mm), or coarse sediment at 30-40 cm in Zone IV (mean = 97 mm, $p \leq 0.05$).

The proportion of fine-grained sediment (≤ 1 mm) at HSB increased after the riverworks were completed at the upstream treatment site, HGB (Table 2.7); *post hoc* Tukey HSD tests confirm the initial proportion of fine sediment (mean = 0.148) was less than at one month or six months after upstream riverworks (means = 0.195, $p \leq 0.05$). Fine sediment decreased along the riffle flowpath (Table 2.7), with less fine sediment in Zone IV (mean = 0.137) than either Zone I or II (means = 0.207 and 0.210, respectively, Tukey HSD tests with $p < 0.001$). With the exception of the surface cobble layer that contained little fine sediment (mean = 0.099), there was no variation with depth (Table 2.7; Games-Howell tests at $p < 0.001$). Most of the significant Zone*Depth interaction (Table 2.7) can be explained by differences between the surface armour layer of cobbles and the deeper layers that contain fine sediment. The exception is Zone II, which had relatively more fine sediment 20-50 cm (ranging 0.187 – 0.348).

Sediments were very poorly sorted at the control riffle. Sorting was slightly worse six months after upstream riverworks than initially (Tukey HSD test at $p = 0.026$, Table 2.7). Sorting declined along the riffle flowpath with sediment in Zones I and II (means = 2.716 and 2.618, respectively) better sorted than in Zone IV (mean = 3.049, Tukey HSD test at $p \leq 0.05$, Table 2.7). The significant Zone*Depth interaction (Table 2.7) was due

to the armour layer (0-10 cm) at the head of the riffle (Zone I) being better sorted than all other sediment (Games-Howell tests with $p \leq 0.05$).

Porosity ranged from 8.3 – 49.4 % at the control riffle HSB (Figure 2.13). The relatively high porosity (36.3 %) in the armour layer one month after upstream riverworks explains the significant Time*Depth interaction (Table 2.7). However, the significant Time*Zone*Depth interaction (Table 2.7) accounts for most of the modelled variance and makes interpretation difficult. Likewise, the significant Time*Zone*Depth interaction in the proportions of FBOM (≤ 0.250 mm) confounds interpretation of terms in the ANOVA model (Table 2.7). However, most of the modelled variance (62.8 %) is explained by a large increase in FBOM after the upstream riverworks. Initial proportions of FBOM (mean = 0.099) were considerably less than one month, six months and 12 months after upstream riverworks (means = 0.364, 0.415 and 0.392, respectively; Games-Howell tests at $p < 0.001$, Table 2.7, Figure 2.14), particularly in the surface layer (0-10 cm) of Zone III (mean = 0.569, Games-Howell tests at $p \leq 0.05$, Table 2.7).

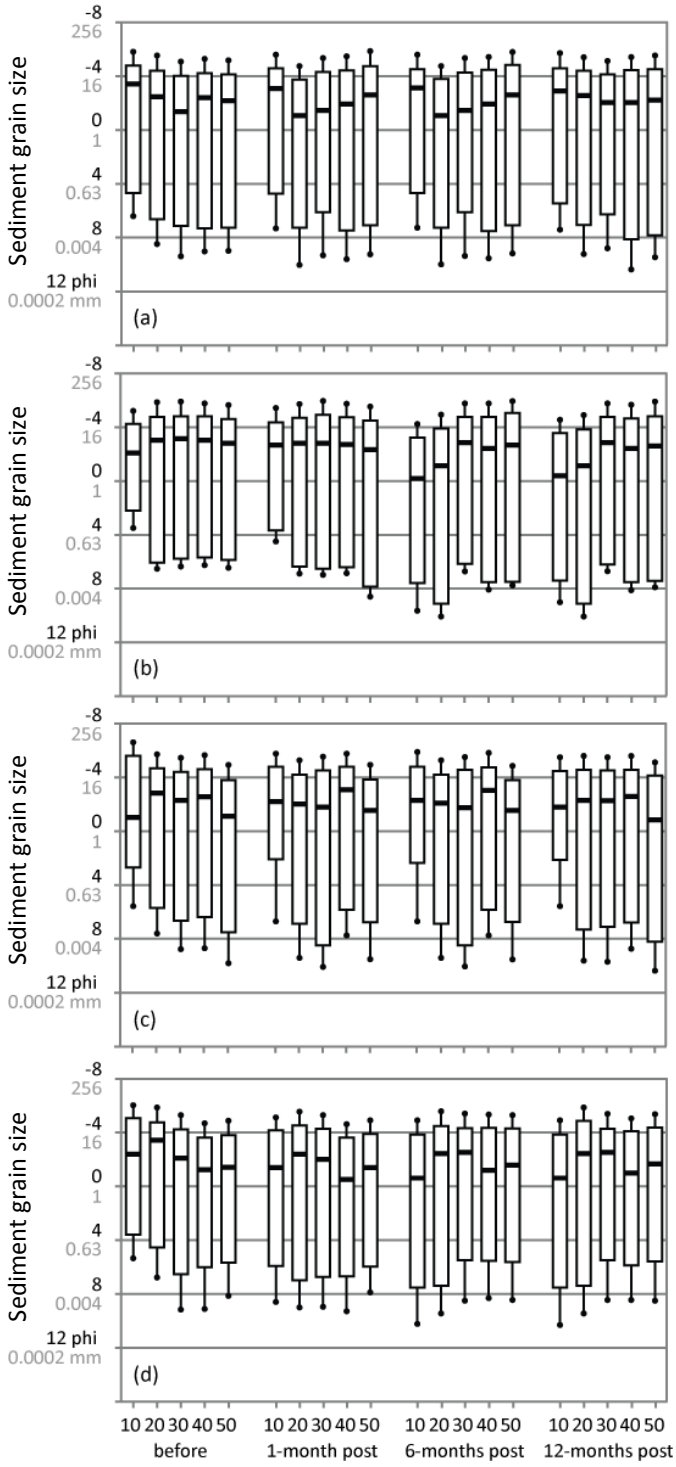

Figure 2.16 Sediment grain size distributions at the control riffle HSB at five depths (0-50 cm) across four zones: **(a)** Zone I, at the head of the riffle, **(b)** Zone II, in the upstream end of the riffle, **(c)** Zone III, towards the downstream end of the riffle, and **(d)** Zone IV, at the tail of riffle (see Figure 2.6 for descriptions of Zones). Each box-and-whisker combination is the mean of three cores. See Figure 2.12 for the key to box-and-whisker combinations.

Table 2.7 ANOVA results of the sediment variables median grain size (d_{50}), proportion of fines, sorting coefficient, porosity, and the proportion of FBOM at the control riffle on the Hunter River, HSB. VC is variance components (%) and *df* is degrees of freedom. Normality was assessed by the Wilk-Shapiro test (*W,* see Note 1 below) and equality of variances by Levene's test (*H*, see Note 2). Significant *p*-values are bold and underlined *p*-values were not supported by nonparametric Kruskal-Wallis tests (see Note 3).

Source	*df*	--- Median Grain Size (d_{50}) ---			----- Proportion of Fines -----			------ Sorting Coefficient ------			---------- Porosity ----------			---- Proportion of FBOM -----		
		F	*p*-value	VC	*F*	*p*-value	VC	*F*	*p*-value	VC	*F*	*p*-value	VC	*F*	*p*-value	VC
Time	3	0.657	0.580		3.472	**0.018**	6.0	2.779	**0.043**	5.6	2.104	0.102	5.8	29.198	**<0.001**	62.8
Zone	3	8.384	**<0.001**	13.5	8.237	**<0.001**	17.7	6.207	**0.001**	16.4	1.887	0.134	4.7	2.075	0.106	2.4
Depth	4	19.173	**<0.001**	44.2	13.083	**<0.001**	39.5	2.731	0.031[1]	7.3	0.432	0.785		3.672	0.007[2]	7.9
Time*Zone	9	0.519	0.859		1.585	0.124	4.1	0.660	0.744		0.730	0.681		0.854	0.567	
Time*Depth	12	0.503	0.911		1.326	0.209	2.9	1.300	0.223	3.8	2.727	**0.002**	36.3	1.310	0.218	2.7
Zone*Depth	12	6.816	**<0.001**	42.4	3.385	**<0.001**	23.1	6.284	**<0.001**	66.7	1.192	0.293	4.0	2.117	**0.018**	9.9
Time*Zone*Depth	36	0.135	>0.999		1.257	0.171	6.7	0.460	0.996		1.782	**0.008**	49.3	1.543	**0.037**	14.3
Error	160									0.2						

Note 1. No variables were normally distributed at HSB: **Median Grain Size (d_{50})** $W = 0.853$, $p < 0.001$; **Proportion of Fines** $W = 0.830$, $p < 0.001$; **Sorting Coefficient** $W = 0.942$, $p < 0.001$; **Porosity** $W = 0.895$, $p < 0.001$; and **Proportion of FBOM** $W = 0.911$, $p < 0.001$.

Note 2. Equality of variances at HSB were tested using Levene's (*H*) test. The following are the significant *p*-values: **Median Grain Size (d_{50})** $p < 0.001$ (Depth); **Proportion of Fines** $p < 0.001$ (Depth); **Sorting Coefficient** $p = 0.019$ (Depth); **Porosity** $p < 0.001$ (Time) and $p = 0.002$ (Depth); and **Proportion of FBOM** $p < 0.001$ (Time) and $p = 0.003$ (Depth).

Note 3. [1]$H = 6.905$, $p = 0.141$, $df = 4$; [2]$H = 5.810$, $p = 0.214$, $df = 4$.

2.3.3 Vertical hydrologic exchange

The installation of log sills at WUM and HGB did increase the magnitude of vertical hydrologic exchange at all sites, but the response varied across zones and with antecedent patterns of surface water–groundwater exchange (Figure 2.17). At WUM1, downwelling increased post-ELS, most notably at the head of the riffle (Zone I) and immediately upstream of the log sill (Zone II, Figure 2.17). The downwelling zone at the tail of the riffle (Zone IV) became an upwelling zone as predicted in the conceptual model (Figure 1.14). Thus, significant Time*Zone interactions explained most of the modelled variance (Table 2.8). *Post hoc* Games-Howell pairwise comparisons of Time*Zone suggest all significant tests are due to increased downwelling in Zones I and II – particularly Zone II – and the creation of an upwelling zone at Zone IV, as described above (Table 2.9). However, the significant Time*Zone*Depth interaction compromises interpretation of the ANOVA results for WUM1 (Table 2.8).

Similar to WUM1, downwelling increased at the head of the riffle (Zones I and II) after the log sill was installed at WUM2 (Figure 2.17). Although upwelling was maintained at the tail of the riffle (Zone IV), downwelling actually decreased immediately downstream of the log sill (Zone III, Figure 2.17). Although Zone was statistically significant and explained most of the modelled variance (Table 2.8), *post hoc* Games-Howell tests found no significant pairwise comparisons between Zones, likely because the significant Time*Zone and Zone*Depth interactions masked factor-level patterns. *Post hoc* Games-Howell tests of Time*Zone (Table 2.8) confirm the difference between downwelling and upwelling zones across all times, the increased downwelling in Zones I and III post-ELS, and to a lesser extent, the decrease in downwelling at Zone III post-ELS (Table 2.9).

At the Hunter River treatment site HGB, initial VHGs were weak across both riffles, i.e. both downwelling and upwelling zones (Figure 2.17). With the installation of log sills, downwelling increased dramatically across Zones I-III at both riffles (Figure 2.17, Table 2.8). Although the downwelling zone at the tail of the riffle at HGB1 (Zone IV) was converted to an upwelling zone with the installation of the log sill, upwelling at both

log sills remained weak, with the exception of one month post-ELS at HGB2 (Figure 2.17). Although Time and Zone were statistically significant and explained substantial variance in the ANOVA model of HGB1 (29.6 and 35.1 %, respectively), it is the significant Time*Zone interaction (Table 2.8) that is of interest, as *post hoc* tests of this interaction confirms the patterns described above (i.e. downwelling *v* upwelling zones, the increase in downwelling in Zones I-III post-ELS, and the conversion of Zone IV from down- to up-welling, Table 2.9). Similarly, the Time*Zone interaction at HGB2 (Table 2.8) confirms the maintenance of upwelling in Zone IV, albeit with a peak one month after the installation of the log sill, and the increase in downwelling in Zones I-III post-ELS (Table 2.9). However, interpretation of the ANOVA model for HGB2 is confounded by the statistical significance of most factors and all interactions (Table 2.8).

In contrast to the antecedent weak downwelling in the riffles at HGB, downwelling was consistently stronger at the control site, HSB (Figure 2.17). VHGs changed little over time at HSB, with differences among Zones explaining most of the modelled variance (Table 2.8). *Post hoc* Games-Howell tests found no significant differences between any pair of Zones, but these were likely masked by the significant Time*Zone interaction (Table 2.8), that was largely driven by differences between down- and up-welling zones, but also due to the strong downwelling in Zones II and III one month post-ELS that were statistically greater than downwelling in Zones I-III at different times (Figure 2.17, Table 2.10).

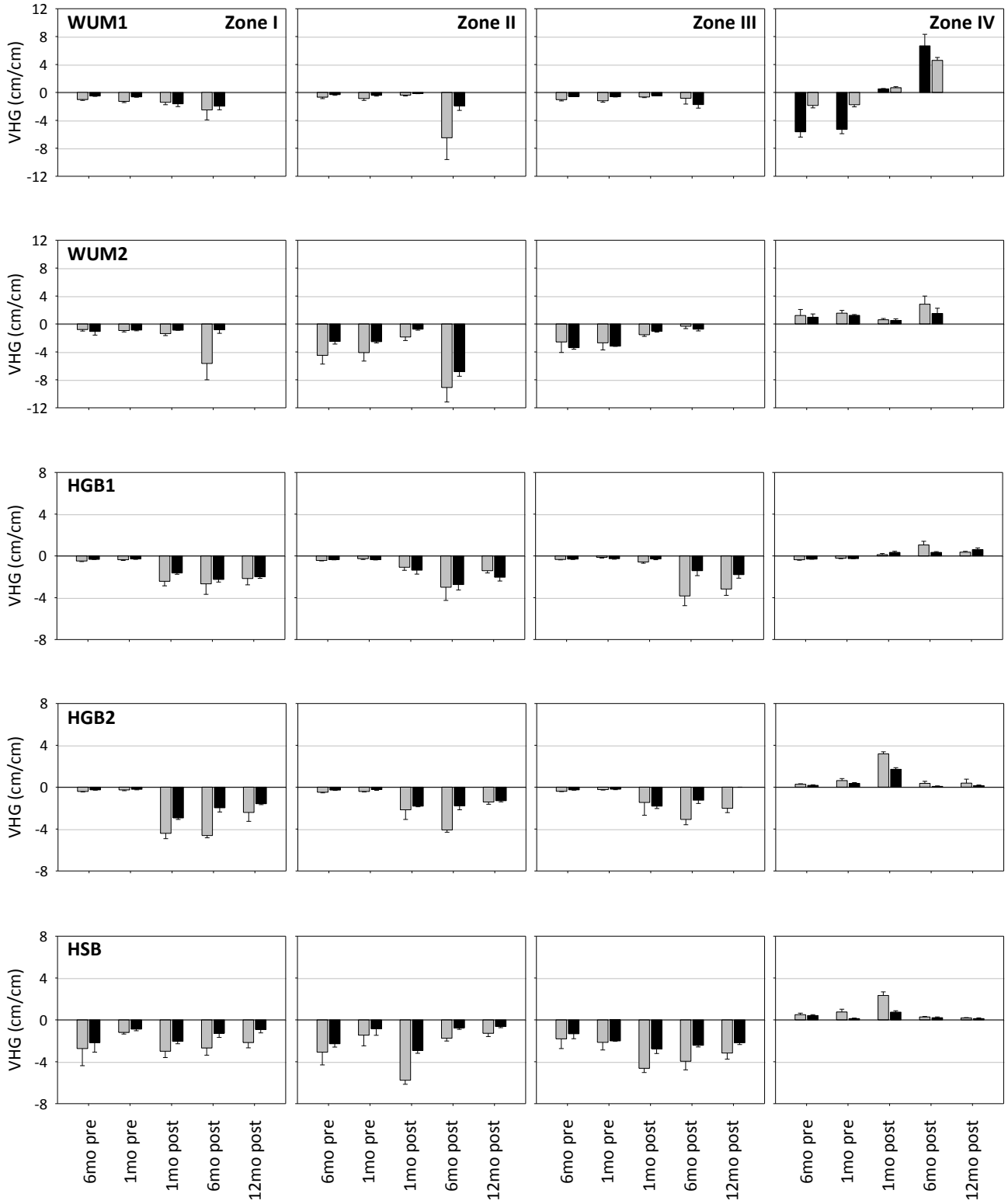

Figure 2.17 Vertical hydraulic gradients (VHG, mean ± SEM) before and after the installation of log sills at WUM and HGB, and the control site HSB. Zones I, II, III and IV are far upstream, immediately upstream, immediately downstream and far downstream of the log sills, respectively, or equivalent locations at HSB. Sites are organised along rows and Zones along columns. Grey and black fills are 20 and 40 cm depths, respectively. Note the scales change on the *y*-axes.

Table 2.8 ANOVA and nonparametric tests of vertical hydraulic gradients (VHG) upstream and downstream of log sills at WUM and HGB, and the control riffle at HSB. MS is Mean Squares, *df* is degrees of freedom and VC is variance components (%). Normality was assessed by the Wilk-Shapiro test (*W*) and equality of variances by Levene's test (*H*). Significant *p*-values are bold and underlined *p*-values are not supported by nonparametric tests. [1] Kruskal-Wallis (*H*) test (*df* = 3), [2] Mann-Whitney (*U*) test (*df* = 1), [3] *H* test (*df* = 4).

	WUM1 (Upstream LS)							**WUM2 (Downstream LS)**					
Source	ANOVA					Nonparametric tests		ANOVA				Nonparametric tests	
	df	MS	*F*	*p*	VC	*test*	*p*	MS	*F*	*p*	VC	*test*	*p*
Time	3	8.063	4.717	**0.005**	4.0	9.521[1]	**0.023**	10.066	5.071	0.003	4.5	1.353[1]	0.717
Zone	3	6.780	3.966	0.012	3.2	4.566[1]	0.206	115.271	58.068	**<0.001**	63.0	63.288[1]	**<0.001**
Depth	1	15.376	8.994	0.004	2.9	929.500[2]	0.103	6.982	3.517	0.065	0.9		
Time*Zone	9	44.260	25.889	**<0.001**	81.1			18.402	9.270	**<0.001**	27.4		
Time*Depth	3	2.092	1.224	0.308	0.2			1.707	0.860	0.467			
Zone*Depth	3	2.715	1.588	0.201	0.6			7.269	3.662	**0.017**	2.9		
Time*Zone*Depth	9	5.825	3.407	**0.002**	7.8			2.745	1.383	0.215	1.3		
Error	64	1.710						1.985					

	HGB1 (Upstream LS)							**HGB2 (Downstream LS)**					
	ANOVA					Nonparametric tests		ANOVA				Nonparametric tests	
	df	MS	*F*	*p*	VC	*test*	*p*	MS	*F*	*p*	VC	*test*	*p*
Time	4	10.916	25.377	**<0.001**	29.6	21.945[3]	**<0.001**	15.603	45.625	**<0.001**	22.3	21.738[3]	**<0.001**
Zone	3	17.024	39.575	**<0.001**	35.1	53.106[1]	**<0.001**	39.576	115.723	**<0.001**	42.9	69.247[1]	**<0.001**
Depth	1	1.651	3.838	0.054	0.9			6.966	20.368	<0.001	2.4	1513.500[2]	0.133
Time*Zone	12	4.061	9.442	**<0.001**	30.7			5.697	16.657	**<0.001**	23.4		
Time*Depth	4	0.348	0.808	0.524				2.911	8.511	**<0.001**	3.7		
Zone*Depth	3	1.340	3.116	**0.031**	1.9			3.282	9.597	**<0.001**	3.2		
Time*Zone*Depth	12	0.646	1.501	0.141	1.8			0.795	2.326	**0.013**	2.0		
Error	80	0.430						0.342					

	HSB (Control Riffle)						
	ANOVA					Nonparametric tests	
	df	MS	*F*	*p*	VC	*test*	*p*
Time	4	5.585	6.322	<0.001	6.9	6.843[3]	0.144
Zone	3	60.672	68.679	**<0.001**	66.1	70.939[1]	**<0.001**
Depth	1	12.545	14.201	<0.001	4.3	1508.500[2]	0.126
Time*Zone	12	5.122	5.798	**<0.001**	18.7		
Time*Depth	4	0.846	0.957	0.436			
Zone*Depth	3	4.429	5.013	**0.003**	3.9		
Time*Zone*Depth	12	0.740	0.838	0.612			
Error	80	0.883					

Tests of normality (W) and equal variances (H)					
	WUM1	WUM2	HGB1	HGB2	HSB
W test	0.743	0.902	0.846	0.825	0.936
p (*W*)	**<0.001**	**<0.001**	**<0.001**	**<0.001**	**<0.001**
H test	5.961	4.424	6.138	7.307	4.365
p (*H*)	**<0.001**	**<0.001**	**<0.001**	**<0.001**	**<0.001**
--- *p*-values of among-group heterogeneity (*H* test) ---					
Time	**<0.001**	**<0.001**	**<0.001**	**<0.001**	**0.007**
Zone	**<0.001**	**0.006**	**0.027**	**0.006**	**0.004**
Depth	**<0.001**	**0.003**	**0.003**	**<0.001**	**<0.001**

Table 2.9 Significant *p*-values of *post hoc* Games-Howell tests of the Time*Zone interactions of VHGs at WUM1 and WUM2 (top half, above and below grey squares), and at HGB1 and HGB2 (bottom half, above and below grey squares), respectively.

		6mo pre-ELS				1mo pre-ELS				1mo post-ELS				6mo post-ELS			
		ZI	ZII	ZIII	ZIV	ZI	ZII	ZIII	ZIV	ZI	ZII	ZIII	ZIV	ZI	ZII	ZIII	ZIV
6mo pre	ZI				0.016				0.038						0.002		<0.001
	ZII				0.005				0.013						0.001		<0.001
	ZIII				0.018				0.044						0.003		<0.001
	ZIV		<0.001	<0.001		0.034	0.010	0.028			0.002	0.007	<0.001				<0.001
1mo pre	ZI														0.005		<0.001
	ZII				<0.001				0.024						0.001		<0.001
	ZIII				0.001										0.004		<0.001
	ZIV		<0.001	<0.001			<0.001	<0.001			0.005	0.017	<0.001				<0.001
1mo post	ZI																<0.001
	ZII														<0.001		<0.001
	ZIII														0.001		<0.001
	ZIV		0.001	0.005			0.001	0.006						0.031	<0.001		<0.001
6mo post	ZI				<0.001				<0.001				0.002				<0.001
	ZII	<0.001	<0.001	<0.001	<0.001	<0.001	<0.001	<0.001	<0.001	<0.001	<0.001	<0.001	<0.001	<0.001		0.021	<0.001
	ZIII		0.041												<0.001		<0.001
	ZIV	0.025	<0.001	<0.001		0.027	<0.001	<0.001		0.012	0.005	0.007		<0.001	<0.001		

		6mo pre-ELS				1mo pre-ELS				1mo post-ELS				6mo post-ELS				12mo pre-ELS			
		ZI	ZII	ZIII	ZIV	ZI	ZII	ZIII	ZIV	ZI	ZII	ZIII	ZIV	ZI	ZII	ZIII	ZIV	ZI	ZII	ZIII	ZIV
6mo pre	ZI									0.007				<0.001	<0.001	<0.001		0.004		<0.001	
	ZII									0.006				<0.001	<0.001	<0.001		0.004		<0.001	
	ZIII									0.003				<0.001	<0.001	<0.001		0.002		<0.001	
	ZIV									0.004				<0.001	<0.001	<0.001		0.002	0.049	<0.001	
1mo pre	ZI									0.003				<0.001	<0.001	<0.001		0.002	0.046	<0.001	
	ZII									0.003				<0.001	<0.001	<0.001		0.002	0.039	<0.001	
	ZIII									0.001				<0.001	<0.001	<0.001		0.001	0.016	<0.001	
	ZIV									0.001				<0.001	<0.001	<0.001		0.001	0.021	<0.001	
1mo post	ZI	<0.001	<0.001	<0.001	<0.001	<0.001	<0.001	<0.001	<0.001			0.009	<0.001				<0.001				<0.001
	ZII	0.001	0.001	0.001	<0.001	<0.001	0.001	<0.001	<0.001	0.001			0.031		0.006	0.046	<0.001				0.003
	ZIII	0.028	0.042	0.025	<0.001	0.011	0.025	0.009	<0.001	<0.001				<0.001	<0.001	<0.001		0.006		<0.001	
	ZIV	<0.001	<0.001	<0.001	<0.001	<0.001	<0.001	<0.001	<0.001	<0.001	<0.001	<0.001		<0.001	<0.001	<0.001		<0.001	<0.001	<0.001	
6mo post	ZI	<0.001	<0.001	<0.001	<0.001	<0.001	<0.001	<0.001	<0.001		0.028	0.001	<0.001				<0.001				<0.001
	ZII	<0.001	<0.001	<0.001	<0.001	<0.001	<0.001	<0.001	<0.001			0.030	<0.001				<0.001				<0.001
	ZIII	<0.001	<0.001	<0.001	<0.001	<0.001	<0.001	<0.001	<0.001	0.004			<0.001				<0.001				<0.001
	ZIV									<0.001	<0.001	<0.001	<0.001	<0.001	<0.001	<0.001		<0.001	<0.001	<0.001	
12mo post	ZI	0.001	0.001	0.001	<0.001	<0.001	0.001	<0.001	<0.001	0.001			<0.001	0.030			<0.001				<0.001
	ZII				0.002				<0.001	<0.001			<0.001	<0.001	0.002		0.002				<0.001
	ZIII								0.004	<0.001			<0.001	<0.001	<0.001						<0.001
	ZIV									<0.001	<0.001	<0.001	<0.001	<0.001	<0.001	<0.001		<0.001	0.001	0.037	

Table 2.10 The *p*-values of significant *post hoc* Games-Howell pairwise comparisons of the Time*Zone interactions accounting for 18.7 % of variance in VHGs at HSB.

		6mo pre-ELS				1mo pre-ELS				1mo post-ELS				6mo post-ELS				12mo pre-ELS			
		ZI	ZII	ZIII	ZIV	ZI	ZII	ZIII	ZIV	ZI	ZII	ZIII	ZIV	ZI	ZII	ZIII	ZIV	ZI	ZII	ZIII	ZIV
6mo pre	ZI				<0.001				<0.001				<0.001				0.001				0.001
	ZII				<0.001				<0.001				<0.001				<0.001				<0.001
	ZIII				0.041				0.046		<0.001	0.024	<0.001								
	ZIV							0.002		<0.001	<0.001	<0.001		0.004		<0.001		0.048		<0.001	
1mo pre	ZI										<0.001	0.001	0.001			0.021					
	ZII										<0.001	0.002	0.001			0.039					
	ZIII								0.002		0.010		<0.001				0.007				0.013
	ZIV									<0.001	<0.001	<0.001		0.004		<0.001				<0.001	
1mo post	ZI												<0.001				<0.001				0.001
	ZII												<0.001	0.005	<0.001		<0.001	<0.001	<0.001		<0.001
	ZIII												<0.001		0.004		<0.001	0.020	<0.001		<0.001
	ZIV													<0.001	<0.001	<0.001		<0.001	0.002	<0.001	
6mo post	ZI																0.014				0.023
	ZII																				
	ZIII																<0.001		0.013		<0.001
	ZIV																			<0.001	
12mo post	ZI																				
	ZII																				
	ZIII																				<0.001
	ZIV																				

2.4 Discussion

The first hypothesis was that log sills increase topographic complexity at the local scale, predicted to occur via the mechanisms of channel steepening from sediment deposited immediately upstream of the log sill, the formation of a scour pool immediately downstream of the log sill and an unconsolidated dune formed from the pool deposits downstream of the scour pool (Figure 1.14). Several metrics suggest that topographic complexity increased after the log sills were installed. Sediments were deposited upstream of all log sills except the upstream log sill on the Hunter River, HGB1. Similarly, dunes were created downstream of all log sills except HGB1. In contrast, the size, location, depth and persistence of the scour pools varied greatly among log sills, even within the same river; generally though, the scour pools were deeper and wider in the Williams River than the Hunter River.

There are several reasons for the greater magnitude of elevation change and resulting topographic complexity in the Williams River than in the Hunter River. Firstly, flow regimes are very different between the unregulated Williams River and larger, regulated Hunter River. In the Williams River, mean daily low flow was 0.93 $m^3 s^{-1}$ and the reach experienced four small floods between 10-20 $m^3 s^{-1}$ during the six months after construction. In contrast, mean daily low flow in the Hunter River was 4.77 $m^3 s^{-1}$ and while there was only one substantial flood during the study period, there were sustained periods of above baseflows due to dam releases. In their previous work on the Williams River, Brooks and co-workers (2006) found the larger floods created the greatest topographic complexity while smaller floods reworked sediments, smoothing and masking the effects of the larger floods. It is likely that the dam releases were sufficient to rework the unconsolidated gravels in the Hunter River. Secondly, flume studies have shown that scour depth is related to sediment sorting irrespective of clast size (Marion *et al.* 2004), and sediments were slightly better sorted in the Williams River than Hunter River. Furthermore, field surveys indicate the scour in the plunge pool downstream of steps contributes most of the step-induced increase in geomorphic complexity (i.e. more important than the upstream deposit or downstream dune, Zimmermann and Church 2001).

DEMs of Difference revealed elevation changes associated with the log sills ranged from -1.40 to +2.17 m in the Williams River and -1.31 to +1.31 m in the Hunter River. Flume studies indicate that scour pools reach their maximum depth very quickly (Tregnaghi *et al.* 2007). In contrast, previous work downstream of Upper Munni in the Williams River (Brooks *et al.* 2004) found elevation changes ranging -0.6 to +1.8 m within one month of the completion of construction (and after two floods with recurrence intervals of 2 and 4 years, and 3 and 19 hours exceeding the reach-scale critical entrainment threshold, respectively). Four years after the completion of riverworks, the elevation range had increased to -1.8 to +2.2 m, with greater deposition and erosion around bank-attached jams than log sills (Brooks *et al.* 2006). Thus, the elevation changes measured in the current study are similar to previous work of similar-sized log structures. Although there are few comparative studies worldwide, these have much smaller ranges of elevation change. For example, in the low-gradient, meandering Middle Fork John Day River in eastern Oregon (U.S.A.), large multi-log bank-attached jams induced elevation changes of -0.9 to +0.5 m (Tu 2011).

Complex flow patterns interacting with heterogeneous sediments caused asymmetrical erosion and deposition around log sills and this resulted in nonregular bed topography. Many researchers argue that a single averaged profile poorly represents step-pool morphology in natural rivers or even in artificial streams and flumes with live-bed conditions (Comiti *et al.* 2005). There is a real need for combined field-based and modelling approaches where modelling parameters are set by field conditions and the modelling is used to identify the mechanisms responsible for observed phenomena to improve the accuracy and detail of predictions of geomorphic and hydrologic responses to riverworks. Computational fluid dynamics (CFD) methods have only recently been able to incorporate reach-scale topographic complexity (Biron *et al.* 2007). Early environmental applications of CFD models have been successfully used to determine high resolution, complex changes in bed topography and its effects on surface water movement through the reach (Casas *et al.* 2010), and how this can influence hyporheic exchange flux around stream restoration structures (Crispell and Endreny 2009).

The second hypothesis was that the increased topographic complexity induced by the log sills would increase vertical hydrological exchange around the log sills by increasing downwelling upstream of the log, and creating or increasing upwelling downstream of the log sill. Strong downwelling was induced upstream of all log sills. Scour pool areas were predominantly downwelling, but whereas this represented a substantial increase in exchange in the Hunter River, downwelling declined from initial levels in the scour zones of the Williams River sills. As predicted by the conceptual model, upwelling zones were created or strengthened at the tail of all riffles, although in the Hunter River, upwelling decreased with time from log sill construction. Given that upwelling also declined in the control site, this may have been due to extreme low flows reducing pressures at the stream-bed interface and/or the clogging of interstices by fine sediments between flood events.

These findings were generally consistent with previous studies, with one significant exception. In their study of an experimental step constructed in an agricultural stream, Kasahara and Hill (2006b) found the step induced an intense downwelling upstream of the sill, with upwelling downstream of the step. A modelling study of a log suspended above a flat bed found downwelling occurred upstream of the log, near the crest of the dune deposited downstream from sediment excavated from the plunge pool and downstream of the dune, with upwelling occurring in the plunge pool (Sawyer *et al.* 2011). The maximum depth of the scour pool in this latter study was 2.6 cm and the dune was 60 cm from the log with a maximum height of 5.6 cm (Sawyer *et al.* 2011). Kasahara and Hill (2006b) appear to have sampled downstream of the plunge pool in their study, but Zone III in my study was in the plunge pool. However, a modelling study of a step conducted over tens of metres also found that the structure induced upwelling immediately downstream of it and extending for about three metres from the step (Hester and Doyle 2008), so the difference in this study is unlikely to be wholly due to sampling location.

Given the depth the log sills penetrated the river bed in this study, it is likely that the extra depth of downwelling flowpaths meant that they returned to the stream further downstream of the log sill and this, combined with the hydraulic ram effect of stream

water over the log sill, induced downwelling in the plunge pool. Although this study and the modelling studies mentioned all found that log sills predominantly triggered downwelling, a study of debris dams in the semi-arid Red Canyon River near Lander, Wyoming (U.S.A.) found this to depend on whether the log structures were in gaining or losing reaches (Lautz *et al.* 2006). As downwelling increased upstream of the log sills despite limited localized channel steepening, the dominant mechanisms of vertical hyporheic exchange can be inferred to be localized head gradients caused by an impermeable object within the streambed and backwater pooling behind the exposed log.

In the Williams River, the proportion of fine-grained sediments peaked immediately after the construction of log sills and then declined. However, it remained above initial levels six months after construction. Although fine-grained sediments also peaked immediately following the construction of log sills in the Hunter River, they declined to below initial levels 12 months later. In the Williams River, fine sediment likely originated from the basaltic silts that comprised the adjacent stream banks (Brooks *et al.* 2004). In the Hunter River, initial proportions of fine bed sediments were greater and the river typically carries a larger suspended load during baseflow and the larger dam releases. High suspended loads are known to clog streambeds, reduce hydraulic conductivity and in turn, hyporheic exchange (Schälchli 1992). In the experimental study of Kasahara and Hill (2006b), high suspended loads caused fine sediments to preferentially clog downwelling zones and reduce the reach hydraulic gradient from 0.017 to 0.015 m m^{-1} within 12 months. The hydraulic permeability of the streambed is thought to exert the greatest control on log-induced hyporheic exchange because hydraulic permeability varies by orders of magnitude while stream velocity and the blockage effect of the log have limited ranges (Sawyer *et al.* 2011). Thus, restoration programs need to address fine sediment inputs and reintroduce bed-moving floods to maximise the success of on-ground investments (Kasahara and Hill 2006b, Kasahara *et al.* 2009). Fine sediment significantly increased at the downstream control riffle, HSB, one month after riverworks were constructed 1.8 river-kilometres upstream, emphasizing the importance of designing restoration strategies that minimize negative

impacts during on-ground works (Palmer *et al.* 2005), and that do not simply shift problems downstream.

The treatment riffles in the Hunter River reach were horizontally stratified before the onset of riverworks. Modelling and flume studies suggest that heterogeneous layering of stream sediments may result in greater and more variable hyporheic flux than in homogeneous beds with the same mean permeability; hyporheic zones in the former are smaller and tend to comprise flowpaths that are relatively shallow, short and have more rapid residence times (Salehin *et al.* 2004). Conversely, a field-based modelling study of the low-gradient, sandy gravel-bed Prairie Creek in central Nebraska (U.S.A.) found residence times in heterogeneous beds increased or decreased relative to homogeneous beds depending on the positions of the heterogeneities in the bed and the bed geometry (Cardenas *et al.* 2004). The strata in HGB were uniform and almost horizontal, and it is likely that the coarser layers were areas of preferential hyporheic flow. As such, horizontal hyporheic exchange likely substantially exceeded vertical hyporheic exchange across these riffles before riverworks began.

Proportions of FBOM were at the low end of the range from published studies (Crenshaw *et al.* 2002, and references within). In the Williams River, FBOM was concentrated in surface sediments of downwelling zones. With the exception of the head of the upstream riffle, proportions of FBOM typically increased above initial levels one month after the construction of log sills, and continued increasing six months after construction. However, they never reached the proportions measured initially in the head of the upstream riffle. In contrast, initial proportions of FBOM in HGB1 closely followed the horizontal stratigraphy, with the greatest proportions of FBOM in the fine-grained strata. With few exceptions, FBOM declined significantly after the construction of log sills and did not recover within one year. Initial FBOM in HGB2 peaked in downwelling zones (Zones II and III) and was consistent across depths; similarly to HGB1, FBOM at HGB2 declined after riverworks and only increased after riverworks in the 0-10 and 40-50 cm sediments. Interestingly, FBOM increased at the control site, HSB, after the upstream riverworks, indicating that much of the fine sediment mobilized by riverworks in the Hunter River was organically derived.

Previous studies have found strong positive correlations between organic matter and fine sediment (Claret *et al.* 1997), and initial sediment conditions in the Hunter River concur. The close correlation between FBOM and the fine sediment layers in HGB1 suggest that FBOM was deposited with the sediment during flood (Olsen and Townsend 2005). Conversely, at both riffles on the Williams River and HGB2, initial proportions of FBOM were greatest in the surface sediments of downwelling zones, suggesting it was deposited during baseflows (Boulton and Foster 1998). Although native gravel was used to backfill structures and the streambed, FBOM decreased markedly after construction. There are several possible reasons for this. Firstly, the increases in fine sediment and FBOM at the downstream control site following riverworks in the Hunter River suggest that FBOM was mobilized and entrained through the disturbance associated with construction, depleting the standing stock of FBOM at the treatment site. This may have also occurred in the Williams River where the same construction techniques were used. The increased FBOM after riverworks in the Williams River may have been associated with the multiple small floods during that time but the temporal resolution of sampling was insufficient to confirm this. In the Hunter River, the lack of noticeable increase in FBOM with time from construction indicates that supply was limited and/or that FBOM was broken down rapidly after deposition.

Although assessments of breakdown rates of interstitial particulate organic matter (POM) are relatively scarce, several researchers identify porosity as a key determinant of POM breakdown by its control of invertebrate distributions in the hyporheic zone (Olsen and Townsend 2003, Navel *et al.* 2010). While early studies suggested invertebrates are only likely to be limited when porosity is less than 3-5 % (Maridet *et al.* 1996, Boulton and Foster 1998), an experimental laboratory study on Rhône hyporheic sediments found that decreases in porosity from 25 % to 12 % were enough to constrain the vertical distribution of medium-sized shredders and thus, the breakdown of buried POM (Navel *et al.* 2010). Critically, this was not due to porosity *per se*, but how porosity changed the availability of electron acceptors (oxygen) and nutrients (nitrogen and phosphorus). In the Williams River, porosity declined immediately following the construction of log sills, but at six months was greater than

initial levels. Although porosity was relatively constant at WUM1, it declined rapidly with depth and along the riffle at WUM2 and this was likely influenced by fine sediment increasing with depth. Overall though, porosity remained > 8 % at all sites across all times.

Communicating restoration outcomes

Given the results of this study, comparing changes in vertical hydraulic gradients against changes in the median grain size of sediment (d_{50}) appears to be the most pragmatic way of communicating the restoration results of this study using Findlay's (1995) model relating hyporheic structure and function as applied by Kasahara and co-workers (2009). The models were constructed for the 20-cm deep VHG and using the average d_{50} of all depths. Only Zones II and IV are shown here (Figure 2.18). The mechanisms by which log sills induce downwelling are the backwater pooling effect and obstruction of an impermeable object and these had the greatest effect in Zone II. Zone IV was selected as it is the upwelling zone.

In the Williams River, median grain size in all zones decreased immediately following construction. Median grain size then increased six months after construction (as the fines were mobilized), with concurrent significant increase in both downwelling and upwelling. Changes in both sediment size and VHG were much more subtle in the Hunter River. Unfortunately, it is difficult to compare these results with the general hypotheses of the previous study of Kasahara and co-workers (2009), as their example does not include the actual sediment variables.

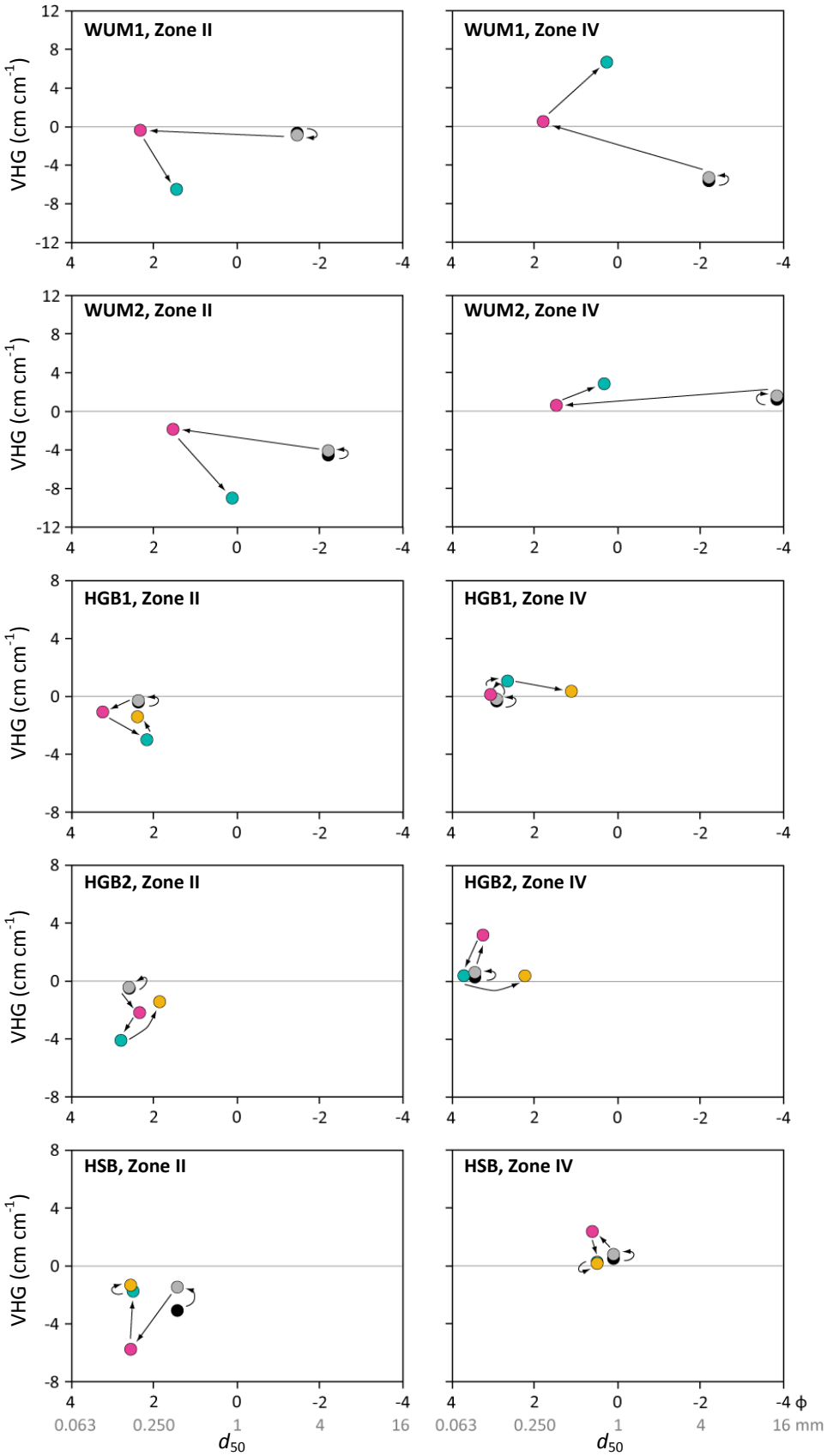

Figure 2.18 Mean change in vertical hydraulic gradients (circles) at 20 cm deep immediately upstream and downstream of log sills six months pre- (black), one month pre- (grey), and one month post- (magenta), six months post- (cyan), and 12 months post-ELSs (yellow). Above and below the grey line is upwelling and downwelling, respectively. Sediment grain size (d_{50}) is the average of all depths across three cores.

Limitations of this study

Few restoration projects undergo comprehensive ecological assessments, and fewer involve the theoretical optimum of long-term monitoring of salient patterns and processes at appropriate temporal and spatial scales with adequate replication of controls and reference sites (Downes *et al.* 2002). Application of even the simplest Before-After-Control-Impact (BACI) experimental designs may be difficult in the absence of data prior to the impact; non-replicable restoration 'treatments' given project objectives, costs, and the lack of appropriate and accessible sites; the lack of suitable and accessible control sites; the difficulty of finding reference sites (Dufour and Piégay 2009); and difficulties in defining the salient patterns and processes at the appropriate temporal and spatial scales (Michener 1997). These limitations inhibit the ability to infer causal relationships between abiotic changes and biological responses. However, even given these constraints, restoration projects can be comprehensively assessed and used to inform fundamental ecological theory (Michener 1997).

The design of this experiment was constrained by the absence of a control site and minimal sampling before the riverworks in the Williams River; this was because I included this restoration project in the study opportunistically and had little warning or lead-time to collect 'before-impact' data. In the Hunter River, extreme low flows immediately preceding the riverworks did not prevent the collection of pre-data, but likely caused below average vertical hydraulic gradients. The restoration strategy to locate two log sills at each treatment site was logistically and financially optimal, but the size of and disturbance associated with installing these structures meant that log sills were not independent of each other. Despite these constraints, this is the first documented study of how large, multi-log structures typical of those installed by river management agencies affect hyporheic structure and function. As such, the results of this study are invaluable for informing future riverworks, especially as they cannot be replicated by modelling, flume studies or even small experimental structures.

The use of DEMS and DEMs of Difference to represent topographic surfaces and geomorphic change is increasingly common given continuing improvements in field

survey hardware and GIS (geographic information system) software (Wheaton *et al.* 2010a). Error can be introduced into the DEM and subsequent analyses from numerous sources including the quality of survey point data, sampling strategy, surface composition, topographic complexity and interpolation methods (Chappell *et al.* 2003, Milan *et al.* 2011). Quantification of the uncertainty associated with DEM construction has typically focused on elevation accuracy to determine the fundamental question of whether real geomorphic change can be distinguished from noise (Wheaton *et al.* 2010b).

Despite widespread acknowledgement that elevation uncertainty increases around topographically complex terrain, the most common procedure for managing DEM uncertainties involves specifying a minimum level-of-detection threshold (e.g. the 84th percentile of the particle size distribution (d_{84}), Chappell *et al.* 2003) and disregarding changes under this threshold (Wheaton *et al.* 2010b). Recent innovations include using fuzzy set theory to estimate spatially variable DEM uncertainty, using Bayes' theorem to calculate conditional probabilities of erosion and deposition based on their predicted spatial cohesion (i.e. known patterns in the location, size and shape of erosional and depositional patches), and calculating spatially distributed error from the relationship between local topographic roughness and the standard deviation of elevation errors (Wheaton *et al.* 2010b, Milan *et al.* 2011). As these methods are tested and integrated in commercial GIS software packages, assessments of DEM uncertainty will become routine for ecological studies. Reassuringly, despite the absence of uncertainty analyses of the DEMs of Difference in this study, elevation changes are within the ranges documented by the earlier study of Brooks and co-workers (2004, 2006), who specified a minimum threshold of detection of ± 0.2 m.

There are a few techniques to estimate the area and volume of the hyporheic zone and residence times of hyporheic flowpaths. Flowpaths can be mapped directly by measuring pressure or head gradients, or by analysing the chemical signatures of exchange patches (Stream Solute Workshop 1990). Conservative tracers are also used and, when combined with reactive tracers, can estimate the absolute and relative importance of hyporheic nutrient cycling processes to the whole stream (Kasahara and

Hill 2006a). In their comparison of an experimental log sill and artificial riffle construction, Kasahara and Hill (2006a) combined a conservative tracer (Br^- or Cl^-) with a biologically reactive tracer (KNO_3) to elegantly quantify the extent of the hyporheic zone, the volume of hyporheic exchange as a proportion of surface flow, and the residence time and nutrient dynamics of riffle flowpaths. However, even the deployment of a conservative tracer such as fluorescent dyes that are ideal for examining smaller spatial and temporal scales (m to km, and hours to days, respectively) and are easily measured at high frequency with a field-portable fluorometer is logistically intensive and expensive in large rivers (Caplow *et al.* 2004). Although the inert gas sulphur hexafluoride (SF_6) has been used successfully as a conservative tracer in large rivers (km and weeks, Ho *et al.* 2006), its operational range is over longer spatial and temporal scales than appropriate here (Figure 2.5, Heffernan *et al.* 2010). This study lacked the resources to conduct repeated high-resolution solute tracer studies given the discharge of the studied rivers, particularly the Hunter River (Boulton and Hancock 2006). Therefore, it had no means of quantifying the extent, volume and residence time of the studied hyporheic zones and hypotheses and conclusions were constrained accordingly.

No previous study has assessed the effects of deeply embedded, multi-log structures, and this study was unable to assess the effects of such structures on large-scale hyporheic flowpaths such as the down-valley movement of groundwater. This may form a significant component of hyporheic exchange in rivers flowing through deep alluvium (Brunke and Gonser 1997), and be particularly important in maintaining baseflow (Church *et al.* 1987). There are two key recommendations for future studies of similar structures: (1) the study needs to measure horizontal as well as vertical hyporheic exchange, and (2) the spatial extent of the impact of these structures needs to be carefully assessed. With respect to the latter point, if these structures sever or impede large-scale, deep flowpaths, they may substantially change the location and magnitude of down- and up-welling both upstream and downstream of the riverworks, i.e. increase hyporheic discharge upstream similar to bedrock outcrops, and reduce hyporheic discharge downstream, reducing the buffering effects and refugia of downstream hyporheic zones.

Techniques used to sample the sediment matrix within the low flow channel range significantly in the effort, cost and effectiveness at sampling specific size classes. Freeze-coring preserves the vertical stratification of sediments (with some disruption as the standpipe is sunk) and provides an estimate of sediment porosity. However, freeze-core samples have a ragged edge with larger particles protruding from the frozen core (Plate 2.9) and are small (relative to bulk core samples), suggesting that the method does not sample all size fractions with equal efficiency and that the sample size may be too small to accurately sample the larger clasts (Wolman 1954, Zimmermann *et al.* 2005). Alternative sampling methods including pebble counts (Kondolf 2000a) and qualitative or semi-quantitative visual estimates estimate only the surface layer and cannot measure fine sediment content (Kondolf 2000a and references within). Bulk-core sampling within the low flow channel involves driving a cylindrical core-sampler (50 cm diameter) into the bed, hand-removing sediment to a predetermined depth and retaining the muddy water within the sampler to sample fine sediments (Wood and Armitage 1997, Olsen and Townsend 2003). Bulk-core sampling is labour-intensive but simple, and typically yields large sample sizes that – at best – are divided into surface and subsurface layers.

Sediment heterogeneity and the amount of fine sediment (63-250 µm and 1 mm) have been identified as key determinants of the distribution of hyporheic invertebrates (Sobczak and Findlay 2002), and physicochemical conditions through altering permeability, residence times and hydrological exchange (Boulton *et al.* 2010). Despite its limitations, freeze-coring provides a quantitative method of estimating changes in sediment size distributions including vertical stratification and infiltration of fine sediments. Furthermore, the small sample size (relative to bulk-core samples) is an advantage for repeated surveys of localized restoration projects where large samples would introduce error in successive topographic surveys and sediment samples. Combining freeze-cores with pebble counts would increase the sampling efficiency of surface layers, particularly where there was an armour layer, but would also overestimate armouring given that only subsurface large clasts would be under-sampled.

This study used a novel method of calculating percentiles of sediment size distributions for use in determining d_{50} and other sediment indices. This method removes the subjectivity of visually interpreting percentiles from cumulative distribution curves and optimises the analysis of large numbers of samples. However, the method overestimates the grain size of the smaller percentiles (i.e. the larger clasts) where these comprise the majority of sample. This overestimation is worse in poorly sorted sediments that consist of a large range of particle sizes. It is difficult to assess the sampling error associated with the combination of freeze-coring that underestimates large clasts with the algebraic calculation of sediment size distributions that overestimates larger clasts.

Finally, although the use of log sills in hyporheic restoration has been the focus of several previous studies, none of these comprises large, multi-log structures deeply embedded in higher-order, degraded rivers, and none included an assessment of the disturbance associated with placing large wood structures within the streambed. Until more such studies are conducted with riverine scientists working closely with restoration practitioners, the ability of science to accurately inform cost-benefit analyses of these types of restoration projects will be restricted. Technological advances that increase the ability to collect both intensive and extensive geomorphic, sedimentary, hydrological and biogeochemical samples, and use these to model hyporheic processes in natural reaches, will both substantially improve the science underpinning future restoration projects and enable these restoration projects to inform fundamental ecological theory (Boulton *et al.* 2003).

Conclusions

This study documents the reach-scale increases in topographic complexity and vertical hyporheic exchange induced by large engineered log sills embedded in two degraded gravel-bed rivers. The magnitude of erosion and deposition around the log sills depends on the size, frequency and duration of floods that exceeded the critical entrainment threshold of the reach. Concurring with previous studies, the log sills predominantly increased downwelling, particularly immediately upstream of the sills

(Zone II). Given this occurred without remarkable localized channel steepening upstream of the log, and the scour pools were sites of weak downwelling, the dominant mechanisms of sill-induced vertical hyporheic exchange are likely to be the backwater pooling effect from the exposed portion of the log sill, and the localized hydraulic gradients caused by the obstruction of an impermeable object within the sediment.

A key part of any similar restoration project should be to manage fine sediments through the reach. In the Williams River, fine sediments were likely introduced to the streambed from the stream banks during construction. In the Hunter River, high antecedent levels of interstitial fine sediment and a high suspended load contributed to high fine sediment levels immediately following construction, even at the undisturbed control site 1.8 river-kilometres downstream. The proportions of interstitial FBOM declined after riverworks and this would have affected hyporheic nutrient cycling processes (Chapter 3) and invertebrate foodwebs.

The findings of this study support the hypothesis that log sills located in riffles increase topographic complexity. It is unclear how much increases in topographic complexity contributed to increases in vertical hydrologic exchange, as topographic responses varied among log sills, and the disturbance associated with their construction substantially altered sediment characteristics and reduced stream discharge and velocity down the right channels. Nonetheless, the increased downwelling induced by the log sills is predicted to increase the supply of dissolved oxygen, solutes and FPOM into the hyporheic zone. Thus, the third hypothesis of my conceptual model is that where log sills predominantly induce localized downwelling, the increase in hyporheic exchange will increase nutrient supply to the hyporheic zone, creating or increasing a hyporheic sink. Conversely, where log sills induce localized upwelling (Lautz *et al.* 2006), the increase in hyporheic exchange will increase nutrient supply to the hyporheic zone as well as creating or increasing hyporheic nutrient input to the surface stream. As this study found predominant downwelling, the research described in Chapter 3 explored whether the log sills created or increased hyporheic sinks.